UC San Diego

UC San Diego Electronic Theses and Dissertations

Title

The organization and diversity of neurons in the developing spinal cord

Permalink

https://escholarship.org/uc/item/6rp7w6sb

Author

Osseward II, Peter James

Publication Date

2021

Supplemental Material

https://escholarship.org/uc/item/6rp7w6sb#supplemental

Peer reviewed|Thesis/dissertation

eScholarship.org Powered by the California Digital Library
University of California

UNIVERSITY OF CALIFORNIA SAN DIEGO

The organization and diversity of neurons in the developing spinal cord

A dissertation submitted in partial satisfaction of the requirements for the degree Doctor of Philosophy

in

Neurosciences

by

Peter James Osseward II

Committee in Charge:

Professor Samuel Pfaff, Chair
Professor Yimin Zou, Co-Chair
Professor Susan Ackerman
Professor Kenta Asahina
Professor Kristin Baldwin
Professor Takaki Komiyama

2021

Copyright

Peter James Osseward II, 2021
All rights reserved.

The dissertation of Peter James Osseward II is approved, and it is acceptable in quality and form for publication on microfilm and electronically:

University of California San Diego

2021

DEDICATION

To Mom, Dad, and JP, for their love and support.

EPIGRAPH

Our life is an apprenticeship to the truth, that around every circle another can be drawn; that there is no end in nature, but every end is a beginning; that there is always another dawn risen on mid-noon, and under every deep a lower deep opens.

Ralph Waldo Emerson, Circles

TABLE OF CONTENTS

Dissertation Approval Page iii

Dedication iv

Epigraph v

Table of Contents vi

List of Abbreviations vii

List of Figures viii

List of Supplementary Material xi

Acknowledgements xii

Vita xvi

Abstract of Dissertation xvii

Chapter 1: Cell type and circuit modules in the spinal cord 1

Chapter 2: Conserved genetic signatures parcellate cardinal spinal neuron classes into local and projection subsetsets 13

Chapter 3: An intersectional genetic system to access interneuron subtypes arrayed across the spinal cord 94

LIST OF ABBREVIATIONS

LTMR	low threshold mechanoreceptors
CPG	central pattern generator
V	ventral interneuron class
MSE	motor synergy encoders
MN	motor neuron
dI	dorsal interneuron class
MMC	medial motor column
LMC	lateral motor column
HMC	hypaxial motor column
GL	gluteus
TA	tibialis anterior
IF	intrinsic foot
LRN	lateral reticular nucleus
GABA	g-aminobutyricacid
scRNA-seq	single cell RNA-sequencing
UMAP	uniform manifold approximation and projection
Glut	glutamatergic
UMIs	unique molecular identifiers
GO	Gene Ontology
CTB	cholera toxin subunit b

LIST OF FIGURES

Figure 1.1: Features encompassing neuronal identity in the spinal cord…… 3

Figure 1.2: Spinal cord regions and cell types…… 4

Figure 1.3: Molecular organization of spinal neurons…… 5

Figure 1.4: Specificity in spinal cord circuitry…… 7

Figure 2.1: scRNA-seq identifies relationships among groups of spinal neurons…… 15

Figure 2.2: Branch points in the hierarchical comparisons define spinal neuron groups with discrete locations……16

Figure 2.3: The group-N and -Z division is linked to neuronal birthdate…… 17

Figure 2.4: Each cardinal class is a mixture of both group-N and -Z neurons…… 18

Figure 2.5: Projection and long-range neurons express group-Z markers…… 19

Figure 2.6: A unified taxonomic index of spinal neurons…… 20

Figure 2.7: Validation of Cre lines and gene expression in Group-N and -Z neurons…… 40

Figure 2.8: Group-H, -E, -N, -Z marker gene expression patterns……42

Figure 2.9: Group-E, -N, and -Z neurons are mixtures of both glutamatergic and GABAergic neurons…… 44

Figure 2.10: Colocalization and spatial analysis of multiple Group-Z and Group-N markers…… 46

Figure 2.11: Group-E, -N, -Z neuron markers label distinct neuronal populations…… 48

Figure 2.12: Characterization of Group-N, -Z, -E marker expression along the rostrocaudal axis of spinal cord neurons……50

Figure 2.13: Summary dendrogram of marker genes for Group-H, -E, -Z, -N neurons……52

Figure 2.14: E12.5 scRNA-seq analysis of neural tube cells…… 54

Figure 2.15: k-means 2 divisions of E12.5 scRNA-seq reveal neuronal groups and states…… 56

Figure 2.16: Embryonic development of Group-N, -Z, and -E neurons…… 58

Figure 2.17: Group-N and -Z neurons develop properly in the absence of sensory or motor neurons…… 60

Figure 2.18: Each cardinal neuron class is a mixture of both Group-N and Group-Z neurons…… 62

Figure 2.19: Quantification of Group-E, -N, and -Z neurons that arise from each cardinal neuron class……64

Figure 2.20: Spatial characterization of Group-N and -Z neurons from each cardinal class…… 66

Figure 2.21: Group-N and -Z divisions amongst the V1 cardinal class clades…… 68

Figure 2.22: Group-N and -Z neurons synapse with motor neurons and receive diverse inputs…… 70

Figure 2.23: Cervical and lumbar spinothalamic neurons express Group-Z markers…… 72

Figure 2.24: Lumbar spinocerebellar neurons express Group-Z markers…… 74

Figure 2.25: Spinomedullary neurons express Group-Z markers…… 76

Figure 2.26: Propriospinal cervicolumbar and lumbocervical neurons express Group-Z markers…… 78

Figure 2.27: Summary of neuronal features encapsulated by cardinal class and Group-Z/N identity…… 80

Figure 3.1: Genetic labeling of Group-N and Group-Z neurons in the spinal cord…… 98

Figure 3.2: Intersectional genetics recapitulates cardinal class immunostaining with Group-N and Z markers…… 100

LIST OF SUPPLEMENTARY MATERIALS

Table S1: P0 neuron 45 cluster solution enriched genes and cardinal class identification

Table S2: Top differentially expressed genes between Group-N and Group-Z neurons

Table S3: E12.5 neuron 27 cluster solution enriched genes and cardinal class identification

Table S4: GO terms analysis comparing Group-N/Z neurons

Table S5: Animal and marker counts for experiments

ACKNOWLEDGEMENTS

There are many individuals I would like to thank for their friendship, support, and guidance over the years. Graduate school has been an arduous but rewarding journey, and I am grateful for all the types of support I have received during it.

I would like to thank my family and friends for their support and compassion.

I would like to thank my previous scientific mentors, Tom Knight, Leena Knight, and David Perkel for welcoming me into their labs, their mentorship, and their encouragement for me to pursue graduate school.

I would like to thank my thesis committee for their feedback and perspectives on my projects over the years.

I would like the thank all the members of the Pfaff lab for their time, effort, and feedback to make this work possible. Neal, Marito, and Lukas, thank you for training and mentoring me during my initial time in the lab. To my fellow graduate students in lab and also the in the neurosciences program, thank you for the conversation, celebration, and commiseration throughout graduate school. Thank you Pfaff lab postdocs for sharing your hard-earned wisdom. Karen, Miriam, Shawn, Fernando, Hannah, Craig, Brendan, Tom, and G, thank you for all the help and support in lab. Your support has been tremendous in allowing me to make the most of my time in the Pfaff lab. Marito, I would like to thank you being a great co-author. Working on our project together has been a collaborative and fantastic experience ever since our initial data sets suggested we were converging on the same interesting research question. Working out the resulting ideas and details over the years has been a great way to go through graduate school.

Sam, thank you for the wonderful time in your lab. You provide an incredible amount of trust and resources for your lab members, as well as encouragement to go for ambitious projects. Furthermore, starting with your kindness and jokes, you have fostered an environment of friendship and collaboration among lab members. Altogether, you have made coming into lab the past years an enjoyable and transformative experience.

Chapter 1, in full, is a reprint of the review as it appears in: Osseward, P. J., 2nd, and S. L. Pfaff. 2019. 'Cell type and circuit modules in the spinal cord', *Curr Opin Neurobiol*, 56: 175-84. The manuscript was written in collaboration with Samuel L. Pfaff. The authors of this manuscript would like to thank Ben Temple, Bianca Barriga, Gokhan Senturk, Kelsey Ladt, and Marito Hayashi for helpful comments on the manuscript. P.J.O was supported by the Christopher and Dana Reeve Foundation. S.L.P. is supported as a Howard Hughes Medical Institute Investigator and as a Benjamin H. Lewis chair in neuroscience. Research in the laboratory is supported by funding from the Howard Hughes Medical Institute and the Sol Goldman Charitable Trust.

Chapter 2, in full, is a reprint of the manuscript as it appears in: Osseward, Peter J., Neal D. Amin, Jeffrey D. Moore, Benjamin A. Temple, Bianca K. Barriga, Lukas C. Bachmann, Fernando Beltran, Miriam Gullo, Robert C. Clark, Shawn P. Driscoll, Samuel L. Pfaff, and Marito Hayashi. 2021. 'Conserved genetic signatures parcellate cardinal spinal neuron classes into local and projection subsets', *Science*, 372: 385. The manuscript was written in collaboration with Marito Hayashi and Samuel L. Pfaff.

We thank K. Lettieri, B. O'Leary, H. Forman, A. J. Levine, M. J. Sternfeld, K. L. Hilde, members of the Pfaff laboratory, the FCCF core (C. O'Connor and C. Fitzpatrick; NIH-NCI CCSG: P30 014195), the NGS core (N. Hah; NIH-NCI CCSG: P30 014195, the Chapman Foundation and the Helmsley Charitable Trust), the UCSD IGM Genomic Center (K. Jepsen and other members), the Biophotonics core (NIH-NCI CCSG: P30 014195 and the Waitt Foundation), the GT3 core (J. Naughton, J. Marlett, and R. Armendariz; NIH-NCI CCSG: P30 014195, NINDS R24 Core Grant, funding from NEI), and the Janelia Viral Vector Core for technical support and advice; M. Goulding, G. Gatto, members of the Goulding laboratory, E. J. Kim and E. M. Callaway for providing reagents and advice; and S. Ackerman, K. Asahina, K. Baldwin, T. Komiyama, and Y. Zou for discussions and advice. Funding: P.J.O. was supported by the Christopher and Dana Reeve Foundation. N.D.A. is supported by the NIMH T32 Training Grant T32MH019938 J.D.M. is supported by NIH-NICHD K99 HD096512. B.K.B. is supported by the UCSD Cell and Molecular Genetics Training Program (T32 GM007240) and the Timken-Sturgis Foundation. M.H. was supported by the Japanese Ministry of Education, Culture, Sports, Science, and Technology Long-Term Student Support Program and the Timken-Sturgis Foundation. S.L.P. is a Benjamin H. Lewis chair in neuroscience. This research was supported by funding from the Howard Hughes Medical Institute, the Christopher and Dana Reeve Foundation, the Sol Goldman Charitable Trust, and National Institutes of Health (1 U19 NS112959-01). Author contributions: Conceptualization: M.H., P.J.O., and S.L.P. Methodology: M.H., P.J.O., J.D.M., and S.P.D. Software: S.P.D., J.D.M., and P.J.O. Validation: M.H., P.J.O., L.C.B., and R.C.C. Formal analysis: S.P.D., J.D.M., P.J.O., and M.H. Investigation: M.H., P.J.O., N.D.A., B.A.T., B.K.B., L.C.B., F.B., and R.C.C. Resources: M.G., S.P.D., J.D.M., P.J.O., and M.H. Data curation: S.P.D., J.D.M., and P.J.O. Writing, original draft: M.H., P.J.O.,

and S.L.P. Writing, review and editing: M.H., P.J.O., N.D.A., J.D.M., B.A.T., B.K.B., S.P.D., and S.L.P. Visualization: M.H., P.J.O., and S.P.D. Supervision: M.H., P.J.O., and S.L.P. Project administration: M.H., P.J.O., and S.L.P. Competing interests: The authors declare no competing interests. Data and materials availability: All data are available in the main text or the supplementary materials. The accession number for the scRNA-seq data reported in this paper is NIH GEO: GSE171607, GSE171605, and GSE171606.

Chapter 3 is preliminary material being prepared for submission. Authors include Peter J. Osseward, Marito Hayashi, Lukas C. Bachmann, Hannah Forman, and Samuel L. Pfaff. The manuscript was written in collaboration with Samuel L. Pfaff.

We thank K. Lettieri, M. Gullo, members of the Pfaff laboratory, the GT3 core (J. Naughton, J. Marlett, and R. Armendariz; NIH-NCI CCSG: P30 014195, NINDS R24 Core Grant, funding from NEI), and the Transgenic Core Facility of the Salk Institute (Y. Dayn and Tsung-Chang Sung; NIH-NCI CCSG: P30 014195). Funding: P.J.O. was supported by the Christopher and Dana Reeve Foundation. M.H. was supported by the Japanese Ministry of Education, Culture, Sports, Science, and Technology Long-Term Student Support Program and the Timken-Sturgis Foundation. S.L.P. is a Benjamin H. Lewis chair in neuroscience. This research was supported by funding from the Howard Hughes Medical Institute, the Christopher and Dana Reeve Foundation, the Sol Goldman Charitable Trust, and National Institutes of Health (1 U19 NS112959-01).

VITA

2012 Bachelor of Arts, Biochemistry, Biophysics, & Molecular Biology (BBMB)
Bachelor of Arts, Philosophy
Whitman College. Walla Walla, Washington

2021 Doctor of Philosophy, Neurosciences
University of California San Diego. La Jolla, CA
Graduate Research
The Salk Institute for Biological Studies. La Jolla, CA

PUBLICATIONS

Osseward, Peter J., Neal D. Amin, Jeffrey D. Moore, Benjamin A. Temple, Bianca K. Barriga, Lukas C. Bachmann, Fernando Beltran, Miriam Gullo, Robert C. Clark, Shawn P. Driscoll, Samuel L. Pfaff, and Marito Hayashi. 2021. 'Conserved genetic signatures parcellate cardinal spinal neuron classes into local and projection subsets', *Science*, 372: 385.

Osseward, P. J., 2nd, and S. L. Pfaff. 2019. 'Cell type and circuit modules in the spinal cord', *Curr Opin Neurobiol*, 56: 175-84.

Wood, W. E., **P. J. Osseward, 2nd**, T. K. Roseberry, and D. J. Perkel. 2013. 'A daily oscillation in the fundamental frequency and amplitude of harmonic syllables of zebra finch song', *PLoS One*, 8: e82327.

ABSTRACT OF DISSERTATION

The organization and diversity of neurons in the developing spinal cord

by

Peter James Osseward II

Doctor of Philosophy in Neurosciences

University of California San Diego, 2021

Professor Samuel L. Pfaff, Chair

Within the nervous system, the spinal cord plays vital roles both at the initial steps of receiving and processing incoming sensory information, and at the final stages of executing appropriate motor plans. Spinal neural networks are sufficient to produce corrective sensorimotor reflexes and locomotor central pattern generator activity, but also must interface with the brain to produce more nuanced and elaborate behavior. Consequently, a diverse array of spinal

interneurons mediate these functions. Significant studies have delineated spinal neurons into cardinal classes with distinct developmental origins and functions. However, recent studies have uncovered extensive molecular and circuit diversity within each cardinal class. As a result, because each cardinal class is comprised of a mixture of subpopulations, it has been difficult to interpret which aspects of each cardinal class are most salient to its function.

This dissertation describes a series of original work that aims to identify a unifying logic for spinal neuron diversification across cardinal classes. The first chapter consolidates recent work on spinal neuron characterization, with a focus on molecular and circuit diversity within single cardinal classes. The second chapter examines molecular diversity conserved across heterogeneous populations of spinal neurons. We found broad genetic signatures which divide the spinal cord into sensory-motor, local-long range, and inhibitory-excitatory groups of neurons. The local-long range signature corresponded to neuronal birthdate and divided each cardinal class into their local and projection subsets. Thus, many aspects of diversity within each cardinal class can be tracked with the same molecular signatures, greatly simplifying the task of identifying discrete functional cell types. The third chapter provides an initial characterization of transgenic mouse lines developed to label the local and long-range groups of spinal neurons identified in chapter two.

In summary, this work identifies a genetic axis which governs aspects of spinal neuron diversity. This genetic axis is organized temporally, reflecting the birthdate of spinal neurons. It corresponds to whether the neuron projects locally or long-range. This genetic axis is orthogonal to the previously defined cardinal classes, and when used together predict many aspects of spinal neuron attributes, including location, neurotransmitter, and synaptic outputs.

Chapter 1: Cell type and circuit modules in the spinal cord

Available online at www.sciencedirect.com

ScienceDirect

Current Opinion in Neurobiology

Cell type and circuit modules in the spinal cord

Peter J Osseward II[1,2] and Samuel L Pfaff[1]

The spinal cord contains an extraordinarily diverse population of interconnected neurons to process somatosensory information and execute movement. Studies of the embryonic spinal cord have elucidated basic principles underlying the specification of spinal cord neurons, while adult and postnatal studies have provided insight into cell type function and circuitry. However, the overarching principles that bridge molecularly defined subtypes with their connectivity, physiology, and function remain unclear. This review consolidates recent work in spinal neuron characterization, examining how molecular and spatial features of individual spinal neuron types relate to the reference points of connectivity and function. This review will focus on how spinal neuron subtypes are organized to control movement in the mouse.

Addresses
[1] Gene Expression Laboratory and the Howard Hughes Medical Institute, Salk Institute for Biological Studies, 10010 North Torrey Pines, La Jolla, CA 92037, USA
[2] Neurosciences Graduate Program, University of California, San Diego, La Jolla, CA 92093, USA

Corresponding author: Pfaff, Samuel L (pfaff@salk.edu)

Current Opinion in Neurobiology 2019, **56**:175–184

This review comes from a themed issue on **Neuronal identity**

Edited by **Sacha Nelson** and **Oliver Hobert**

For a complete overview see the Issue and the Editorial

Available online 5th April 2019

https://doi.org/10.1016/j.conb.2019.03.003

0959-4388/© 2019 The Authors. Published by Elsevier Ltd. This is an open access article under the CC BY-NC-ND license (http://creativecommons.org/licenses/by-nc-nd/4.0/).

Introduction

The spinal cord is a major site of output of the nervous system, where neural activity is converted into precise muscle contractions. It is also a place of integration, containing neural networks capable of processing a variety of sensory and descending inputs. Thus, the spinal cord is both a site of convergence and divergence, where multiple streams of information are synthesized and transformed into patterned activation of motor neurons.

A heterogeneous network of spinal neurons underlies this sophisticated sensorimotor processing. Historically, investigators have identified spinal cord neuron types using one or two features at a time, through the lens of morphology, location, physiology, connectivity, molecular markers, developmental lineage, or behavior (Figure 1). These studies have provided a basic understanding of the major classes of spinal neurons and their most prominent features [1,2]. Experiments perturbing specific sets of interneurons point toward a modular organization of cell types and circuits within the spinal cord, where populations of neurons play somewhat independent roles [2–5].

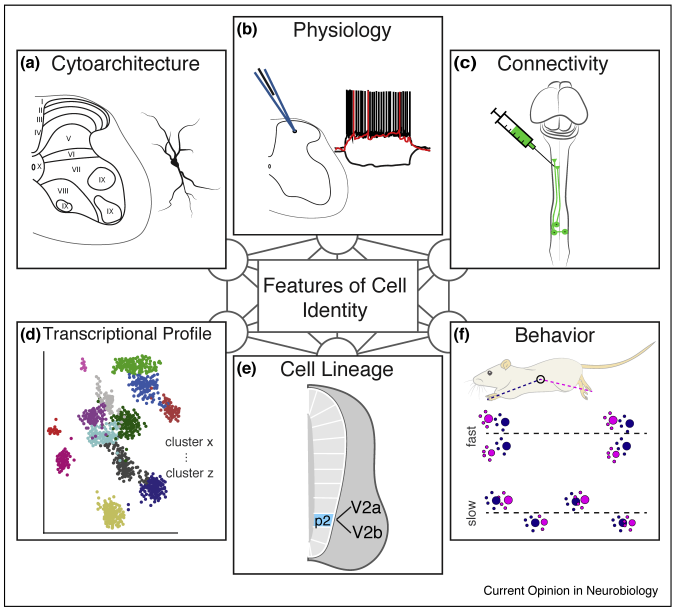
Despite this division of function among cell types, recent studies using transcriptional profiling have uncovered an impressive array of molecular divisions *within* individual classes of spinal neurons, suggesting an even finer-grained level of cellular heterogeneity. The significance of many of these molecular subtypes are still obscure. In this review, we will examine how features of neuronal identity link to one another and attempt to understand what these relationships may suggest for spinal cord circuit assembly and function. We present evidence that interneuron molecular subtypes correspond to a complex mixture of neuronal features. Given this abstract relationship between molecular-identity and functional-identity, we suggest that mapping neuron subtypes into a multidimensional space of features will be necessary for uncovering the principles of spinal neuron diversity and motor control.

Spinal regions, their cell types, and segregated functions

The spinal cord can coarsely be divided into three regions: dorsal, intermediate, and ventral (Figure 2a). While these divisions are somewhat arbitrary anatomical, physiological, and functional studies provide evidence for distinct functions between these regions. The dorsal horn mediates exteroceptive sensory processing [4]. The ventral cord is critical for motor execution and the generation of rhythmic motor behaviors [3,5]. The intermediate spinal cord is thought to play a major role in integrating sensory and descending information to fine tune motor output [6]. Within each of these spinal regions, studies have characterized and manipulated molecularly defined cell populations (Figure 2b). The results of these studies point toward distinct molecular populations that make specific contributions to each region's overall function.

In the dorsal horn, cutaneous sensory neurons terminate in modality-specific patterns (Figure 2c) [4,7,8]. Noxious sensory afferents primarily terminate within laminae I–II, transmitting thermal or painful touch sensations. Innocuous touch is transmitted by a variety of low threshold mechanoreceptors (LTMRs) which terminate within laminae II–IV. These receptors transduce sensations such

Figure 1

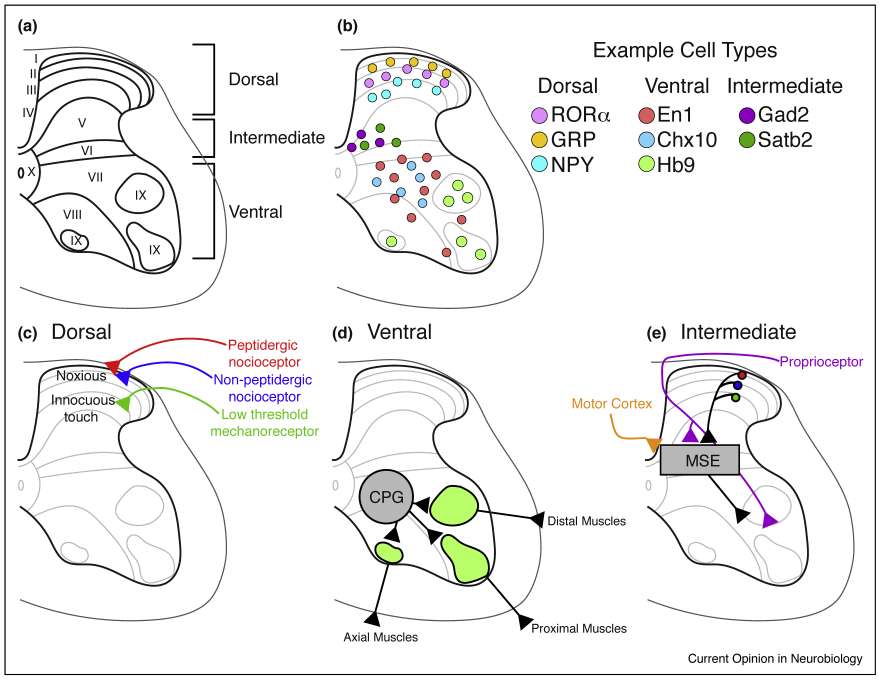


Features encompassing neuronal identity in the spinal cord. Spinal neurons can be classified based on many individual features, but the relationships between these features are still unclear.
(a) Spinal neurons can be classified based on cell morphology and location. Laminar designation, originally described by Bror Rexed, is a common method to categorize spinal neurons.
(b) Spinal neurons possess a variety of intrinsic electrophysiological properties. Furthermore, cell recordings paired with stimulation (such as dorsal root stimulation) can reveal functional connections between neuronal populations.
(c) Various tracers and viral approaches have been used to examine connectivity between spinal neurons. Anterograde, retrograde, and trans-synaptic tracing have been used to identify neuronal populations with specific projection patterns.
(d) RNA sequencing, both at the population and single cell level, have identified many transcriptionally distinct populations within the spinal cord.
(e) Developmental studies have examined genes involved in the specification of spinal neurons. Overexpression and knockout studies have provided insight into gene function, while lineage tracing has allowed investigators to probe the anatomy and function of developmentally defined cell types.
(f) Spinal neurons can be classified based on their role in behaviors. Early activity gene markers such as c-fos have been used to identify cohorts of neurons active during specific behaviors. Activation, silencing, and ablation studies have allowed spinal neurons to be categorized by the behaviors they mediate.

as skin indentation or hair vibration. Consequently, the ablation of dorsal spinal neuron subtypes results in selective deficits of sensory behaviors [4]. For example, ablation of spinal neurons expressing Retinoid-Related Orphan Receptor Alpha (RORα), which receive input from light touch LTMR subtypes, results in deficiencies in fine motor control and the detection of static and dynamic touch [9].

The ventral spinal cord contains motor neurons and a diverse network of interneurons that regulate motor neuron firing. Motor neuron subtypes are organized into pools that are arrayed in a musculotopic map [10–12]. In the lumbar spinal cord, ventral interneurons assemble into a network named the locomotor central pattern generator (CPG) (Figure 2d) [3,5]. The CPG drives rhythmic motor pool activity, alternating between left and right limbs, as well as between flexor and extensor muscles, producing a crude stepping pattern independent of sensory inputs [13]. The CPG comprises a variety of developmentally distinct classes of neurons identified through lineage tracing studies (Figure 3a–d) [3]. Manipulation of each ventral interneuron class has revealed a highly modular functional organization [3]. For example, V2a interneurons are excitatory, project ipsilaterally, and express the gene *Chx10*. Ablation of V2a interneurons does not stop or randomize the CPG, instead it disrupts high speed left–right alternation [14,15]. Many of the molecularly defined

Figure 2

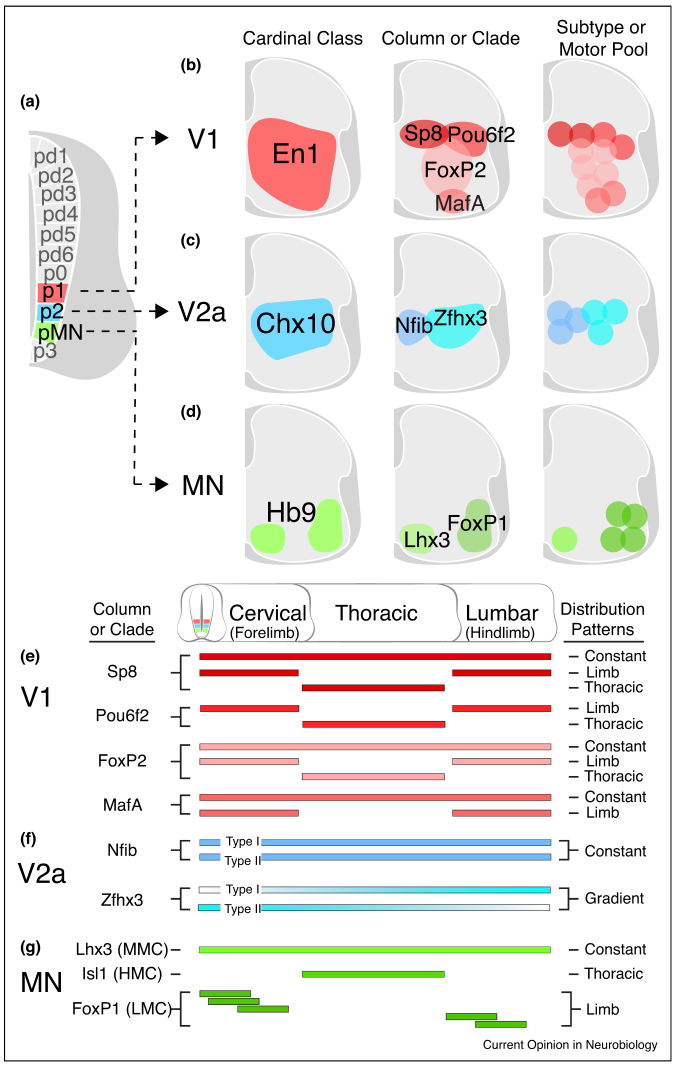


Spinal cord regions and cell types.
(a) Spinal regions and corresponding Rexed laminae.
(b) Examples of molecularly defined cell types located in each region. In some cases, the gene of interest is also expressed in other spinal regions. Example dorsal cell types are RORα, GRP, and NPY expressing neurons [4,9,52–54]. Ventral cell types include En1, Chx10, and Hb9 expressing neurons [2,32••,34••]. Gad2 and Satb2 expressing neurons are intermediate spinal cord cell types [19,22•,26–28].
(c) Exteroceptive sensory fibers terminate in the dorsal cord in a topographic fashion [4,7,8]. Noxious sensory afferents primarily terminate within laminae I–II. Low threshold mechanoreceptors terminate within laminae II–IV of the spinal cord.
(d) Motor neurons are organized into columns and pools which reflect a musculotopic map [10–12]. Lumbar ventral interneurons form a network named the locomotor central pattern generator (CPG), which rhythmically excites motor neurons to generate locomotion [3,13].
(e) Many intermediate interneurons are monosynaptically connected to motor neurons [19,21]. Stimulation of intermediate premotor neurons evokes synergistic activity in multiple motor pools, thus these neurons are designated motor synergy encoders (MSE) [19]. The intermediate spinal cord receives a variety of sensory and descending inputs. Dorsal interneurons relay exteroceptive information onto intermediate spinal interneurons [20]. The corticospinal tract and proprioceptive afferents also densely terminate in the intermediate spinal cord [19,21]. Proprioceptive afferents also innervate motor neurons and subsets of ventral interneurons.

ventral classes of interneurons in the lumbar spinal cord are also present in other segments, where they support motor behaviors such as breathing and reaching [16–18].

The intermediate spinal cord is a nodal point, receiving convergent input from proprioceptive, exteroceptive, and corticospinal neurons [19–21]. Subsets of intermediate neurons also project onto ventral CPG interneurons and directly onto motor neurons (Figure 2e) [19,22•]. Stimulation of intermediate premotor neurons, termed motor synergy encoders (MSE), evokes activation of multiple motor pools [19]. This may serve to coordinate the use of synergistic limb muscles for complex movements [19,23]. While the ventral spinal cord is pivotal for generating rhythmic motor patterns, the confluence of incoming sensory modalities allows the intermediate spinal cord to fine tune motor actions. Intermediate spinal neurons guide the movements necessary to withdraw the limb from sources of painful stimuli [20]. Recent studies have begun to identify and manipulate molecularly defined neuron populations enriched in the intermediate cord, such as Satb2, Gad2, and RORβ expressing interneurons [22•,24,25•,26–28]. Conditional deletion of *Satb2* in the spinal cord results in a hyperflexion response during the

Figure 3



Molecular organization of spinal neurons.
(a) During embryonic development, spinal interneurons are derived from 13 progenitor domains (including the late born dILa and dILb domains). Highlighted are the pMN, p1, and p2 domains. After neurogenesis, cells migrate to their final settling positions [2].
(b) The p1 domain generates V1 interneurons, which express En1. V1 interneurons settle throughout the ventral horn. The majority of V1 interneurons can be divided into 4 clades, expressing either Sp8, Pou6f2, FoxP2, or MafA. V1 clades can be further divided into many subtypes based on combinatorial expression of additional transcription factors. These additional transcriptional divisions often correspond to spatial divisions as well [32••].
(c) The p2 domain generates V2a–V2d interneurons [2,55]. V2a interneurons are divided into a medial and lateral column based on Nfib and Zfhx3 expression. Each column comprises multiple transcriptionally distinct subtypes; however, the spatial locations of these subtypes have yet to be examined in detail [34••].
(d) The pMN domain gives rise to motor neurons, which express Hb9 and settle in the ventral spinal cord. Motor neurons are organized into

limb withdrawal reflex. In general, it has been remarkable that targeted perturbations of spinal interneurons cause discrete functional phenotypes rather than an entire breakdown of motor control. One interpretation is that cell types are organized in modular systems within the spinal cord, rather than having broadly distributed functionality.

Hierarchical divisions of spinal neuron types

Developmental studies have identified 13 neural progenitor populations (i.e. lineages) that produce distinct cardinal classes of spinal neurons (Figure 3a) [2]. Analysis of these lineages has revealed that neurons arising from a common progenitor share particular features, often including neurotransmitter, settling location, and axonal projection pattern. While developmental origin offers a convenient way to organize spinal neurons into coherent groups, these lineage-defined classes are still rather broad cohorts of heterogeneous cells. The neural diversity arising from a single progenitor population is best understood for motor neurons, generated from pMN progenitors (Figure 3a,d) [12]. Motor neurons are organized hierarchically. As a first division, motor neurons are arranged into separate columns which each target a different peripheral structure such as limb muscle, axial muscle, or sympathetic ganglia. Within each column, somatic motor neurons form pools, each with a unique muscle target. Molecular studies have uncovered transcriptional codes that mark each motor column (e.g. LIM-Hd factors) and label individual motor pools (e.g. Hox and ETS factors) [11,12].

Extensive heterogeneity within interneuron classes has also been observed. A variety of molecular markers such as peptides and their receptors, calcium binding proteins, and transcription factors further divide interneuron classes into subtypes. In some cases, these molecular subtypes have been tied to specialized aspects of circuitry and function [1–4]. For example, Renshaw cells are a type of inhibitory neuron which receive input from motor neurons and in turn project on to motor neurons (Figure 4a) [29]. This circuit configuration allows Renshaw cells to provide feedback inhibition to motor neurons. Renshaw cells express Calbindin and are a subtype of V1 interneurons, a large ventral inhibitory class which express the gene *En1* (Figure 3b) [30,31,32••].

Recent studies have used transcriptional profiling to examine the fine-grained heterogeneity among ventral spinal interneuron classes [32••,34••,35•,36]. For V1 interneurons, transcriptional diversity assayed by 19 transcription factors correlated with differing position, electrophysiological properties, and input connectivity [32••]. The majority of V1 interneurons are organized into four non-overlapping clades defined by Sp8, MafA, FoxP2, and Pou6f2 expression [32••,33] (Figure 3b). Each clade can be further divided, resulting in ~50 subtypes of V1 interneurons based on their combinatorial expression of transcription factors. Likewise, considerable diversity was also demonstrated within V2a interneurons, with differentially expressed molecular markers corresponding to spatial location, projection targets, and timing of neurogenesis [34••]. Single cell RNA-sequencing revealed that V2a interneurons are divided into medial and lateral columns based on Nfib and Zfhx3 expression (Figure 3c). Additional molecular subtypes within each V2a columnar population were also found. A theme that has emerged for each interneuron population is the hierarchical organization of neuronal types into increasingly specialized cell groups, analogous to the way motor columns are divided into motor pools. While the function of each interneuron subtype remains poorly understood, elegant studies have begun to combine single cell sequencing and behavior to detect subsets of interneurons associated with specific sensorimotor responses [35•,37•]. Functionally targeting the discrete subtypes of V1 and V2a interneurons will help to define the role of these smaller neuronal units in motor control.

Rostrocaudal position as an additional axis of cellular diversity

Motor neuron columns are organized segmentally in registration with their peripheral muscle targets (Figure 3g). There is also increasing evidence for segmental specialization of interneurons. A recent study examined V1 molecular diversity in the thoracic spinal

(Figure 3 Legend Continued) columns. While all motor neurons initially express Lhx3, only the MMC (Medial motor column) maintains its expression. The LMC (Lateral motor column) expresses FoxP1. Within each column, motor neurons can be further divided into motor pools, each of which is spatially clustered and has a unique muscle target [10–12].

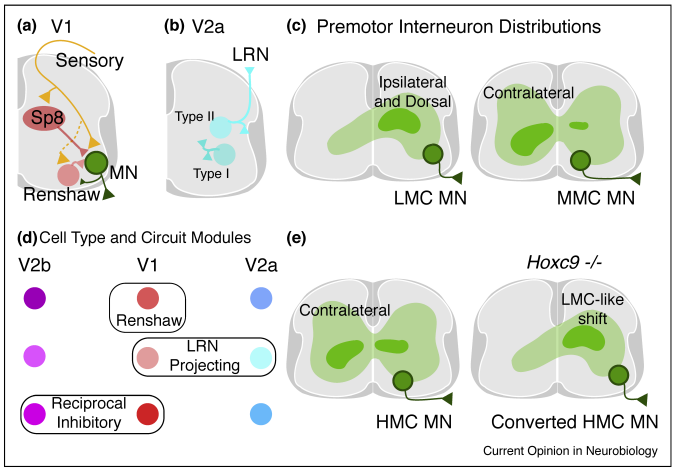
(e–g) Categories of neurons based on their rostrocaudal distribution. Constant: a population of neurons which are present throughout the length of the spinal cord. Limb: neurons which reside in the cervical and lumbar cord. Thoracic: neurons which are located in the thoracic cord. Gradient: neurons that are arrayed in a gradient along the cord.

(e) V1 interneuron clades are preserved across the rostrocaudal axis. However, V1 subtypes specific to limb segments or thoracic segments can be identified based on the expression of two transcription factors [38••].

(f) V2a columns span the rostrocaudal axis. The composition of each column is a combination of Type I V2a interneurons (which maintain Chx10 expression) and Type II V2a interneurons (which downregulate Chx10). The ratio of the two types remains constant in the medial column. In the lateral column, the ratio is organized in a gradient manner which is dependent on spinal segment. Cervical segments are composed of primarily Type II V2a interneurons, while lumbar segments are primarily Type I V2a interneurons [34••].

(g) The MMC, HMC (Hypaxial motor column), and LMC synapse onto axial, intercostal, and limb muscles, respectively. The MMC spans the spinal cord, while the HMC and LMC are segment specific. Motor pools are segmentally organized as well [10–12]. Example LMC motor pools are shown (MMC and HMC pools are not shown). Motor pools generally span a few segments [10,12].

Figure 4



Specificity in spinal cord circuitry.
(a) Microcircuits in V1 interneurons for the Sp8 clade and Renshaw cells. Sp8 neurons receive proprioceptive input from Gluteus (GL) and Tibialis Anterior (TA) muscles while Renshaw cells only receive input from the GL. Renshaw cells receive input from GL and TA motor neurons while Sp8 neurons do not. Both Sp8 neurons and Renshaw cells synapse onto GL, TA, and intrinsic foot (IF) motor neurons [32••].
(b) Type II V2a interneurons, which downregulate Chx10 during development, are predominately located in cervical segments and project supraspinally to the lateral reticular nucleus (LRN). Type I V2a interneurons, which maintain Chx10 expression, project within the spinal cord [34••].
(c) Spatial distribution of premotor interneurons for different motor neuron column types. LMC (Lateral motor column) neurons predominately receive input from spinal interneurons located ipsilaterally and dorsally. MMC (Medial motor column) neurons receive a greater portion of input from contralaterally located spinal interneurons [19,21,42].
(d) Schematic depicting the relationship between spinal interneuron classes and circuit subtypes. Renshaw cells, which provide feedback inhibition to motor neurons, are a subtype exclusively found in V1 interneurons [49–51]. Subtypes of both V1 and V2a interneurons project to the brainstem lateral reticular nucleus (LRN) [39]. Reciprocal inhibitory neurons receive proprioceptive input from a limb muscle and inhibit the corresponding antagonist motor pool. Subtypes of V1 and V2b interneurons are reciprocal inhibitory neurons [51].
(e) Location of premotor HMC interneurons in the thoracic spinal cord. In *Hoxc9* mutants, HMC neurons are converted into an LMC fate and their premotor interneuron distribution shifts accordingly [41••,42].

cord using the same set of 19 transcription factors initially identified in the lumbar cord. The study revealed V1 thoracic and limb-specific subtypes, as well as subtypes located throughout the spinal cord (Figure 3e) [38••]. Genetic manipulations demonstrated that segment-specific V1 interneuron subtypes were dependent on Hox genes and not dependent on extrinsic cues from segmentally organized motor neurons [38••].

Interestingly, RNA-sequencing of purified V2a interneurons revealed molecular distinctions which corresponded to V2a projection patterns [18,34••,39]. In more rostral segments, a portion of V2a interneurons possess an axon which bifurcates—one branch synapses locally and the other projects supraspinally, including to the lateral reticular nucleus (LRN) in the brainstem (Figure 4b). The ascending branch provides the brain with an efference copy of motor plans, allowing for predictions of the consequences of motor actions [18]. Transcriptional analysis revealed that the canonical V2a marker, *Chx10*, was downregulated in a subset of cells during embryonic development, resulting in Type I V2a neurons which maintain Chx10 expression and Type II V2a neurons which downregulate it. Type II V2a interneurons are primarily the brainstem-projecting population. Type I and Type II V2a neurons formed a counter-gradient along the spinal cord, with the majority of lumbar V2a interneurons being Type I and cervical V2a interneurons being a mix of the two types (Figure 3f). These observations have led to the speculative idea that V2a neurons participate in segment-specific activity using a Type I/Type II ratiometric computation.

These studies demonstrate that interneuron subtypes exhibit rostrocaudal spatial specificity, like their motor pool counterparts. Additionally, spinal cord segments are specialized through both qualitative differences in interneuron subtypes (e.g. V1 interneurons) and quantitative differences in the ratio of interneuron subtypes (e.g. V2a interneurons). The rostrocaudal specificity of interneuron

subtypes likely relates to the functions of each spinal segment. Lumbar segments, which produce CPG activity, are essential for locomotion. Type I V2a neurons, which are enriched in lumbar segments, form extensive connections within the spinal cord (Figure 4b) [34••]. Stimulation of lumbar V2a interneurons drives motor neuron activity more quickly and reliably than stimulation of cervical V2a interneurons [34••]. Cervical segments play a smaller role in locomotion but are also vital for reaching behavior. Accordingly, the cervical spinal cord contains less Type I V2a interneurons but far more Type II V2a interneurons, whose supraspinal projection supports dexterity [18]. Interneuron subtypes present throughout the rostrocaudal axis presumably have broad-use functionality. An example is the V1 subtype Renshaw cells, which are prevalent throughout the spinal cord and provide feedback inhibition to multiple types of motor neurons (Figure 4a) [38••,40]. The identification of molecularly distinct interneuron subtypes with specific distributions in limb segments, thoracic segments, all segments, or in gradients suggests substantial circuit and physiological specialization of spinal interneurons across the spinal cord.

Molecular subtypes and their connectivity

Given the similarities in the hierarchical division of motor neurons and interneurons into motor pools and subtypes, it is intriguing to speculate that interneuron subtypes may be tailored to innervate single motor pools. However, at present there is not a clear indication that interneuron subtypes connect to motor pools in an exclusive relationship. For V1 interneurons, Sp8 clade neurons and Renshaw cells both form synapses onto the Gluteus (GL), Tibialis Anterior (TA), and intrinsic foot (IF) motor pools. Renshaw cells are a subtype of the MafA clade, which indicates that multiple clades can innervate a single motor pool and that the same clade can innervate multiple motor pools (Figure 4a) [32••].

While a variety of interneuron types connect to a single motor pool, the overall spatial distribution of spinal premotor interneurons has a stereotyped pattern [21,41••,42]. Interestingly, a major factor in premotor connectivity is the identity of the motor neuron itself [43]. Limb premotor neurons have distributions concentrated dorsally and ipsilaterally while axial and hypaxial premotor neurons have a tendency to be located contralaterally (Figure 4c,e) [41••,42]. Converting thoracic HMC (Hypaxial motor column) neurons into a LMC (Lateral motor column) identity resulted in a corresponding shift in premotor interneuron distribution (Figure 4e) [41••]. Perturbing motor neuron identity also alters the timing of motor neuron activity during CPG activation. Flexor-extensor motor timing is altered while rhythmicity and left–right alternation is maintained, indicating that motor neuron identity influences some, but not all components of the locomotor CPG [44,45]. Interneurons also play a role in establishing motor circuitry. Deletion of the midline guidance molecule *EphA4* in dorsal interneurons results in aberrant contralateral premotor connections, indicating premotor connectivity is governed by an interplay of presynaptic and postsynaptic factors [46•].

Conclusion

With their unique muscle targets, motor pools have a pleasing simplicity across their features of development, genetics, connectivity, and function. As investigators begin to study spinal interneuron subtypes with equal precision and resolution, the correlations between neuronal features appear comparatively intricate and multidimensional. Differences between interneuron molecular subtypes may reflect a multitude of possible differences including inputs (sensory, descending, or other spinal interneurons), outputs (supraspinal, premotor, or other spinal interneurons), and physiology. The increasing division of neuron subtypes appears to apply to other regions of the central nervous system as well. Recent studies have demonstrated that the corticospinal tract can be divided into many parallel pathways based on cortical regions, which connect topographically onto different sets of spinal interneurons [47•,48].

Despite this complexity, it is likely that principles will emerge governing spinal interneuron identity as a variety of features of identity are cataloged for subtypes across spinal lineages. Developmental lineage often establishes certain neuronal features. For example, all V1 interneurons project ipsilaterally and express inhibitory neurotransmitters. However, additional layers of regulation help specify other aspects of spinal interneuron circuitry and physiology. Renshaw cells are a subtype that arise exclusively from the V1 interneuron lineage, thus other sets of transcription factors likely differentiate the Renshaw cell subtype from other V1 interneuron subtypes (Figure 4d) [30,32••,38••,49,50]. Neuron subtypes that are derived from separate lineages, but share aspects of circuitry or physiology, are potential entry points to uncovering overarching principles of subtype specification. In addition to V2a neurons, a subset of neurons from other lineages such as V1, V3, and dI3 also project supraspinally to the LRN [39]. This raises the possibility that Type I and Type II differences found in V2a interneurons extend to other populations [34••,39]. Comparing the transcriptional profiles of these interneuron subtypes which project to the LRN may reveal a common genetic signature for generating a brainstem-projecting subtype regardless of lineage (Figure 4d). Another example of a specialized circuit-defined interneuron subtype are reciprocal inhibitory neurons. Reciprocal inhibitory neurons receive proprioceptive input from a limb muscle and inhibit the corresponding antagonist motor pool [3]. They prevent unwanted co-contraction of flexor and extensor muscles [51]. Interestingly, populations of reciprocal inhibitory neurons include cells from both the V1 and

V2b classes [51]. Thus, two separate lineages which generate inhibitory interneurons potentially share a genetic program for generating an interneuron input–output pattern (Figure 4d).

Beyond surveying and characterizing spinal interneuron diversity, it is critical to test the functional role of interneuron subtypes. Ablating and silencing spinal interneuron classes has proven to be an effective technique for examining how a circuit functions in the absence of a population of neurons. Additionally, studies which switch or perturb the genetic identity of cells without outright eliminating them are vital to understanding the function of neuronal diversity itself. Genetically converting the identity of one motor column into another type of motor column has revealed many insights into spinal neuron organization and function. Molecular studies in motor neurons initially identified mechanisms guiding motor neuron specification and their axon guidance [11,12]. Recently, motor neuron manipulations have also been used to study the role of motor neuron identity in establishing premotor circuitry and physiology [41••,44,45]. Thus, extending these types of studies to interneuron clades and subtypes will likely prove fruitful. While the role of molecular markers for establishing spinal interneuron lineages has been examined in some detail, less is known about the function of interneuron subtype markers [8]. Manipulating interneuron subtypes could potentially allow investigators to change subtype ratios or flatten subtype diversity altogether. Genetic manipulations may consequently alter spinal circuitry and physiology, providing causal insight into how molecular-identity relates to functional-identity and ultimately how subtypes shape behavior.

Conflict of interest statement

Nothing declared.

Acknowledgements

We would like to thank Ben Temple, Bianca Barriga, Gokhan Senturk, Kelsey Ladt, and Marito Hayashi for helpful comments on the manuscript. P.J.O was supported by the Christopher and Dana Reeve Foundation. S.L.P. is supported as a Howard Hughes Medical Institute Investigator and as a Benjamin H. Lewis chair in neuroscience. Research in the laboratory is supported by funding from the Howard Hughes Medical Institute and the Sol Goldman Charitable Trust.

References and recommended reading

Papers of particular interest, published within the period of review, have been highlighted as:

- • of special interest
- •• of outstanding interest

1. Alaynick WA, Jessell TM, Pfaff SL: **SnapShot: spinal cord development**. *Cell* 2011, **146** 178-178 e171.

2. Lu DC, Niu T, Alaynick WA: **Molecular and cellular development of spinal cord locomotor circuitry**. *Front Mol Neurosci* 2015, **8**:25.

3. Kiehn O: **Decoding the organization of spinal circuits that control locomotion**. *Nat Rev Neurosci* 2016, **17**:224-238.

4. Koch SC, Acton D, Goulding M: **Spinal circuits for touch, pain, and itch**. *Annu Rev Physiol* 2018, **80**:189-217.

5. Gosgnach S, Bikoff JB, Dougherty KJ, El Manira A, Lanuza GM, Zhang Y: **Delineating the diversity of spinal interneurons in locomotor circuits**. *J Neurosci* 2017, **37**:10835-10841.

6. Granmo M, Petersson P, Schouenborg J: **Action-based body maps in the spinal cord emerge from a transitory floating organization**. *J Neurosci* 2008, **28**:5494-5503.

7. Abraira VE, Ginty DD: **The sensory neurons of touch**. *Neuron* 2013, **79**:618-639.

8. Lai HC, Seal RP, Johnson JE: **Making sense out of spinal cord somatosensory development**. *Development* 2016, **143**:3434-3448.

9. Bourane S, Grossmann KS, Britz O, Dalet A, Del Barrio MG, Stam FJ, Garcia-Campmany L, Koch S, Goulding M: **Identification of a spinal circuit for light touch and fine motor control**. *Cell* 2015, **160**:503-515.

10. Romanes GJ: **The motor cell columns of the lumbo-sacral spinal cord of the cat**. *J Comp Neurol* 1951, **94**:313-363.

11. Bonanomi D, Pfaff SL: **Motor axon pathfinding**. *Cold Spring Harb Perspect Biol* 2010, **2**:a001735.

12. Dasen JS, Jessell TM: **Hox networks and the origins of motor neuron diversity**. *Curr Top Dev Biol* 2009, **88**:169-200.

13. Kiehn O: **Locomotor circuits in the mammalian spinal cord**. *Annu Rev Neurosci* 2006, **29**:279-306.

14. Crone SA, Quinlan KA, Zagoraiou L, Droho S, Restrepo CE, Lundfald L, Endo T, Setlak J, Jessell TM, Kiehn O *et al.*: **Genetic ablation of V2a ipsilateral interneurons disrupts left-right locomotor coordination in mammalian spinal cord**. *Neuron* 2008, **60**:70-83.

15. Crone SA, Zhong G, Harris-Warrick R, Sharma K: **In mice lacking V2a interneurons, gait depends on speed of locomotion**. *J Neurosci* 2009, **29**:7098-7109.

16. Francius C, Harris A, Rucchin V, Hendricks TJ, Stam FJ, Barber M, Kurek D, Grosveld FG, Pierani A, Goulding M *et al.*: **Identification of multiple subsets of ventral interneurons and differential distribution along the rostrocaudal axis of the developing spinal cord**. *PLoS One* 2013, **8**:e70325.

17. Romer SH, Seedle K, Turner SM, Li J, Baccei ML, Crone SA: **Accessory respiratory muscles enhance ventilation in ALS model mice and are activated by excitatory V2a neurons**. *Exp Neurol* 2017, **287**:192-204.

18. Azim E, Jiang J, Alstermark B, Jessell TM: **Skilled reaching relies on a V2a propriospinal internal copy circuit**. *Nature* 2014, **508**:357-363.

19. Levine AJ, Hinckley CA, Hilde KL, Driscoll SP, Poon TH, Montgomery JM, Pfaff SL: **Identification of a cellular node for motor control pathways**. *Nat Neurosci* 2014, **17**:586-593.

20. Schouenborg J: **Action-based sensory encoding in spinal sensorimotor circuits**. *Brain Res Rev* 2008, **57**:111-117.

21. Tripodi M, Stepien AE, Arber S: **Motor antagonism exposed by spatial segregation and timing of neurogenesis**. *Nature* 2011, **479**:61-66.

22. • Hilde KL, Levine AJ, Hinckley CA, Hayashi M, Montgomery JM, Gullo M, Driscoll SP, Grosschedl R, Kohwi Y, Kohwi-Shigematsu T *et al.*: **Satb2 is required for the development of a spinal exteroceptive microcircuit that modulates limb position**. *Neuron* 2016, **91**:763-776.
This study characterizes a population of inhibitory interneurons located in the intermediate spinal cord which express Satb2. Deletion of *Satb2* from the interneurons causes the cells to be mispositioned in the spinal cord and form altered sensorimotor reflex circuitry.

23. Giszter SF, Mussa-Ivaldi FA, Bizzi E: **Convergent force fields organized in the frog's spinal cord**. *J Neurosci* 1993, **13**:467-491.

24. Fink AJ, Croce KR, Huang ZJ, Abbott LF, Jessell TM, Azim E: **Presynaptic inhibition of spinal sensory feedback ensures smooth movement**. *Nature* 2014, **509**:43-48.

25. • Koch SC, Del Barrio MG, Dalet A, Gatto G, Gunther T, Zhang J, Seidler B, Saur D, Schule R, Goulding M: **RORbeta spinal interneurons gate sensory transmission during locomotion to secure a fluid walking gait**. *Neuron* 2017, **96**:1419-1431 e1415.
The authors demonstrate inhibitory spinal interneurons expressing RORβ play a key role in providing presynaptic inhibition to proprioceptive afferents. Ablation of RORβ interneurons results in a hyperflexion phenotype during locomotion.

26. Wildner H, Das Gupta R, Brohl D, Heppenstall PA, Zeilhofer HU, Birchmeier C: **Genome-wide expression analysis of Ptf1a- and Ascl1-deficient mice reveals new markers for distinct dorsal horn interneuron populations contributing to nociceptive reflex plasticity**. *J Neurosci* 2013, **33**:7299-7307.

27. Zhang J, Weinrich JAP, Russ JB, Comer JD, Bommareddy PK, DiCasoli RJ, Wright CVE, Li Y, van Roessel PJ, Kaltschmidt JA: **A role for dystonia-associated genes in spinal GABAergic interneuron circuitry**. *Cell Rep* 2017, **21**:666-678.

28. Betley JN, Wright CV, Kawaguchi Y, Erdelyi F, Szabo G, Jessell TM, Kaltschmidt JA: **Stringent specificity in the construction of a GABAergic presynaptic inhibitory circuit**. *Cell* 2009, **139**:161-174.

29. Renshaw B: **Influence of discharge of motoneurons upon excitation of neighboring motoneurons**. *J Neurophysiol* 1941, **4**:167-183.

30. Stam FJ, Hendricks TJ, Zhang J, Geiman EJ, Francius C, Labosky PA, Clotman F, Goulding M: **Renshaw cell interneuron specialization is controlled by a temporally restricted transcription factor program**. *Development* 2012, **139**:179-190.

31. Carr PA, Alvarez FJ, Leman EA, Fyffe RE: **Calbindin D28k expression in immunohistochemically identified Renshaw cells**. *Neuroreport* 1998, **9**:2657-2661.

32. •• Bikoff JB, Gabitto MI, Rivard AF, Drobac E, Machado TA, Miri A, Brenner-Morton S, Famojure E, Diaz C, Alvarez FJ *et al.*: **Spinal inhibitory interneuron diversity delineates variant motor microcircuits**. *Cell* 2016, **165**:207-219.
This study surveys subtype diversity in V1 interneurons. Subtypes, defined by differential expression of transcription factors, settle in distinct locations in the spinal cord and form specialized circuits.

33. Gabitto MI, Pakman A, Bikoff JB, Abbott LF, Jessell TM, Paninski L: **Bayesian sparse regression analysis documents the diversity of spinal inhibitory interneurons**. *Cell* 2016, **165**:220-233.

34. •• Hayashi M, Hinckley CA, Driscoll SP, Moore NJ, Levine AJ, Hilde KL, Sharma K, Pfaff SL: **Graded arrays of spinal and supraspinal V2a interneuron subtypes underlie forelimb and hindlimb motor control**. *Neuron* 2018, **97**:869-884 e865.
The authors explore how V2a interneurons are specialized across the rostrocaudal axis to support hindlimb and forelimb behaviors. They identify two subtypes of V2a interneurons, the first subtype is enriched in lumbar segments and supports locomotion, the second subtype is enriched in cervical segments and projects supraspinally to support dexterous movement.

35. • Sathyamurthy A, Johnson KR, Matson KJE, Dobrott CI, Li L, Ryba AR, Bergman TB, Kelly MC, Kelley MW, Levine AJ: **Massively parallel single nucleus transcriptional profiling defines spinal cord neurons and their activity during behavior**. *Cell Rep* 2018, **22**:2216-2225.
In this study, the authors use single nucleus RNA-seq in the adult mouse spinal cord to identify transcriptionally distinct groups of neurons and assess their activity during different sensorimotor behaviors. During rotarod and formalin injection behavioral assays, different sets of neurons throughout the spinal cord are activated.

36. Delile J, Rayon T, Melchionda M, Edwards A, Briscoe J, Sagner A: **Single cell transcriptomics reveals spatial and temporal dynamics of gene expression in the developing mouse spinal cord**. *Development* 2019:146 http://dx.doi.org/10.1242/dev.173807.

37. • Haring M, Zeisel A, Hochgerner H, Rinwa P, Jakobsson JET, Lonnerberg P, La Manno G, Sharma N, Borgius L, Kiehn O *et al.*: **Neuronal atlas of the dorsal horn defines its architecture and links sensory input to transcriptional cell types**. *Nat Neurosci* 2018, **21**:869-880.
This study characterizes cellular diversity in the dorsal horn using single cell RNA-seq. Excitatory and inhibitory neurons can be hierarchically organized, with subtypes demonstrating enrichment in specific dorsal laminae. Using the immediate early gene *Arc*, the authors identify neuronal subtypes that are activated during noxious heat or cold exposure.

38. •• Sweeney LB, Bikoff JB, Gabitto MI, Brenner-Morton S, Baek M, Yang JH, Tabak EG, Dasen JS, Kintner CR, Jessell TM: **Origin and segmental diversity of spinal inhibitory interneurons**. *Neuron* 2018, **97**:341-355 e343.
This study examines V1 subtype diversity across the rostrocaudal axis. Limb and thoracic-specific subtypes were identified. The authors show development of these subtypes were not dependent on cues from motor neurons.

39. Pivetta C, Esposito MS, Sigrist M, Arber S: **Motor-circuit communication matrix from spinal cord to brainstem neurons revealed by developmental origin**. *Cell* 2014, **156**:537-548.

40. Saywell SA, Ford TW, Kirkwood PA: **Axonal projections of Renshaw cells in the thoracic spinal cord**. *Physiol Rep* 2013, **1**:e00161.

41. •• Baek M, Pivetta C, Liu JP, Arber S, Dasen JS: **Columnar-intrinsic cues shape premotor input specificity in locomotor circuits**. *Cell Rep* 2017, **21**:867-877.
This study examines the role of motor neuron identity in shaping their sensory and interneuron inputs. Using *Hoxc9* mutants to convert the columnar identity of HMC neurons to a LMC identity, the authors demonstrate that presynaptic input to motor neurons is converted as well.

42. Goetz C, Pivetta C, Arber S: **Distinct limb and trunk premotor circuits establish laterality in the spinal cord**. *Neuron* 2015, **85**:131-144.

43. Dasen JS: **Master or servant? emerging roles for motor neuron subtypes in the construction and evolution of locomotor circuits**. *Curr Opin Neurobiol* 2017, **42**:25-32.

44. Hinckley CA, Alaynick WA, Gallarda BW, Hayashi M, Hilde KL, Driscoll SP, Dekker JD, Tucker HO, Sharpee TO, Pfaff SL: **Spinal locomotor circuits develop using hierarchical rules based on motorneuron position and identity**. *Neuron* 2015, **87**:1008-1021.

45. Machado TA, Pnevmatikakis E, Paninski L, Jessell TM, Miri A: **Primacy of flexor locomotor pattern revealed by ancestral reversion of motor neuron identity**. *Cell* 2015, **162**:338-350.

46. • Satoh D, Pudenz C, Arber S: **Context-dependent gait choice elicited by EphA4 mutation in Lbx1 spinal interneurons**. *Neuron* 2016, **89**:1046-1058.
By deleting the EphA4 axon guidance receptor from Lbx1 expressing interneurons, the authors demonstrate that dorsal premotor interneurons form bilateral premotor connections instead of ipsilateral connections. This ectopic bilateral wiring corresponds with an increase of left–right limb gait synchrony during swimming and airstepping.

47. • Wang X, Liu Y, Li X, Zhang Z, Yang H, Zhang Y, Williams PR, Alwahab NSA, Kapur K, Yu B *et al.*: **Deconstruction of corticospinal circuits for goal-directed motor skills**. *Cell* 2017, **171**:440-455 e414.
Using viral tracing and genetically encoded calcium indicators, the authors examine the activity of corticospinal neurons during a food-pellet retrieval task. Populations of corticospinal neurons are activated sequentially throughout the task and project to distinct premotor populations within the spinal cord.

48. Ueno M, Nakamura Y, Li J, Gu Z, Niehaus J, Maezawa M, Crone SA, Goulding M, Baccei ML, Yoshida Y: **Corticospinal circuits from the sensory and motor cortices differentially regulate skilled movements through distinct spinal interneurons**. *Cell Rep* 2018, **23**:1286-1300 e1287.

49. Sapir T, Geiman EJ, Wang Z, Velasquez T, Mitsui S, Yoshihara Y, Frank E, Alvarez FJ, Goulding M: **Pax6 and engrailed 1 regulate two distinct aspects of renshaw cell development**. *J Neurosci* 2004, **24**:1255-1264.

50. Benito-Gonzalez A, Alvarez FJ: **Renshaw cells and Ia inhibitory interneurons are generated at different times from p1 progenitors and differentiate shortly after exiting the cell cycle**. *J Neurosci* 2012, **32**:1156-1170.

51. Zhang J, Lanuza GM, Britz O, Wang Z, Siembab VC, Zhang Y, Velasquez T, Alvarez FJ, Frank E, Goulding M: **V1 and v2b interneurons secure the alternating flexor-extensor motor activity mice require for limbed locomotion**. *Neuron* 2014, **82**:138-150.

52. Bourane S, Duan B, Koch SC, Dalet A, Britz O, Garcia-Campmany L, Kim E, Cheng L, Ghosh A, Ma Q *et al.*: **Gate control of mechanical itch by a subpopulation of spinal cord interneurons**. *Science* 2015, **350**:550-554.

53. Mishra SK, Hoon MA: **The cells and circuitry for itch responses in mice**. *Science* 2013, **340**:968-971.

54. Sun S, Xu Q, Guo C, Guan Y, Liu Q, Dong X: **Leaky gate model: intensity-dependent coding of pain and itch in the spinal cord**. *Neuron* 2017, **93**:840-853 e845.

55. Dougherty KJ, Zagoraiou L, Satoh D, Rozani I, Doobar S, Arber S, Jessell TM, Kiehn O: **Locomotor rhythm generation linked to the output of spinal shox2 excitatory interneurons**. *Neuron* 2013, **80**:920-933.

Acknowledgements

Chapter 1, in full, is a reprint of the review as it appears in: Osseward PJ 2nd, Pfaff SL. Cell type and circuit modules in the spinal cord. Curr Opin Neurobiol. 2019 Jun;56:175-184. doi: 10.1016/j.conb.2019.03.003. Epub 2019 Apr 5. PMID: 30954861. The manuscript was written in collaboration with Samuel L. Pfaff. The authors of this manuscript would like to thank Ben Temple, Bianca Barriga, Gokhan Senturk, Kelsey Ladt, and Marito Hayashi for helpful comments on the manuscript. P.J.O was supported by the Christopher and Dana Reeve Foundation. S.L.P. is supported as a Howard Hughes Medical Institute Investigator and as a Benjamin H. Lewis chair in neuroscience. Research in the laboratory is supported by funding from the Howard Hughes Medical Institute and the Sol Goldman Charitable Trust.

Chapter 2: Conserved genetic signatures parcellate cardinal spinal neuron classes into local and projection subsets

NEURODEVELOPMENT

Conserved genetic signatures parcellate cardinal spinal neuron classes into local and projection subsets

Peter J. Osseward II[1,2]†, Neal D. Amin[1]‡, Jeffrey D. Moore[3], Benjamin A. Temple[1,2], Bianca K. Barriga[1,4], Lukas C. Bachmann[1], Fernando Beltran Jr.[1], Miriam Gullo[1], Robert C. Clark[1], Shawn P. Driscoll[1], Samuel L. Pfaff[1]*, Marito Hayashi[1]†§

Motor and sensory functions of the spinal cord are mediated by populations of cardinal neurons arising from separate progenitor lineages. However, each cardinal class is composed of multiple neuronal types with distinct molecular, anatomical, and physiological features, and there is not a unifying logic that systematically accounts for this diversity. We reasoned that the expansion of new neuronal types occurred in a stepwise manner analogous to animal speciation, and we explored this by defining transcriptomic relationships using a top-down approach. We uncovered orderly genetic tiers that sequentially divide groups of neurons by their motor-sensory, local-long range, and excitatory-inhibitory features. The genetic signatures defining neuronal projections were tied to neuronal birth date and conserved across cardinal classes. Thus, the intersection of cardinal class with projection markers provides a unifying taxonomic solution for systematically identifying distinct functional subsets.

From a functional perspective, spinal neurons can be divided along several axes, including motor-sensory, excitatory-inhibitory, and locally connected neurons for intracord processing versus projection neurons for communication with the brain (*1*–*6*). Neuron heterogeneity is often characterized on the basis of landmarks such as their neurotransmitter type, connectivity, cytoarchitecture, morphology, physiology, developmental origin, and genetic profile (*7*). In the spinal cord, separate cardinal neuron classes arise from molecularly distinct progenitor cells arrayed along the dorsoventral axis of the neural tube (*2*, *8*). Neurons within each cardinal class share properties such as the same neurotransmitter identity and have been targeted in functional studies (*1*, *2*). However, it is increasingly apparent that each cardinal class is itself composed of heterogeneous populations of neuron types, impeding a detailed understanding how spinal circuits function (*9*–*13*). We sought to determine whether there was a coherent logic for spinal neuron diversification in mice that could be used to systematically describe the heterogeneity within all the cardinal classes.

[1]Gene Expression Laboratory, Salk Institute for Biological Studies, La Jolla, CA 92037, USA. [2]Neurosciences Graduate Program, University of California, San Diego, 9500 Gilman Drive, La Jolla, CA 92037, USA. [3]Howard Hughes Medical Institute, Department of Molecular and Cellular Biology, Center for Brain Science, Harvard University, Cambridge, MA, USA. [4]Biological Sciences Graduate Program, University of California, San Diego, 9500 Gilman Drive, La Jolla, CA 92037, USA.
†These authors contributed equally to this work.
‡Present address: Department of Psychiatry and Behavioral Sciences, Stanford University, Stanford, CA 94305, USA. §Present address: Howard Hughes Medical Institute, Department of Cell Biology, Harvard Medical School, Boston, MA 02115, USA.
*Corresponding author. Email: pfaff@salk.edu

One perspective of neuronal diversity is that it arose through evolution in order to expand neural functions (*14*–*16*). In this view, primitive neuron types served as the precursors for more specialized subtypes, leading to the prediction that individual neuronal attributes may have emerged in a stepwise fashion with ordered hierarchical relationships (*14*, *16*, *17*). This analogy to animal speciation prompted us to investigate whether molecular and cellular correlates for this type of stepwise diversification could be detected among large heterogeneous populations of spinal neurons. Thus, rather than focusing on fine-grained molecular differences that may or may not correspond to functional cellular features, we used a top-down approach to identify the transcriptomic signatures linked to the emergence of different neuronal types. At each branch point in our established hierarchy, we defined the molecular, developmental, cytoarchitectural, neurotransmitter, and connectivity properties of the neurons. Our analysis uncovered molecular markers for local and projection neurons regardless of cardinal class or neurotransmitter. By combining markers for cardinal classes with those for conserved genetic signatures for projection status, we established a simple combinatorial matrix that systematically identified discrete subsets of spinal neurons.

Group-E and -H neurons divide the spinal motor-sensory circuitry

To enrich for neurons while minimizing technical and biological variability, we genetically labeled glutamatergic and γ-aminobutyric acid (GABA)–ergic neurons in postnatal day 0 (P0) mice, sorted lumbar spinal neurons separately, pooled them, and performed single-cell RNA-sequencing (scRNA-seq) on the combined sample (Fig. 1A and fig. S1). At P0, spinal neurons have been generated and the basic functional features of adult spinal circuitry have been established, but expression persists for many developmental markers of neuronal subtype diversity (*2*, *9*, *10*, *18*). Using marker analyses, 6743 cells passed quality control and were identified as neurons (Fig. 1A). Glutamatergic and GABAergic neurons largely segregated in the uniform manifold approximation and projection (UMAP) space, and a graph-based comparison using the highly variable genes conservatively identified 45 distinct clusters (Fig. 1, B and C). As expected, many of these clusters were enriched for genes that have been previously identified as marker genes for cardinal classes (Fig. 1D and table S1) (*1*, *2*).

To explore the conserved relationships that exist among lumbar spinal neurons, we developed a divisive clustering pipeline using the *k*-means algorithm to split spinal neurons into pairwise groups iteratively on the basis of their overall transcriptional composition (Fig. 1, E and F). We focused on transcription factors because they regulate neuronal identity and function (*2*, *14*, *15*). We anticipated that this approach would first reveal the glutamatergic and GABAergic neurotransmitter division in the cell population because it is such a prominent phenotypic difference, and the two cell types were isolated from separate litters. However, the neuronal populations split along an axis unrelated to neurotransmitter identity (Fig. 1, B and G) (*11*, *19*). Differential gene expression of the first division indicated that transcription factor Ebf1 is highly expressed in a cell group we defined as group-E neurons, whereas transcription factor Hoxc10 is enriched in a different group we termed group-H neurons (Fig. 1G). Histological analysis of Ebf1$^+$ and Hoxc10$^+$ neurons identified a spatial division of these groups (Fig. 2, A and B, and fig. S2). Ebf1$^+$ neurons were located in laminae I to III of the superficial dorsal horn, corresponding to the site where many exteroceptive sensory inputs terminate. By contrast, Hoxc10$^+$ neurons were predominantly located in laminae IV to X, areas involved in proprioception and motor control (*3*, *4*). Although group-E and group-H neurons broadly differ in motor-sensory functions associated with their positions, both types are composed of a mixture of glutamatergic and GABAergic neurons (Fig. 1, B and G, and fig. S3) (*3*, *4*).

Group-N and -Z neurons are arrayed along the mediolateral axis of the spinal cord

Using the hierarchical-divisive strategy outlined above (Fig. 1F), we further split the group-E neurons into two subgroups and found that this division identifies glutamatergic-related and GABAergic-related genes and their corresponding neurons (Fig. 1, B and H) (*2*, *4*). Division of the group-H population produced

Downloaded from http://science.sciencemag.org/ on April 22, 2021

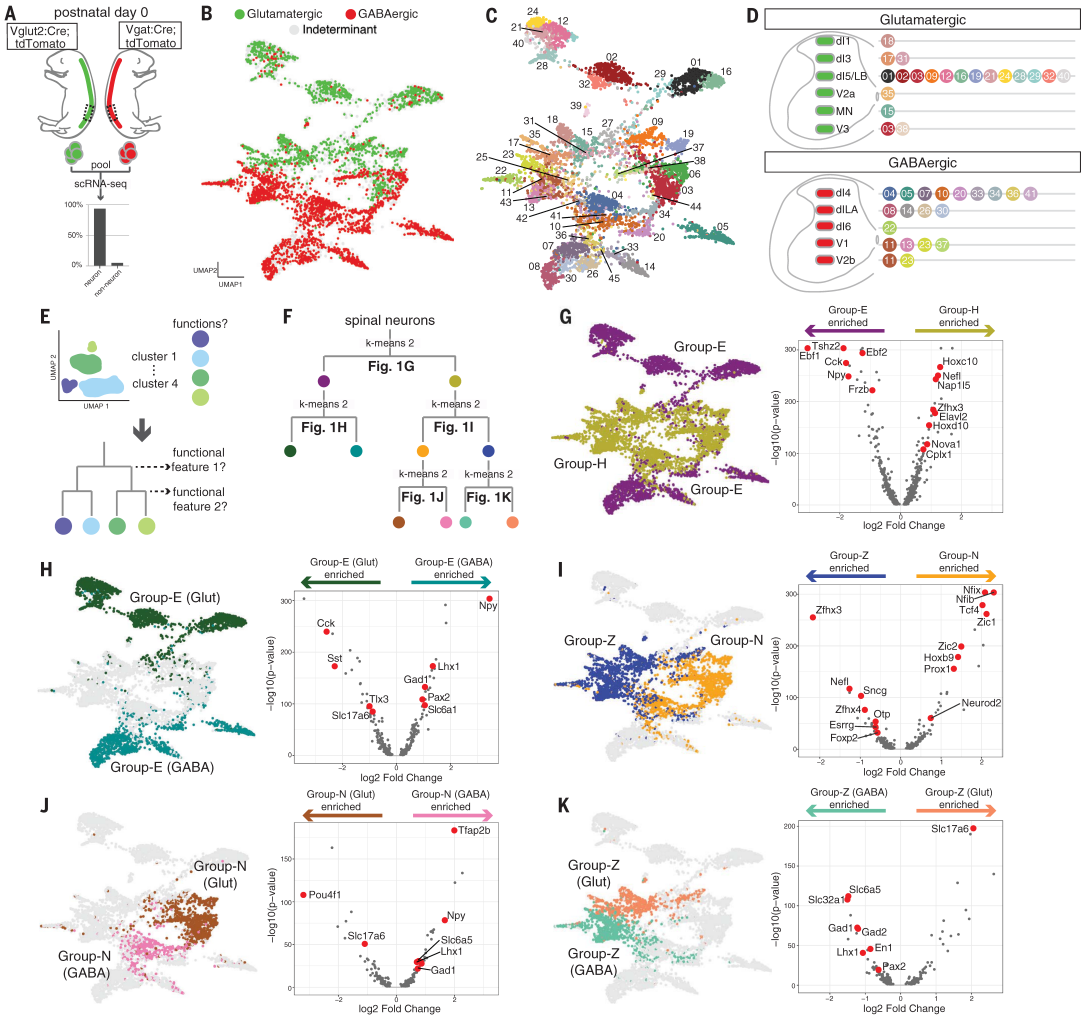


Fig. 1. scRNA-seq identifies relationships among groups of spinal neurons. (**A**) Lumbar segments from P0 Vglut2:Cre; Ai14 and Vgat:Cre; Ai14 neonates (two females and one male from each litter) were microdissected. tdTomato$^+$ cells were sorted and pooled as one sample before scRNA-seq. Using marker analyses and quality control measures, 6743 cells were identified as neurons (94.4% of total cells detected). These neurons had 1012 median genes per cell and 1606 median unique molecular identifiers (UMIs) per cell. (**B**) UMAP visualization of neurons identifies that glutamatergic neurons and GABAergic neurons largely segregate in UMAP space. (**C**) Forty-five identified clusters are color coded in UMAP space. (**D**) Colored dots with numbers correspond to clusters from Fig. 1C. As expected, clusters corresponded to known cardinal neuron classes, defined by their marker expression. V1 and V2b markers were found in the same clusters (*12*). Several clusters are not shown because they were not enriched for obvious cardinal class marker genes (table S1). (**E**) Schematic outlining methods to identify neuronal subtypes. (Top) Dimensionality reduction tools can be used to define the maximum number of genetically distinct clusters. Functions must be independently defined for each cluster. (Bottom) Hierarchical comparisons of neuronal populations can be used to define branch points. The functional differences at the branch points can be used to identify increasingly more specific neuronal attributes linked to function. (**F**) Schematic of analysis used to investigate the higher-order relationships across spinal neuron populations conducted with iterative *k*-means 2 divisive clustering. Data for each color-coded division are indicated for (G) to (K). (**G** to **K**) (Left) UMAP color coded according to identified division. (Right) Volcano plot depicting differentially expressed genes across each *k*-mean division. [(G) and (I)] Further analysis of highlighted genes are available in Fig. 2 and fig. S2. [(H), (J), and (K)] Glutamatergic- and GABAergic-related genes are highlighted. (G) Group-E: 3360 cells, Jaccard similarity [across bootstraps (supplementary materials, materials and methods)] = 0.960; group-H: 3383 cells, Jaccard similarity = 0.959. (H) Group-E (Glut): 1851 cells, Jaccard similarity = 0.960; group-E (GABA): 1509 cells, Jaccard similarity = 0.922. (I) Group-Z: 1707 cells, Jaccard similarity = 0.867; group-N: 1676 cells, Jaccard similarity = 0.809. (J) Group-N (Glut): 1040 cells, Jaccard similarity = 0.791; group-N (GABA): 636 cells, Jaccard similarity = 0.613. (K) Group-Z (Glut): 768 cells, Jaccard similarity = 0.769; group-Z (GABA): 939 cells, Jaccard similarity = 0.760.

Downloaded from http://science.sciencemag.org/ on April 22, 2021

a different result. Rather than splitting group-H neurons into glutamatergic and GABAergic cell populations, we found a subgroup of neurons enriched for Nfib, NeuroD2, and Prox1 (designated group-N) and a separate subgroup enriched for Zfhx3, Zfhx4, and FoxP2 (group-Z) (Fig. 1I and table S2). Histological analysis found that these two sets of genes spatially divided the spinal cord into large wedge patterns: group-N cells located dorsomedially and group-Z cells positioned ventrolaterally (Fig. 2, C and D, and fig. S4). Group-N and group-Z neurons occasionally intermingle (Fig. 2, C to H, and fig. S5), but few cells coexpressed markers for both group-N and group-Z neurons (Fig. 2, E and G, and fig. S5). Although group-N and group-Z neurons are defined by gene sets, we found that NeuroD2 and Zfhx3 were representative markers of group-N and -Z neurons, respectively (Figs. 1I and 2, C and D; and figs. S2 to S5). Our sequencing was conducted on cells from the lumbar spinal cord, but we found that NeuroD2 and Zfhx3 labeled neurons in the same mediolateral pattern along the entire rostrocaudal axis of the cord (figs. S6 and S7). Further *k*-means splitting of group-N and -Z neurons resolved the glutamatergic and GABAergic subsets in each population (Fig. 1, J and K, and fig. S3) (*2*, *4*). Our findings unmask a stepwise hierarchy of genetic divisions among spinal neurons with layers that supersede neurotransmitter physiology (Fig. 2H).

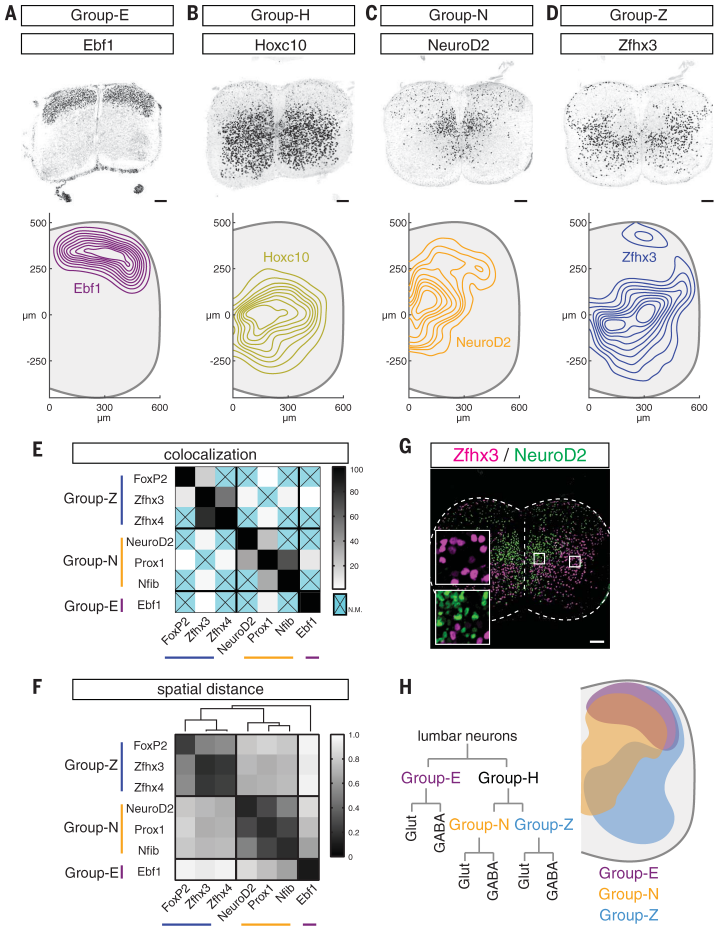


Fig. 2. Branch points in the hierarchical comparisons define spinal neuron groups with discrete locations. (**A** to **D**) (Top) Immunostaining against representative markers for group-E, -H, -N, and -Z neurons in lumbar segments at P0. All images are 20-µm cryosections. Scale bars, 100 µm. (Bottom) Spatial analysis of representative markers displayed on right half of lumbar spinal cord. Contours indicate density of representative markers at the 10th to 90th percentiles. *y* axis = 0 represents the top end of the central canal, and *x* axis = 0 represents the midline. (**E**) Matrix of pairwise mean colocalization rates between group-Z, -N, and -E markers. "N.M." (blue boxes with X) indicates not measured because of antibody incompatibility (figs. S4 and S5). NeuN$^+$ Nfib$^+$ neurons were quantified to exclude Nfib$^+$ glial cells. (**F**) Matrix of pairwise weighted Jaccard distance between group-Z, -N, and -E markers. 1.0, no overlap; 0, complete overlap. Hierarchical clustering dendrogram reveals closer spatial associations among marker genes within each group than between separate groups. (**G**) Immunostaining of Zfhx3 and NeuroD2 in lumbar spinal cord at P0 reveals low incidences of colocalization. Cryosection, 20 µm. Scale bar, 100 µm. This image is a composite of Fig. 2, C and D. (**H**) (Left) Transcriptomic hierarchy of lumbar spinal neurons. (Right) Schematic of spatial enrichments of group-Z, -N, and -E neurons.

Group-N and -Z neurons have distinct birth dates

Although the group-E–group-H division appeared to correspond to neurons involved in exteroception and motor control, respectively, we hypothesized that the group-N and -Z subsets derived from the group-H population might segregate along alternative features. To investigate a possible developmental distinction between group-N and group-Z neurons, we performed scRNA-seq of embryonic day 12.5 (E12.5) spinal cord cells composed of the embryonically defined cardinal cell classes (Fig. 3, A and B; fig. S8; and table S3). The E-H division was not evident at E12.5; however, the group-N and group-Z neuronal populations were detected (Fig. 3, C and D, and figs. S8 and S9). We birth-dated the neurons marked by NeuroD2 and Zfhx3 at P0 using EdU pulses embryonically. The peak of Zfhx3$^+$ neuron birth was at E10.5, whereas the peak of NeuroD2$^+$ neuron generation was later at E13.5 (Fig. 3E and fig. S10). To examine whether group-N and group-Z identity is dependent on neuronal connectivity, we genetically ablated proprioceptive sensory neurons or motor neurons. Despite the absence of sensory and motor neurons, Zfhx3 and NeuroD2 expression patterns were unaltered (fig. S11). Furthermore, we found that Zfhx3 and NeuroD2 expression was maintained in adult spinal neurons (P70), approximating the labeling pattern observed at P0 (Fig. 3F). Taken together, our findings indicate that the group-N and -Z populations have distinct timings of neurogenesis and are present embryonically through adulthood (Fig. 3G).

Group-N and -Z neurons divide each cardinal neuron class into subsets

We set out to understand how group-E, group-N, and group-Z neurons identified here spatially

Downloaded from http://science.sciencemag.org/ on April 22, 2021

and molecularly intersect with the previously characterized cardinal classes. Cre lines labeling the cardinal classes dI1, dI3, dI4/dILA, dI5/dILB, V1, V2a, and V3 were immunostained for Ebf1 (group-E), NeuroD2 (group-N), and Zfhx3 (group-Z) (Fig. 4A). Group-E neurons were found to be restricted to the dI4/dILA and dI5/dILB classes (figs. S12 and S13), whereas all tested cardinal classes were composed of a mixture of both group-N and group-Z neurons derived from the group-H population (Fig. 4, B to F, and figs. S12 and S13). Analysis of E12.5 scRNA-seq data confirmed that the dI2, dI6, and V2b classes also were a mixture of both group-N and group-Z neurons (fig.

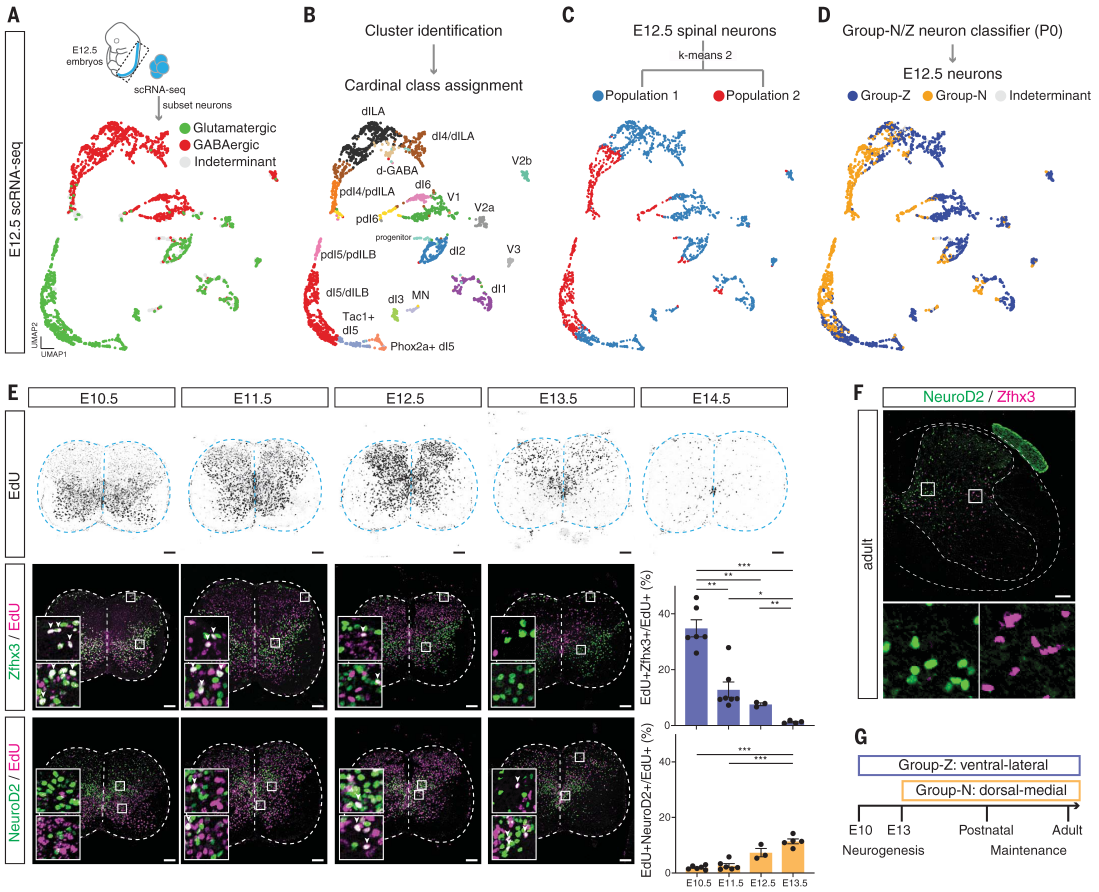


Fig. 3. The group-N and -Z division is linked to neuronal birth date. (**A**) Cells along the entire spinal cord were isolated from two E12.5 embryos from two litters and were subjected to scRNA-seq as separate samples. These datasets were merged post hoc. We bioinformatically identified 2945 neurons, which were selected for further analysis (fig. S8). These neurons had 3566 median genes per cell and 12,189 median UMIs per cell. Glutamatergic and GABAergic neurons are labeled on the UMAP. (**B**) Cardinal classes segregate in UMAP space. Twenty-seven clusters were identified (fig. S8). On the basis of the top 20 differentially expressed genes for each cluster, cardinal classes were identified. Clusters from the same cardinal class were merged (table S3). (**C**) Higher-order groups of spinal neurons were identified with *k*-means 2 divisive clustering (Fig. 1F). Embryonic neurons are color coded according to the first *k*-means 2 division. Population 1: 1971 cells, Jaccard similarity = 0.978; population 2: 974 cells, Jaccard similarity = 0.955. Further divisions are provided in fig. S9. (**D**) The first *k*-means 2 division of embryonic neurons largely corresponded to group-N and group-Z identity established from P0: 79% of population 1 [(C), blue cells] neurons expressed group-Z markers, and 84% of population 2 [(C), red cells] neurons expressed group-N markers. Thus, the *k*-means 2 division identifies group-N and group-Z neurons at an early embryonic stage. (**E**) EdU was injected into multiple pregnant females (E10.5 to E14.5), and lumbar segments were collected from their pups at P0. Representative markers Zfhx3 and NeuroD2 were used to birth date group-Z and group-N neurons, respectively. The peak birth date for group-Z neurons was E10.5, whereas the peak for group-N neurons was E13.5. Each dot represents the colocalization rate for a single animal. Welch one-way analysis of variance (ANOVA) comparing every time point to every other time point, with Dunnett T3 correction for multiple comparisons. $^{*}P \leq 0.05$, $^{**}P \leq 0.01$, $^{***}P \leq 0.001$. Cryosections, 20 μm. Scale bars, 100 μm. (**F**) Immunostaining of Zfhx3 and NeuroD2 in lumbar spinal cord at P70. The mediolateral location and marker expression patterns in adult P70 animals were similar to P0. Cryosection, 25 μm. Scale bar, 100 μm. (**G**) Summary. Group-Z neurons are born before group-N neurons. Molecular markers for both groups are expressed embryonically, postnatally, and into adulthood. Markers for group-Z and group-N neurons are not coexpressed.

Downloaded from http://science.sciencemag.org/ on April 22, 2021

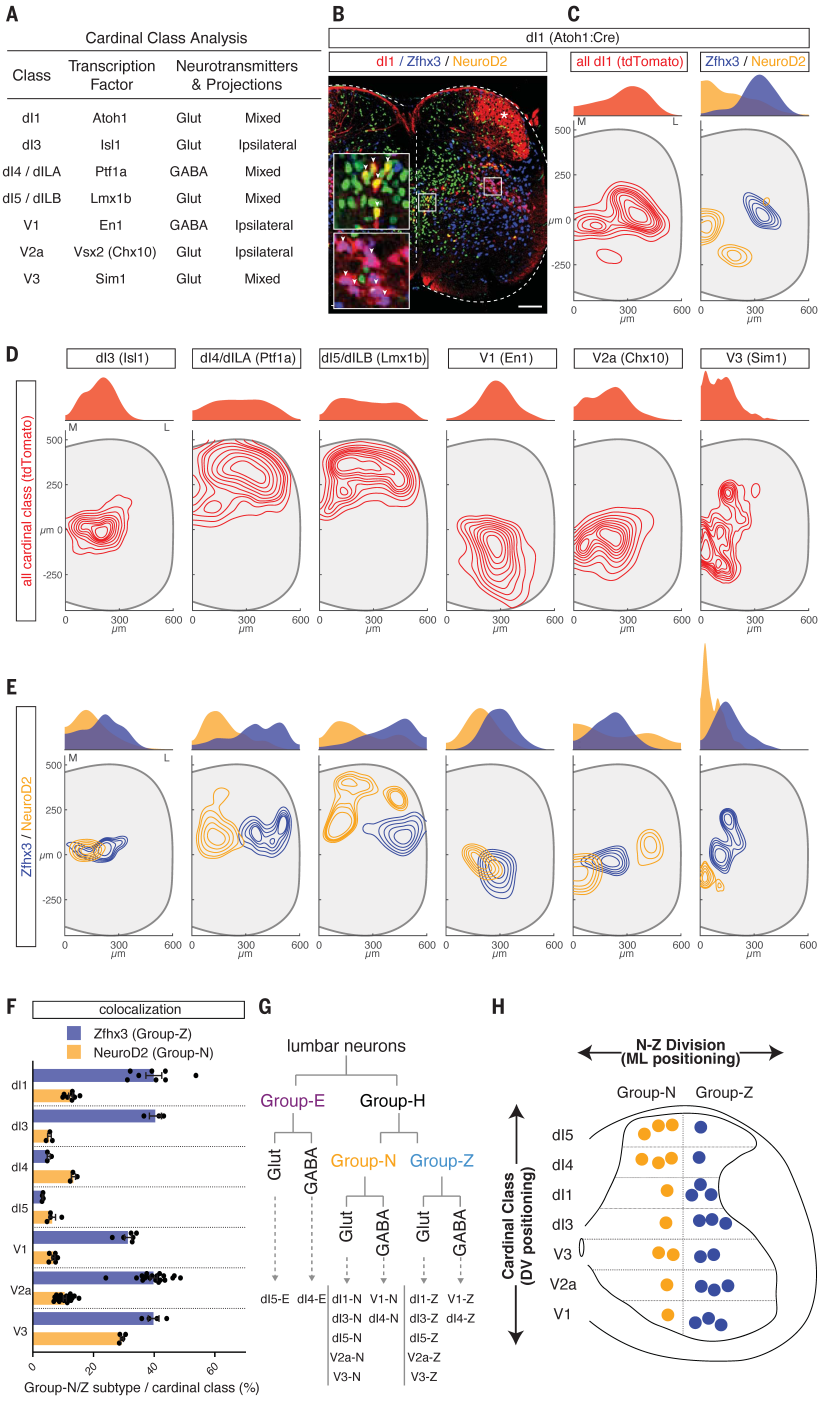


Fig. 4. Each cardinal class is a mixture of both group-N and -Z neurons. (**A**) Summary of mouse lines used to label cardinal classes. Each cardinal class has a characteristic transcription factor expression, neurotransmitter, and axon laterality profile. (**B**) Atoh1:Cre was crossed to a tdTomato reporter to indelibly label dI1 neurons. Immunostaining for NeuroD2 (group-N) and Zfhx3 (group-Z) reveals discrete dI1 populations marked by the two genes. Asterisk in the dorsal horn indicates ectopic sensory fibers from the DRG (*29*). Cryosection, 20 μm. Scale bar, 100 μm. (**C**) (Left) Contours indicate density of dI1 neurons at the 10th to 90th percentiles. Mediolateral density displayed above a two-dimensional contour plot. (Right) Contours indicate densities of group-N and group-Z dI1 neurons at 50th to 90th percentiles. Group-N dI1 neurons were generally located medially, whereas group-Z dI1 neurons were located laterally. (**D**) Contours and mediolateral densities of indicated cardinal classes. Contours indicate density of cardinal class neurons at the 10th to 90th percentiles. Dorsoventral densities are provided in fig. S14. (**E**) Distributions of group-N and group-Z neurons within each cardinal class. Contours indicate density of interneuron subpopulations at the 50th to 90th percentiles. Each cardinal class was split into medial group-N and lateral group-Z neurons. (**F**) Quantification of group-Z and group-N neurons within each cardinal class. Each dot indicates one animal. The ratio of group-N to -Z neurons varies across cardinal classes. (**G**) Summary of the cardinal class types within the hierarchical comparisons of neurons. (**H**) Stylized overview of cell spatial relationships defined by coexpression of cardinal and N-Z markers. Cardinal classes have stereotyped dorsoventral settling positions. Neurons composing each cardinal class are split into medial group-N and lateral group-Z cells.

Downloaded from http://science.sciencemag.org/ on April 22, 2021

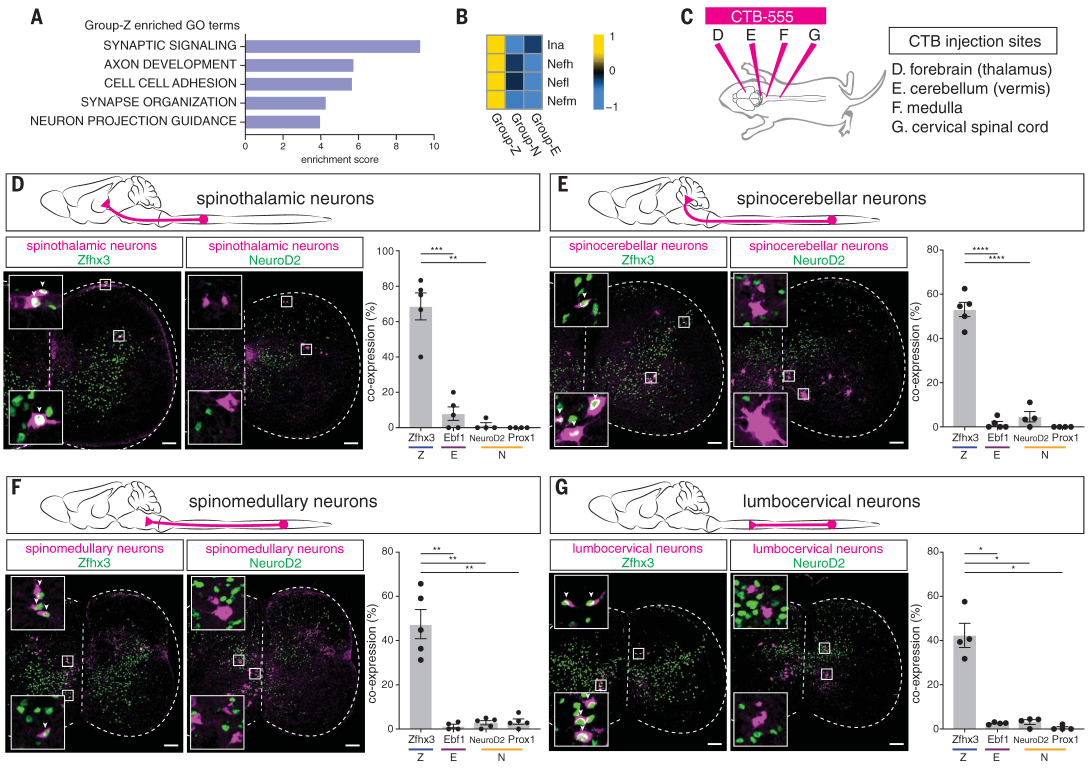


Fig. 5. Projection and long-range neurons express group-Z markers. (**A**) Neuronal morphology-related GO terms are enriched in group-Z compared with group-N neurons (table S4). (**B**) Heatmap of neurofilament genes expressed in spinal neurons showing enrichment in group-Z neurons (log2 scale). (**C**) Schematic of retrograde tracing analysis. CTB was injected into the forebrain (thalamus), cerebellum (vermis), medulla, and cervical spinal cord, respectively, to retrogradely label long-range projection neurons within the spinal cord. Injections were done in neonates, and tissue was collected 4 to 5 days later. (**D** to **G**) Immunostaining against group-Z (Zfhx3), -E (Ebf1), and -N (NeuroD2 and Prox1) markers combined with indicated CTB labeling. White arrowheads indicate group-Z long-range neurons. Each dot on the graph indicates the colocalization rate of one animal. Cryosections, 20 μm. Scale bars, 100 μm. Welch one-way ANOVA comparing Zfhx3 to every other marker, with Dunnett T3 correction for multiple comparisons. *$P \leq 0.05$, **$P \leq 0.01$, ***$P \leq 0.001$. (D) Spinothalamic neurons within cervical segments (region of greatest abundance) expressed group-Z markers. Spinothalamic neurons within lumbar segments are shown in fig. S17. (E) Spinocerebellar neurons within lumbar segments expressed group-Z markers. Additional markers are provided in fig. S18. (F) Spinomedullary neurons within lumbar segments expressed group-Z markers. Additional markers are provided in fig. S19. (G) Cervicolumbar neurons expressed group-Z markers. Additional markers are provided in fig. S20.

S13) (*13*). Moreover, the group-N neurons from each cardinal class were always medial to the group-Z cells (Fig. 4, C to E and H, and fig. S14) (*9*, *10*, *20*). Although each cardinal class contained both group-N and group-Z neurons, the ratio of these types varied within each class (Fig. 4, F and H, and figs. S13 and S15) (*10*, *20*). Group-N and group-Z neurons do not obey cardinal class divisions; rather, all cardinal classes are a mix of group-N and group-Z cells with discrete mediolateral positions. Thus, the group-N–group-Z division is an orthogonal molecular and spatial axis that intersects with cardinal class identity (Fig. 4H).

Local versus long-range projection neuron types underlie the N-Z division

To further understand the cellular features of group-N and group-Z neurons, we explored the connectivity patterns of spinal neurons. We first tested whether the group-N and group-Z neurons represented premotor interneurons, using monosynaptic rabies virus tracing. We found that both the group-N and group-Z populations contained ipsi- and contralateral premotor neurons (fig. S16A) (*21*–*23*). Next, using immunostaining and mouse genetics to visualize presynaptic terminals, we found that both group-N and group-Z neurons receive a variety of inputs (for example, dorsal root ganglia sensory, descending serotonergic, dI1, dI4-6, V1, and V3) (fig. S16, B and C) (*24*). Gene Ontology (GO) term analysis revealed that group-Z neurons were enriched for genes involved in axon and synapse development, including high neurofilament (Nef-l, -m, and -h) expression (Fig. 5, A and B). Consequently, we speculated that group-Z neurons may contain one or more populations of long-range projection neurons (*25*). Subsets of neurons from multiple cardinal classes have been shown to share projection targets, further raising the possibility that group-Z neurons represent

Downloaded from http://science.sciencemag.org/ on April 22, 2021

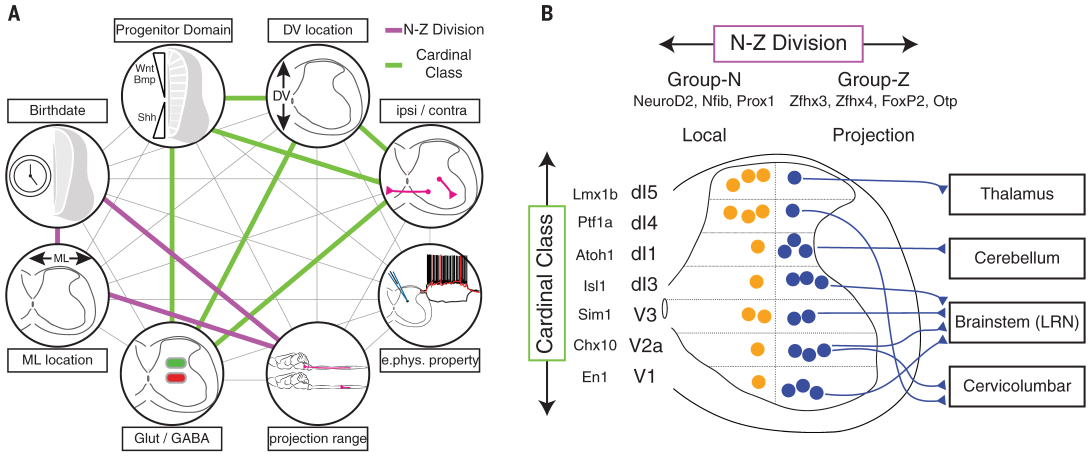


Fig. 6. A unified taxonomic index of spinal neurons. (**A**) Summary of relationships of neuronal attributes. Neuronal subtypes can be viewed as a composite of distinct properties that fall into a range of categories (circles). Neuronal subtypes arise by joining different combinations of these attributes. Cardinal class and N-Z markers simplify the task of defining neuronal subtypes because both correspond to multiple neuronal features (magenta and green lines). (**B**) Summary of neuronal subsets defined by coexpression of cardinal class markers and N-Z labels. This matrix provides a simple labeling index to define neuronal subsets. The postsynaptic targets of group-Z neurons within each cardinal population are predicted from projection neuron–tracing studies (*26*, *29*, *31*, *37*, *38*). Local connections and collaterals are not shown (*26*, *27*).

long-range projections across neuronal classes (*7*, *9*, *26*, *27*). We labeled spinothalamic, spinocerebellar, spinomedullary, and lumbocervical projection neurons with retrograde tracer cholera toxin subunit β (CTB) in combination with group-E, -N, and -Z marker immunostaining (Fig. 5C). Although group-N and group-Z neurons are approximately equal in number (fig. S6), the long-range projection neurons in both the lumbar and cervical cord were preferentially enriched for Zfhx3$^+$ neurons (Fig. 5, D to G, and figs. S17 to S20). Because the single marker Zfhx3 does not label all group-Z neurons, we also performed the supraspinal labeling and immunostaining with additional group-Z markers, including Zfhx4, Otp, and Foxp2. We found that multiple group-Z markers identify additional long-range projection neurons, providing further evidence that many group-Z cells project long axons (figs. S18 and S19). By contrast, markers for group-N (NeuroD2 and Prox1) and group-E (Ebf1) rarely (0 to 7.9%) labeled long-range neurons (Fig. 5, D to G, and figs. S17 to S20). As a positive control, injection of CTB directly into the cord labeled group-N neurons near the injection site (fig. S20). Taken together, our labeling studies indicate that group-Z neurons are composed of long-range projecting cells, whereas group-N and group-E neurons appear to be preferentially composed of local interneurons.

Although most of our studies focused on the lumbar spinal cord, we found one counterexample to the group-N–group-Z correlation with axon projection in the thoracic region. Namely, a fraction of spinocerebellar projection Clarke's column neurons was found to express the group-N marker NeuroD2 (fig. S18) (*28*). The reason for this discrepancy is unclear; however, these cells form a distinct medial nucleus with unusual molecular features, such as the expression of Vglut1 rather than Vglut2 (*29*, *30*). Previous gene profiling of Clarke's column neurons also revealed that they cluster separately from other thoracic spinal neurons (*28*). The non–Clarke's column spinocerebellar neurons in the thoracic cord express group-Z genes that are typical for projection neurons (fig. S18) (*28*).

In principle, the correlation between group-Z markers and projection neuron labeling might have arisen as a byproduct of long-range neurons predominantly being located laterally within the spinal cord where group-Z markers are expressed for independent reasons. Therefore, we sought to define the axon projection pattern of group-Z neurons in atypical locations within the spinal cord. A sparse population of Zfhx3$^+$ neurons were situated in the very superficial lamina of the spinal cord (Figs. 2D and 3E). The superficial Zfhx3$^+$ neurons were labeled after injection of CTB into the thalamus (Fig. 5D). These unusual Zfhx3$^+$ projection neurons were further confirmed to represent spinothalamic cells by using Nk1r/Tacr1 labeling and were also born early like other group-Z neurons (Fig. 3E and fig. S17) (*5*, *31*). Near the midline, the boundary between group-N and group-Z is not absolute, and there is sparse intermingling of NeuroD2$^+$ and Zfhx3$^+$ neurons. To further test the relationship between group-N and group-Z markers and their axonal projection patterns, we examined the marker profile of projection neurons in this region of the spinal cord. Retrograde fills of projection neurons preferentially labeled the Zfhx3$^+$ neurons but not the NeuroD2$^+$ neurons (Fig. 5, E to G). Thus, the molecular features that distinguish group-N from group-Z neurons reveal a core phenotypic difference: Group-N (and group-E) neurons are restricted to forming local connections within the spinal cord, whereas group-Z neurons can also form long-range connections with distant targets (Fig. 6).

Discussion

In this study, we sought to identify a unifying logic for spinal neuron diversification. We used a top-down approach to identify the conserved genetic relationships among heterogeneous cell types and used the branch points of this hierarchical system to find marker genes that were linked to neuronal birth date, cytoarchitecture, neurotransmitter, and projection status. The divide between group-E neurons marked by Ebf1 and group-H cells marked by Hoxc10 corresponded to a split between sensory and motor circuits, respectively (Fig. 2H). The H-neuron population was further divided into group-N and -Z types, in which NeuroD2 labeled medial, late born, locally projecting interneurons and Zfhx3 marked lateral, early

Downloaded from http://science.sciencemag.org/ on April 22, 2021

born, projection neurons (Figs. 2H, 3G, and 6, A and B).

The N-Z division giving rise to local versus projection neurons may have occurred early in evolution because the genetic signatures for these two groups are conserved across broad populations of spinal neurons. Consistent with this, group-N and -Z genes are conserved in many vertebrates, and functional studies of these factors have revealed roles in neural diversification (*32*–*34*). The correlation between birth date and N-Z identity is consistent with neuronal diversity being tied to neurogenesis (*9*, *22*, *35*, *36*).

We anticipated that the most basic characteristic associated with neurons is their neurotransmitter phenotype (*11*, *15*, *19*) but instead found that this was superseded by the distinctions between motor-sensory and local-projection neuron types (Fig. 2H). Motor neurons in different species, although homologous cells, use different neurotransmitters, suggesting that there is flexibility and adaptability in the signals for neurotransmission (*15*). At a molecular level, the same neurotransmitter phenotype across cardinal classes can be specified by different transcriptional pathways (*2*). These findings suggest that spinal neuron neurotransmitter identity can arise through convergent evolutionary processes, causing the genetic signatures for neurotransmitter identity to appear lower in the hierarchical relationships because there are fewer cells with similar genetic characteristics.

Because the lineage-based markers of cardinal interneurons are orthogonal to the conserved markers for the N-Z neuronal sets, we found that the intersection of these two systems systematically labeled neurons with specific dorsoventral and mediolateral positions, birth dates, neurotransmitter phenotypes, ipsilateral-contralateral projections, and local–long-range connectivity (Fig. 6, A and B, and fig. S21). In isolation, neither cardinal class nor N-Z markers precisely define the postsynaptic targets of spinal neurons (*2*, *9*, *10*). However, the spinal neurons innervating the lateral reticular nucleus, thalamus, cerebellum, and long-range spinal targets (propriospinal) can be predicted on the basis of the intersection of their cardinal and N-Z genetic status (Fig. 6B and fig. S21). By identifying markers associated with diversification for the purpose of expanding cellular functions—in this case, evolution and development—it may be possible to create more unified and practical systematics for identifying functionally different cell types in many systems.

REFERENCES AND NOTES

1. D. C. Lu, T. Niu, W. A. Alaynick, *Front. Mol. Neurosci.* **8**, 25 (2015).
2. H. C. Lai, R. P. Seal, J. E. Johnson, *Development* **143**, 3434–3448 (2016).
3. O. Kiehn, *Nat. Rev. Neurosci.* **17**, 224–238 (2016).
4. S. C. Koch, D. Acton, M. Goulding, *Annu. Rev. Physiol.* **80**, 189–217 (2018).
5. A. J. Todd, *Nat. Rev. Neurosci.* **11**, 823–836 (2010).
6. J. Jiang, E. Azim, C. F. Ekerot, B. Alstermark, *Front. Comput. Neurosci.* **9**, 75 (2015).
7. P. J. Osseward 2nd, S. L. Pfaff, *Curr. Opin. Neurobiol.* **56**, 175–184 (2019).
8. J. Ericson *et al.*, *Cell* **90**, 169–180 (1997).
9. M. Hayashi *et al.*, *Neuron* **97**, 869–884.e5 (2018).
10. J. B. Bikoff *et al.*, *Cell* **165**, 207–219 (2016).
11. M. Häring *et al.*, *Nat. Neurosci.* **21**, 869–880 (2018).
12. A. Sathyamurthy *et al.*, *Cell Rep.* **22**, 2216–2225 (2018).
13. J. Delile *et al.*, *Development* **146**, dev173807 (2019).
14. D. Arendt *et al.*, *Nat. Rev. Genet.* **17**, 744–757 (2016).
15. O. Hobert, P. Kratsios, *Curr. Opin. Neurobiol.* **56**, 97–105 (2019).
16. D. Arendt, P. Y. Bertucci, K. Achim, J. M. Musser, *Curr. Opin. Neurobiol.* **56**, 144–152 (2019).
17. H. Zeng, J. R. Sanes, *Nat. Rev. Neurosci.* **18**, 530–546 (2017).
18. D. R. Ladle, E. Pecho-Vrieseling, S. Arber, *Neuron* **56**, 270–283 (2007).
19. B. Tasic *et al.*, *Nature* **563**, 72–78 (2018).
20. M. I. Gabitto *et al.*, *Cell* **165**, 220–233 (2016).
21. A. E. Stepien, M. Tripodi, S. Arber, *Neuron* **68**, 456–472 (2010).
22. M. Tripodi, A. E. Stepien, S. Arber, *Nature* **479**, 61–66 (2011).
23. A. J. Levine *et al.*, *Nat. Neurosci.* **17**, 586–593 (2014).
24. F. J. Alvarez, R. M. Villalba, R. Zerda, S. P. Schneider, *J. Comp. Neurol.* **472**, 257–280 (2004).
25. A. Yuan, M. V. Rao, R. A. Veeranna, R. A. Nixon, *Cold Spring Harb. Perspect. Biol.* **9**, a018309 (2017).
26. C. Pivetta, M. S. Esposito, M. Sigrist, S. Arber, *Cell* **156**, 537–548 (2014).
27. E. Azim, J. Jiang, B. Alstermark, T. M. Jessell, *Nature* **508**, 357–363 (2014).
28. M. Baek, V. Menon, T. M. Jessell, A. W. Hantman, J. S. Dasen, *Cell Rep.* **27**, 2620–2635.e4 (2019).
29. R. Yuengert *et al.*, *Cell Rep.* **13**, 1258–1271 (2015).
30. A. W. Hantman, T. M. Jessell, *Nat. Neurosci.* **13**, 1233–1239 (2010).
31. K. Nishida, S. Ito, *Eur. J. Neurosci.* **46**, 2608–2619 (2017).
32. Z. Zhang *et al.*, *Exp. Neurol.* **322**, 113055 (2019).
33. M. Tambalo, R. Mitter, D. G. Wilkinson, *Development* **147**, dev184143 (2020).
34. S. A. Wilke *et al.*, *Neural Dev.* **7**, 9 (2012).
35. L. C. Greig, M. B. Woodworth, M. J. Galazo, H. Padmanabhan, J. D. Macklis, *Nat. Rev. Neurosci.* **14**, 755–769 (2013).
36. C. Q. Doe, *Annu. Rev. Cell Dev. Biol.* **33**, 219–240 (2017).
37. R. B. Roome *et al.*, *Cell Rep.* **33**, 108425 (2020).
38. L. Ruder, A. Takeoka, S. Arber, *Neuron* **92**, 1063–1078 (2016).

ACKNOWLEDGMENTS

We thank K. Lettieri, B. O'Leary, H. Forman, A. J. Levine, M. J. Sternfeld, K. L. Hilde, members of the Pfaff laboratory, the FCCF core (C. O'Connor and C. Fitzpatrick; NIH-NCI CCSG: P30 014195), the NGS core (N. Hah; NIH-NCI CCSG: P30 014195, the Chapman Foundation and the Helmsley Charitable Trust), the UCSD IGM Genomic Center (K. Jepsen and other members), the Biophotonics core (NIH-NCI CCSG: P30 014195 and the Waitt Foundation), the GT3 core (J. Naughton, J. Marlett, and R. Armendariz; NIH-NCI CCSG: P30 014195, NINDS R24 Core Grant, funding from NEI), and the Janelia Viral Vector Core for technical support and advice; M. Goulding, G. Gatto, members of the Goulding laboratory, E. J. Kim and E. M. Callaway for providing reagents and advice; and S. Ackerman, K. Asahina, K. Baldwin, T. Komiyama, and Y. Zou for discussions and advice. **Funding:** P.J.O. was supported by the Christopher and Dana Reeve Foundation. N.D.A. is supported by the NIMH T32 Training Grant T32MH019938 J.D.M. is supported by NIH-NICHD K99 HD096512. B.K.B. is supported by the UCSD Cell and Molecular Genetics Training Program (T32 GM007240) and the Timken-Sturgis Foundation. M.H. was supported by the Japanese Ministry of Education, Culture, Sports, Science, and Technology Long-Term Student Support Program and the Timken-Sturgis Foundation. S.L.P. is a Benjamin H. Lewis chair in neuroscience. This research was supported by funding from the Howard Hughes Medical Institute, the Christopher and Dana Reeve Foundation, the Sol Goldman Charitable Trust, and National Institutes of Health (1 U19 NS112959-01). **Author contributions:** Conceptualization: M.H., P.J.O., and S.L.P. Methodology: M.H., P.J.O., J.D.M., and S.P.D. Software: S.P.D., J.D.M., and P.J.O. Validation: M.H., P.J.O., L.C.B., and R.C.C. Formal analysis: S.P.D., J.D.M., P.J.O., and M.H. Investigation: M.H., P.J.O., N.D.A., B.A.T., B.K.B., L.C.B., F.B., and R.C.C. Resources: M.G., S.P.D., J.D.M., P.J.O., and M.H. Data curation: S.P.D., J.D.M., and P.J.O. Writing, original draft: M.H., P.J.O., and S.L.P. Writing, review and editing: M.H., P.J.O., N.D.A., J.D.M., B.A.T., B.K.B., S.P.D., and S.L.P. Visualization: M.H., P.J.O., and S.P.D. Supervision: M.H., P.J.O., and S.L.P. Project administration: M.H., P.J.O., and S.L.P. **Competing interests:** The authors declare no competing interests. **Data and materials availability:** All data are available in the main text or the supplementary materials. The accession number for the scRNA-seq data reported in this paper is NIH GEO: GSE171607, GSE171605, and GSE171606.

SUPPLEMENTARY MATERIALS

science.sciencemag.org/content/372/6540/385/suppl/DC1
Materials and Methods
Figs. S1 to S21
Tables S1 to S5
References (*39*–*52*)
MDAR Reproducibility Checklist

View/request a protocol for this paper from *Bio-protocol*.

29 July 2020; accepted 15 March 2021
10.1126/science.abe0690

Downloaded from http://science.sciencemag.org/ on April 22, 2021

Science

Conserved genetic signatures parcellate cardinal spinal neuron classes into local and projection subsets

Peter J. Osseward II, Neal D. Amin, Jeffrey D. Moore, Benjamin A. Temple, Bianca K. Barriga, Lukas C. Bachmann, Fernando Beltran Jr., Miriam Gullo, Robert C. Clark, Shawn P. Driscoll, Samuel L. Pfaff and Marito Hayashi

Science **372** (6540), 385-393.
DOI: 10.1126/science.abe0690

Neuronal identities

Neurons of the mouse spinal cord can be identified by any of several metrics, including what neurotransmitters they use, what cells they connect to, where they are located, and what neuroprogenitor gave rise to them. Osseward *et al.* generated a different metric, genetic signatures, and identified classes of local and projection neurons that were otherwise heterogeneous by other classification systems. With this focus on a cell's genetic signature, its neurotransmitter phenotype, which is accessible by a variety of transcriptional routes, can be seen as a parallel to convergent evolution in development.

Science, this issue p. 385

ARTICLE TOOLS http://science.sciencemag.org/content/372/6540/385

SUPPLEMENTARY MATERIALS http://science.sciencemag.org/content/suppl/2021/04/21/372.6540.385.DC1

REFERENCES This article cites 51 articles, 7 of which you can access for free
http://science.sciencemag.org/content/372/6540/385#BIBL

PERMISSIONS http://www.sciencemag.org/help/reprints-and-permissions

Use of this article is subject to the Terms of Service

Science (print ISSN 0036-8075; online ISSN 1095-9203) is published by the American Association for the Advancement of Science, 1200 New York Avenue NW, Washington, DC 20005. The title *Science* is a registered trademark of AAAS.

Copyright © 2021 The Authors, some rights reserved; exclusive licensee American Association for the Advancement of Science. No claim to original U.S. Government Works

Downloaded from http://science.sciencemag.org/ on April 22, 2021

science.sciencemag.org/content/372/6540/385/suppl/DC1

Supplementary Material for

Conserved genetic signatures parcellate cardinal spinal neuron classes into local and projection subsets

Peter J. Osseward II, Neal D. Amin, Jeffrey D. Moore, Benjamin A. Temple, Bianca K. Barriga, Lukas C. Bachmann, Fernando Beltran, Miriam Gullo, Robert C. Clark, Shawn P. Driscoll, Samuel L. Pfaff*, Marito Hayashi

*Corresponding author. Email: pfaff@salk.edu

Published 23 April 2021, *Science* **372**, 385 (2021)
DOI: 10.1126/science.abe0690

This PDF file includes:

Materials and Methods
Figs. S1 to S21
References

Other Supplementary Material for this manuscript includes the following:
(available at science.sciencemag.org/content/372/6540/385/suppl/DC1)

Tables S1 to S5 as separate Excel files
MDAR Reproducibility Checklist

Materials and Methods

Mouse lines

The following strains of mice were used:

ROSA-CAG:lsl:tdTomato (Ai14, JAX, 007908),

ROSA-CAG:lsl:Synaptophysin-tdTomato (Ai34D, JAX, 012570),

ROSA-CAG:lsl:H2B-tdTomato (Ai75, JAX, 025106),

Isl2:lsl:DTA (JAX, 007942)

Vgat:Cre (JAX, 016962),

Vglut2:Cre (JAX, 016963),

Atoh1:Cre (JAX, 011104),

ChAT:Cre (JAX, 028861),

Chx10:Cre (*39*),

En1:Cre (JAX, 007916),

Fev:Cre (JAX, 012712),

Isl1:Cre (*40*),

Lbx1:Cre (*41*),

Lmx1b:Cre (provided by R. Johnson, University of Texas MD Anderson Cancer Center, (*42*)),

Olig2:Cre (*43*),

Ptf1a:Cre (*44*),

Pvalb:Cre (JAX, 008069),

Sim1:Cre (*45*),

Hb9:GFP (*46*)

Mouse lines obtained from the JAX laboratory were maintained in a C57BL/6J background, and all other lines were maintained in a CB6F1/J background. All mouse work was conducted in accordance with IACUC guidelines of the Salk Institute for Biological Studies. Both male and female mice were used in all studies.

Postnatal day 0 single cell RNA-seq

In order to minimize technical and biological variabilities, timed-matings were set up to obtain both Vglut2:Cre; tdTomato and Vgat:Cre; tdTomato neonates at postnatal day 0 on the experiment day. Sex of the animals were visually inspected and verified by genotyping (*47*). Lumbar segments were dissected from Vglut2; tdTomato (2 females and 1 male) and Vgat; tdTomato (2 females and 1 male) in aCSF. Cell dissociation was conducted using Papain following the manufacturer's instruction (Worthington Biochemical) with 5% Trehalose, 50uM APV, and 800uM KA added during the dissociation process (*48*). Via FACS (FACSDIVA, BD), 30,000 Vglut2; tdTomato cells and 30,000 Vgat;tdTomato cells were sequentially collected into 500ul of FACS buffer (DMEM w/o Phenol Red; 1mM EDTA; 25mM Hepes pH7.0; 5% FBS). Cell suspension was centrifuged at 300 rcf for 2 minutes, and supernatant was removed leaving 60 ul of FACS buffer and cell pellet. The cells were resuspended, and 33.4 ul of the resuspended cells (~30,000 cells) were loaded onto the 10X Chromium Controller using Chromium Single Cell 3' v2 reagents.

Sequencing library was prepared following the manufacturer's instructions (10X Genomics). 9 cycles were used for cDNA amplification, and 12 cycles were used for library amplification. The resulting sequencing library was sequenced with Paired End reads, with a Read 1 of

26 basepairs and a Read 2 of 98 basepairs, on an Illumina HiSeq 4000 and demultiplexed using bcl2fastq v2.18.0.12 at the UCSD IGM Genomics Center.

Alignment and preprocessing of scRNA-seq data

Alignment to Gencode annotated transcripts for mouse and UMI-collapsing were performed using Kallisto and Bustools. Barcodes (potential cells) were discarded if they had fewer than 500 detected features, more than 3500 detected features (based on histogram), or if they had greater than 5% of their UMI counts coming from mitochondrial genes (threshold based on histogram of all potential cells). To identify and remove non-neuronal cells from downstream analysis we used dbscan clustering (fpc package, R) on a UMAP transform of the cells (see next section for description of this method). Clusters of cells with the expression of neuronal markers were retained for downstream analysis as described in the following section, while non-neuronal cells were discarded.

Normalization, dimensionality reduction and UMAP transformation

Raw UMI counts were normalized by first dividing, for each cell, the UMI counts for all genes by the total sum of UMI counts at each cell and scaling by 10,000. To construct the UMAP transformation, we first reduced the dimensionality of the expression data by PCA and then used only the significant principal components as input to the UMAP transformation. Prior to PCA, we identified highly variable genes (HVG) using the method described elsewhere (*49*). Normalized expression values for the identified highly variable genes was then offset by 1 and log-scaled. PCA was performed using the irlba function for partial singular value decomposition (irlba package, R). Identification of the number of significant components was determined automatically

using the 95th percentile of the appropriate Wishart distribution as a threshold for the eigenvalues. The reduced dimensionality expression matrix of significant components (number of cells by number of significant principal components) was then used as the input for UMAP and retained for other downstream analysis. The UMAP transform was calculated using the umap function (umap package, R) with 'n_neighbors=20' and default settings. Additional clustering solutions were performed on the reduced dimensionality expression matrix.

Identification of glutamatergic and GABAergic cells

Identification of glutamatergic and GABAergic cells was performed by associating each cell to the closest of the two stats using a list of known marker genes (Slc17a6, Tlx3 and Lmx1b for glutamatergic; and Slc32a1, Slc6a5, Gad1, Gad2 and Pax2 for GABAergic). The unnormalized UMI count matrix was binarized using a threshold of one UMI, and cell-to-target distances were calculated by Euclidean distance (*13*). For each cell we found the closest target (either glutamatergic or GABAergic). If a cell did not express any markers or if it had equal Euclidean distance to more than one target, its state was marked as indeterminant.

Identification of neuronal cardinal classes

We clustered the reduced dimensionality matrix, described above, by building a nearest neighbors graph linking each cell to its 20 nearest neighbors. We chose 20 neighbors to generate relatively small clusters of cells. The graph was then partitioned using the 'infomap.community' (alias of 'cluster_infomap', igraph package, R) using default settings. The resulting 45 clusters were evaluated for enriched genes by performing differential expression of each cluster's cells verses all other cells. Differential expression was performed using the quasi-likelihood (QL) F-

test in the edgeR R package. Gene dispersions were calculated with monocle and provided for the 'dispersion' parameter to the 'glmQLFit' function. P-values were then calculated via the 'glmQLFtest' function. Each cluster was compared to all other cells (one DE test per cluster) to find top enriched genes at each cluster. Genes were considered significant with post-hoc corrected p-values < 0.05. We assigned cardinal classes by manually inspecting the top 20 enriched genes from each cluster for known marker genes (*1, 2*). See Table 1.

Identification of divisions of neurons

To identify major divisions of neurons and their associated genes we reasoned a top-down divisive clustering strategy would be the most intuitive approach. We developed a simple variation of top-down divisive clustering. Rather than preprocessing the expression matrix, transforming with PCA, and then running a divisive clustering algorithm on the significant components, we opted to include the preprocessing and PCA transformation at each division stage to help bring out variation within partitions of the data that may be hidden when considering all of the cells. At each division stage we started from raw UMI (the full expression matrix at the first stage and partitions of the data at subsequent stages), calculate highly variable genes (HVG), normalize and log-transform, transform with PCA, automatically identify the number of significant components, and finally partition the PCA transformed data into 2 clusters with k-means. For this analysis we filtered out genes detected in fewer than 1% of cells before each HVG calculation. To identify broadly expressed genes, we chose to filter conservatively for 1% minimum detection. We designed the analysis so that it could be stopped after a set number of divisions because our focus was to investigate only the high level divisions in the cells.

To evaluate robustness of the partitions we used bootstrapping and Jaccard similarities. At each bootstrap iteration we bootstrap-sampled the cells and carried out the entire divisive clustering pipeline. Each division stage was compared against the corresponding division stage in the divisive partitioning of the full data and Jaccard scores were calculated. We ran 1000 bootstrap iterations. The final Jaccard scores are the average of the scores calculated across all bootstrap iterations.

Pairwise differential gene expression at split stages was performed using the quasi-likelihood (QL) F-test in the edgeR R package. Gene dispersions were calculated with monocle and provided for the 'dispersion' parameter to the 'glmQLFit' function. P-values were then calculated via the 'glmQLFtest' function.

Gene set enrichment analysis

Gene set enrichment analysis (GSEA) was performed similarly to the method described elsewhere (*50*). Instead of the statistical method described originally, we used the hypergeometric test at each partition of the ranked gene list and identified the position of the minimum p-value, which is called the minimum-hypergeometric test (mHG). *Posthoc* correction was performed on the mHG p-value for each term by scaling the p-value by the number of genes in the ranked gene list. mHG p-values were converted into ES scores by taking the -log10, if the term was enriched, or +log10 if the term was depleted.

Tissue preparation, immunohistochemistry, and imaging

Primary antibodies used were:

Rabbit anti-Calbindin (D-28K, Swant, CB38, 1:500),

Goat anti-ChAT (Millipore, AB144P, lot#NG1915294, 1:300)

Rabbit anti-Ebf1 (Millipore, AB10523, lot# 2930985, 1:2000),

Rabbit anti-Foxp2 (Abcam AB16046, lot# GR252393-1, 1:5000),

Guinea pig anti-Hb9 (Thaler et al. 1999, #723, 1:2000)

Rabbit anti-Hoxc10 (Abcam, AB153904, lot# GR116551-4, 1:500),

Sheep anti-Lrrn1 (R&D systems, AF4990, lot# CBFE011906A, 1:1000),

Rabbit anti-NeuN (Millipore, ABN78, lot# 3305071, 1:1000),

Rabbit anti-NeuN alexa fluor 488 conjugate (Millipore, ABN78A4, lot# 2916039, 1:100),

Rabbit anti-NeuroD2 (abcam, AB104430, lot# GR3263783-2/GR3185621-1, 1:1000),

Rabbit anti-Nfib (Novus, NBP1-81000, lot#A104664, 1:1000),

Rabbit Anti-Nk1r (Millipore, S8305, lot# 049M4810V/098M4766V, 1:1000),

Sheep anti-Onecut2 (R&D Systems, AF6294, lot#CDKS0116081, 1:2000),

Rabbit anti-Otp (Novus, NBP2-19642, lot# 40674, 1:1000),

Rabbit anti-Parvalbumin (Swat, PV25, 1:2000),

Goat anti-Prox1 (Novus, AF2727, lot# VIY0319011/VIY0218072, 1:1000),

Rabbit anti-Pou6f2 (Sigma, HPA008699, lot# A104522, 1:1000),

Guinea pig anti-Vglut1 (Millipore, B5905, lot# 2932489, 1:3000),

Guinea pig anti-Vglut2 (Millipore, AB2251, lot# 2041594, 1:3000),

Sheep anti-Zfhx3 (Novus, AF7384, lot# CGHE011709A/ CGHE0111121, 1:1000),

Rabbit anti-Zfhx4 (Novus, NBP1-82156, lot#G105409/G119343, 1:1000),

Secondary antibodies and counter stains used were:

Donkey anti-rabbit (Thermo Fisher, 1:1000), anti-sheep (Thermo Fisher, 1:1000), anti-goat (Thermo Fisher, 1:1000), and anti-guinea pig (Jackson Immuno, 1:300), Hoescht (Thermo Fisher, 1:2000)

Embryos were fixed with 2-4% PFA for 60-120 min at 4°C. Postnatal spinal cords were isolated and fixed with 4% PFA for 60-120 min at 4°C. Adult mice were transcardially-perfused with PBS followed by 4% PFA. No post-fixation was performed. Tissues were washed with PBS, equilibrated in 30% sucrose for 2hr – overnight at 4°C, embedded in Tissue-Tek OCT (Sakura), and subjected for cryosectioning onto glass slides (VWR). Immunohistochemistry was performed by incubating with primary antibodies (1-2 overnights, 4°C) and fluorophore-conjugated secondary antibodies (1:1000, 1-2hr, room temperature; life technologies, Jackson ImmunoResearch). Sections were mounted with VectaShield (VECTOR) or Mowiol and coverslipped (VWR). Images were acquired using an Olympus FV3000. Images are presented as z-projections unless otherwise noted.

Image and colocalization analysis

Images were loaded into IMARIS (Bitplane) and analyzed using the "spot detection" function. To identify cells labeled by immunostaining, EdU labeling, or tdTomato expression, "Quality" or "Median signal intensity" (with IMARIS default auto-threshold setting) was used as the spot detection parameter for thresholding to exclude non-specific background signal. This was followed by manual validation, such as deleting spots detected outside of the spinal cord. For detecting NeuN labeled cells, an additional threshold parameter for "median signal intensity" for the NeuN channel was used. For cardinal class analysis, tdTomato spots detected from labeled axons were manually deleted. For Isl1:Cre;tdTomato analysis to label dI3 interneurons,

tdTomato expressing motor neurons were manually excluded based on their ventral location and larger soma size.

Colocalization of detected spots was performed using the IMARIS "colocalization" function, with the colocalization distance set to 6um. Because CTB signal is generally excluded from cell nuclei, CTB spot detection and colocalization analysis was performed manually in IMARIS. First, CTB cells were manually labeled as spots in IMARIS using Hoechst/DAPI to identify the nuclei of the CTB labeled cell (this was done blind to Group-Z/N/E marker expression). Next, marker^{+} spots were identified using standard spot detection parameters. Finally, the Group-Z/N/E markers colocalization with CTB cells was assessed manually.

To analyze the position of cells across spinal cord sections and animals, the dorsal edge of the central canal was used as a reference frame in IMARIS, set as position (0,0). To account for variability in spinal cord size, the distances from the reference frame to the dorsal, ventral, and lateral edges of the spinal cord were measured in order to normalize position values. Spot position with respect to the reference frame and cord size measurements were exported as Excel files and loaded into MATLAB for further analysis.

Quantification and statistical analysis

No statistical methods were used to predetermine sample sizes. Quantification of neurons was performed by analyzing 2-8 sections per cord/spinal region. For each animal, the total number of each marker of interest was summed across the spinal cord sections analyzed. The total counts of each marker were used to calculate the colocalization rate for each animal based on the markers of interest. For the colocalization data presented, each dot represents the colocalization rate of a

single animal, with mean ± S.E.M. presented. See Table 5 for total number of animals and cells or markers counted for each experiment.

Prism8 (Graph Pad) software was used for statistical analyses and visualizations of colocalization data in Figures 2, 3, 4, and 5. Comparisons of colocalization rates were performed using Brown-Forsythe and Welch ANOVA with post hoc Dunnett's T3 multiple comparison test, with p values below 0.05 considered statistically significant. In Figure 5D-E, we observed zero colocalizations of Prox1 with the 33 spinothalamic and 178 spinocerebellar cells counted when staining for Group-N markers NeuroD2 and Prox1.

Spatial analysis and statistics

For spatial analysis, spinal cord spot positions were analyzed and plotted in MATLAB (Mathworks) using custom scripts. To account for variability in spinal cord size across the rostrocaudal axis, the spinal cord spot positions were normalized using the length measurements of the spinal cord section. The normalized position values were defined using the top of the central canal as the reference point. The distance from the reference point to the dorsal edge of the spinal cord was normalized to 500um, to the ventral edge as 450um, and lateral edge as 600um. Due to the symmetry of the spinal cord and the markers analyzed, spots from the left and right half of the spinal cord were combined into a single dataset by collapsing the spots detected on the left half of the spinal cord onto the right half.

To examine the spatial distributions of select markers, one- and two-dimension kernel density estimations were calculated in MATLAB using the 'kde' and 'kde2d' functions (Matlab file exchange). The range of the function was set as the limits of the normalized spinal cord. A kernel density estimation was calculated for each individual animal and averaged to create a

mean kernel density estimation. Mediolateral and dorsoventral average kernel densities were individually plotted. For the visualization of two-dimensional kernel density estimates, contour plots were generated with each contour representing a given percentile of the underlying data.

To measure the spatial overlap between two distributions, the Weighted Jaccard Distance was calculated using the mean two-dimensional kernel density estimate for each marker. Also known as Soergel Distance, the formula for Weighted Jaccard Distance is 1 minus sum(min(A,B))/sum(max(A,B)). To hierarchically cluster the Weighted Jaccard Distances, the Matlab 'linkage' function was used with the 'average' method. To test the statistical significance of a Weighted Jaccard Distance, a null distribution was generated via bootstrapping. For the first marker, each animal was randomly paired with an animal from the second marker. The positions of the markers of the two animals were shuffled and the kernel density estimates were calculated for the first animal. This was repeated for each of the animals for the first marker to generate a mean kernel density estimate for the first animal with shuffled data. The process is repeated for the second marker. Finally, the Weighted Jaccard Distance was calculated for the shuffled mean kernel density estimates for each of the two markers. This process was repeated 1000 times to generate a distribution of Weighted Jaccard Distances to compare to the actual Weighted Jaccard Distance.

Spinal Cord *in situ* hybridization Images from Allen Institute

Images of the spinal cord *in situ* hybridization were obtained from the Allen Spinal Cord Atlas (*51*).

E12.5 single cell RNA-seq

The entire developing spinal cord was dissected from one Hb9:GFP embryo from one litter and another Hb9:GFP embryo from another litter in HBSS with HEPES (note: cells were not sorted for GFP). Cell dissociation was conducted using Papain following the manufacturer's instruction (Worthington Biochemical). Specifically, spinal cords were placed in 750 uL papain solution in 37C water bath for 20 minutes, gently triturated, incubated again for additional 25 minutes, fully triturated, and quenched with 250 uL ovomucoid solution. Dissociated cells were then spun down at 150 rcf for 5 minutes. The cell pellet was resuspended in 5% FCS in DMEM/F12 with HEPES without phenol red, and the cells were passed through a cell strainer. Via FACS (FACSDIVA, BD), 20,000 cells were collected (not gated for GFP) into 500 uL of 5% FCS with DMEM/F12 with HEPES without phenol red. Sorted cells were spun down at 300 rcf for 2 minutes, and 370uL were removed to leave remaining 130 uL. The cells were resuspended in this remaining media. 32.5uL of the resuspended cells (~5,000 cells) were loaded into 10X Chromium Controller using Chromium Single Cell 3' v2 reagents.

Sequencing library was prepared following the manufacturer's instructions (10X Genomics). 14 cycles were used for cDNA amplification, and 10 cycles were used for library amplification. The resulting sequencing library was sequenced with Paired End reads, with a Read 1 of 26 basepairs and a Read 2 of 98 basepairs, on an Illumina HiSeq 4000 at the UCSD IGM Genomics Center. Raw sequencing data was demultiplexed using bcl2fastq v2.18.0.12.

Sequencing and demultiplexing of two biological replicates into FASTQ format files were performed by the UCSD sequencing core. Reads from the two samples were aligned and quantified separately for gene expression using Cellranger (10x genomics) and then combined into a single expression matrix using Cellranger's 'aggr' program. We used the estimated cell

count from Cellranger for downstream analysis. This experiment did not require additional QC steps to further analysis.

Normalization of expression values, selection of variable genes, PCA and UMAP calculations were performed as described previously for the P0 neuron experiment. These steps were repeated on the neuron-only data after separating the neurons from non-neurons based in the following way. Neurons were separated from progenitors and a small amount of contaminate cells by classifying cells against lists known markers for neurons, progenitors, oligos, glial cells, endothelial cells, and vascular cells using the euclidean distance method described for identification of glutamatergic and GABAergic cells in the P0 data. Out of 3,645 cells exported from Cellranger we identified 2,945 neurons with the majority of the remaining cells identified as progenitors.

Identification of neurotransmitter type was performed as described for the P0 neuron data.

Clustering of the E12.5 neurons was performed using the same method described for the P0 neuron data using 50 nearest neighbors for constructing the network. We found that using the same setting as in the P0 data, 20 neighbors, produced more clusters than were necessary for our purposes so we arbitrarily chose 50 to reduce the number of clusters. Top 20 genes enriched in each cluster were manually inspected and assigned to a cardinal class based on known marker genes (*1, 2*). See Table 3.

Divisive k-means partitioning was performed using the method described for the P0 neuron data.

Group-N and -Z identification was performed using the euclidean distance method described for cell type identification using pre-determined Group-N and -Z enriched genes. For

Group-Z we used Zfhx3, Zfhx4, Foxp2, and Otp. For Group-N we used Nfib, Neurod2, and Prox1.

Rostrocaudal segmental identity was estimated using expression of Hox genes in each cell. Reference expression patterns of Hox genes for cervical, thoracic and lumbar segments of the spinal cord were determined from bulk RNA-seq of cervical, thoracic and lumbar dissected spinal cords (*9*). Expression of Hox genes within the E12.5 scRNA-seq data was cross correlated against the reference expression data. For each cell the segment with the highest correlation was selected as the identity for that cell.

Ablation of proprioceptors and motor neurons

To understand whether proprioceptive inputs contribute to the emergence or maintenance of the N-Z division, Pvalb:Cre was crossed to Isl2:lsl:DTA (the Isl2 locus is active in the dorsal root ganglion (DRG) and motor neurons). Crossing Isl2:lsl:DTA to Pvalb:Cre restricts the expression of DTA to the proprioceptor of the DRG.

To examine whether the presence of motor neurons contributes to the N-Z division, Olig2:Cre was crossed to Isl2:lsl:DTA to ablate motor neurons.

Birthdating analysis

Co-expression of EdU and Group-E, -Z, and -N markers were analyzed to track the eventual settling locations and identities of neurons born around the EdU-injection time. For each time point, EdU in saline was administered into a pregnant female (20mg/kg) via intraperitoneal

injection twice with a 3hr interval (typically at 10am and 1pm of each time point). Immunostaining was performed first, and EdU signal was visualized using Click-iT EdU Alexa Fluor 647 imaging kit (Life Technologies) following the manufacturer's instruction.

Retrograde tracing

For retrograde tracing experiments, Cholera Toxin Subunit B (Recombinant), Alexa Fluor 555 Conjugate (ThermoFischer C22843, 0.5% in PB) was injected into neonatal mice, and tissue was collected 4-5 days later. Neonatal brain injections were established based on the Allen Developing Mouse Brain Atlas (E18 and P4 reference atlas) (*51*) and the Atlas of the Developing Mouse Brain (*52*). Given the variable body sizes at postnatal stages, 2-3 neonates from each experimental litter were used for injection practice using fast green followed by immediate brain dissection to confirm and adjust the injection coordinates prior to experimental CTB injections using the remaining neonates from the litter. For forebrain injections, CTB was unilaterally injected at P1 targeting the thalamus and adjacent regions (approximately 0.5mm lateral, 0.5mm rostral to bregma, multiple depths from surface at 2.5mm, 2mm, 1.5mm). For cerebellum injections, CTB was injected at P3 into the midline of the vermis (approximately 0.1mm depth). For brainstem injection, CTB was unilaterally injected at P1 into the brainstem just posterior to the end of the developing cerebellum (which correspond to the rhombomere 8 and 9 in early neonates) halfway between midline and lateral edge of brainstem at depths 0.3mm and 0.6mm up from bottom. For cervical injections, CTB was unilaterally injected into lower cervical segments at P1 (approximately 0.3mm lateral, multiple depths at 1.0mm, 0.7mm, 0.4mm). For lumbar injections, CTB was unilaterally injected into upper lumbar segments at P0 (approximately 0.3mm lateral, multiple depths at 1.0mm, 0.7mm, 0.4mm).

Viral Tracing Experiments

All monosynaptic rabies tracing experiments were performed using ChAT:Cre mice. AAV6-CAG-Flex-oG-WPRE-SV40-pA (Addgene 74292) at a titer of $4.6x10^{12}$ GC/mL was obtained from the GT3 Core at the Salk Institute. ΔG-Rabies-GFP (Addgene 52487) at a titer of $1.9x10^{9}$ IU/mL was obtained from the Janelia Viral Vector Core. At P4, AAV was delivered by anesthetizing mice on ice and injecting 0.5 uL of virus through the skin into the tibialis anterior using a Hamilton Syringe. At P7, mice were anesthetized with isoflurane and a small incision was made in the skin to target hindlimb muscles. A Drummond Nanoject II was used to deliver ~250 nL of rabies virus into the muscle at a speed of 9.2 nL/second. Mice were sacrificed one week later at P14 by perfusion with PBS followed by 4% PFA.

Figure S1

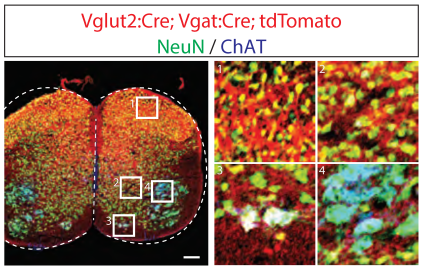


Fig. S1. Validation of Cre lines and gene expression in Group-N and -Z neurons

NeuN and ChAT immunostaining was conducted to assess the extent of neuronal labeling in lumbar segments from P0 Vglut2:Cre; Vgat:Cre; Ai14 mice. Nearly all $NeuN^+$ cells were marked by tdTomato in both the dorsal and ventral spinal cord (insets 1, 2). Medial motor neurons were labeled (inset 3), however the lateral motor column lacked tdTomato (inset 4). Thus, nearly all lumbar spinal interneurons are marked by either Vglut2:Cre or Vgat:Cre. 20um cryosection. Scale bar 100um.

Figure S2

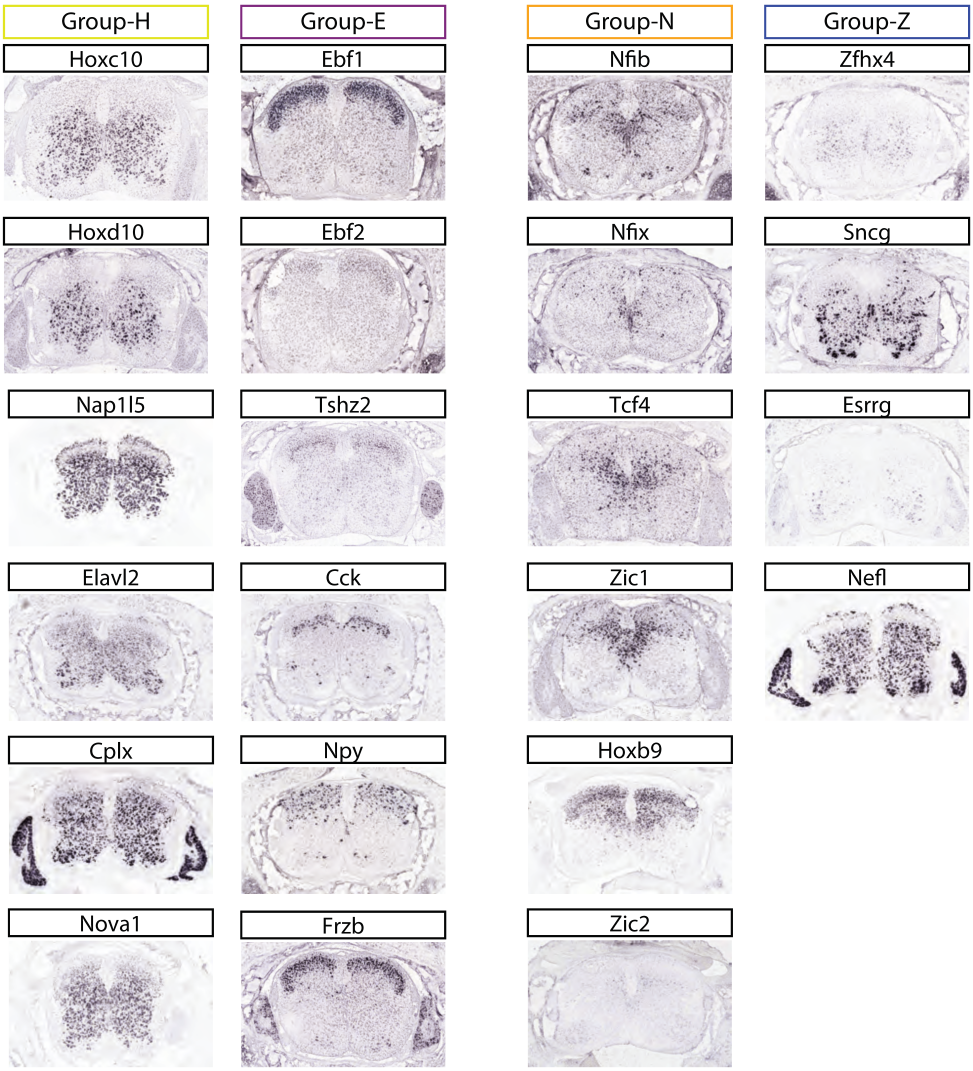

Group-H
Hoxc10
Hoxd10
Nap1l5
Elavl2
Cplx
Nova1
Group-E
Ebf1
Ebf2
Tshz2
Cck
Npy
Frzb
Group-N
Nfib
Nfix
Tcf4
Zic1
Hoxb9
Zic2
Group-Z
Zfhx4
Sncg
Esrrg
Nefl

Fig. S2. Group-H, -E, -N, -Z marker gene expression patterns

In situ hybridization of genes enriched in Group-H, -E, -N, -Z spinal neurons from P4 spinal cords. Images from the Allen Institute Mouse Spinal Cord Atlas.

Figure S3

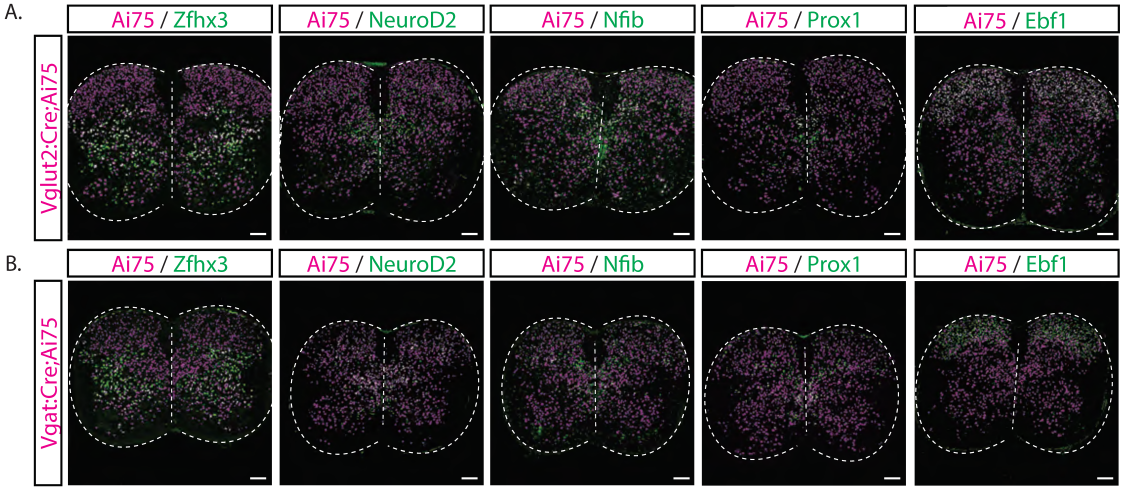

A.
Ai75 / Zfhx3
Ai75 / NeuroD2
Ai75 / Nfib
Ai75 / Prox1
Ai75 / Ebf1
Vglut2:Cre;Ai75
B.
Ai75 / Zfhx3
Ai75 / NeuroD2
Ai75 / Nfib
Ai75 / Prox1
Ai75 / Ebf1
Vgat:Cre;Ai75

Fig. S3. Group-E, -N, and -Z neurons are mixtures of both glutamatergic and GABAergic neurons

(A) Glutamatergic neurons were labeled by crossing Vglut2:Cre to a nuclear-tdTomato reporter Ai75. Double labeling of lumbar P0 spinal cords was performed with tdTomato and Group-Z (Zfhx3), Group-N (Nfib, NeuroD2, Prox1), or Group-E (Ebf1) markers. 20um cryosections. Scale bar 100um.

(B) GABAergic neurons were labeled by crossing Vgat:Cre to a nuclear tdTomato reporter Ai75. Double labeling of lumbar P0 spinal cords was performed with tdTomato and Group-Z (Zfhx3), Group-N (Nfib, NeuroD2, Prox1), or Group-E (Ebf1) markers. 20um cryosections. Scale bar 100um.

Figure S4

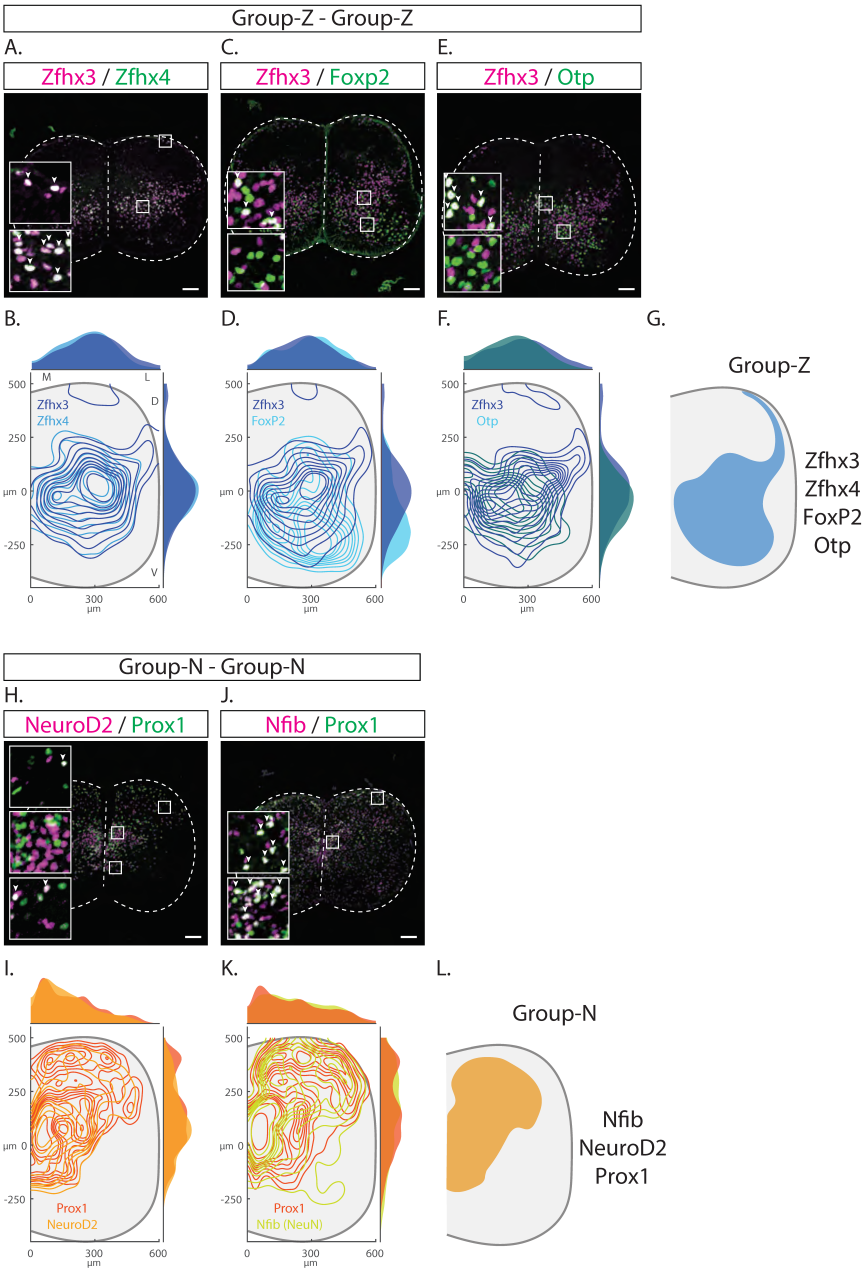

Group-Z - Group-Z
A.
Zfhx3 / Zfhx4
C.
Zfhx3 / Foxp2
E.
Zfhx3 / Otp
B.
D.
F.
G.
Group-Z
Zfhx3
Zfhx4
FoxP2
Otp
Group-N - Group-N
H.
NeuroD2 / Prox1
J.
Nfib / Prox1
I.
K.
L.
Group-N
Nfib
NeuroD2
Prox1

Fig. S4. Colocalization and spatial analysis of multiple Group-Z and Group-N markers

(A-L) Group-Z (Zfhx3, Zfhx4, FoxP2, Otp) and Group-N (Nfib, NeuroD2, Prox1) molecular marker analysis on P0 lumbar spinal cords using immunostaining and cell density contour plots. Y=0 represents the top end of the central canal, and X=0 represents the midline.

(A-G) Group-Z markers partially overlap in expression.

(G) Composite summation of Group-Z marker expression.

(H-L) Group-N markers partially overlap in expression. For the Nfib analysis, $NeuN^{+}$ $Nfib^{+}$ double positive cells were quantified in order to exclude $Nfib^{+}$ glial cells.

(L) Composite summation of Group-N marker expression.

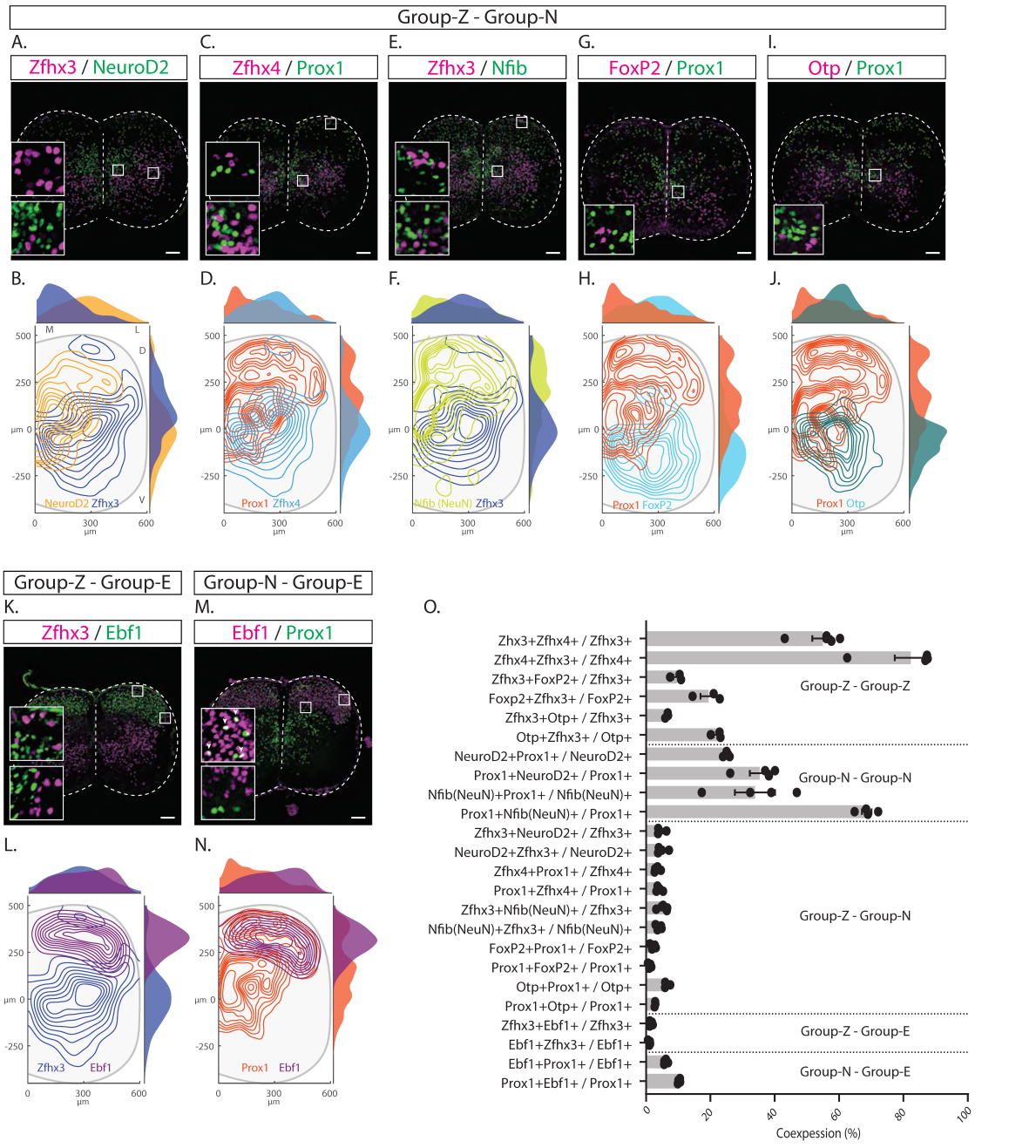

Group-Z - Group-N
A.
Zfhx3 / NeuroD2
C.
Zfhx4 / Prox1
E.
Zfhx3 / Nfib
G.
FoxP2 / Prox1
I.
Otp / Prox1
B.
D.
F.
H.
J.
M
L
D
V
NeuroD2 Zfhx3
Prox1 Zfhx4
Nfib (NeuN) Zfhx3
Prox1 FoxP2
Prox1 Otp
500
250
µm 0
-250
0
300
600
µm
Group-Z - Group-E
Group-N - Group-E
K.
Zfhx3 / Ebf1
M.
Ebf1 / Prox1
L.
N.
Zfhx3 Ebf1
Prox1 Ebf1
O.
Zhx3+Zfhx4+ / Zfhx3+
Zfhx4+Zfhx3+ / Zfhx4+
Zfhx3+FoxP2+ / Zfhx3+
Foxp2+Zfhx3+ / FoxP2+
Zfhx3+Otp+ / Zfhx3+
Otp+Zfhx3+ / Otp+
NeuroD2+Prox1+ / NeuroD2+
Prox1+NeuroD2+ / Prox1+
Nfib(NeuN)+Prox1+ / Nfib(NeuN)+
Prox1+Nfib(NeuN)+ / Prox1+
Zfhx3+NeuroD2+ / Zfhx3+
NeuroD2+Zfhx3+ / NeuroD2+
Zfhx4+Prox1+ / Zfhx4+
Prox1+Zfhx4+ / Prox1+
Zfhx3+Nfib(NeuN)+ / Zfhx3+
Nfib(NeuN)+Zfhx3+ / Nfib(NeuN)+
FoxP2+Prox1+ / FoxP2+
Prox1+FoxP2+ / Prox1+
Otp+Prox1+ / Otp+
Prox1+Otp+ / Prox1+
Zfhx3+Ebf1+ / Zfhx3+
Ebf1+Zfhx3+ / Ebf1+
Ebf1+Prox1+ / Ebf1+
Prox1+Ebf1+ / Prox1+
Group-Z - Group-Z
Group-N - Group-N
Group-Z - Group-N
Group-Z - Group-E
Group-N - Group-E
0
20
40
60
80
100
Coexpression (%)

Fig. S5. Group-E, -N, -Z neuron markers label distinct neuronal populations

(A-N) Molecular marker analysis on P0 lumbar spinal cords using immunostaining and cell density contour plots. Y=0 represents the top end of the central canal, and X=0 represents the midline. Dorsoventral and mediolateral marker densities shown along edge of contour plots.

(A-J) Group-N (Nfib, NeuroD2, Prox1) and Group-Z (Zfhx3, Zfhx4, FoxP2, Otp) markers label separate cells even at the boundaries where the two neuronal groups intermingle. Note, image in A is from Figure 2E. $NeuN^+$ $Nfib^+$ double positive cells were quantified to exclude $Nfib^+$ glial cells.

(K-L) Markers for Group-Z (Zfhx3) and Group-E (Ebf1) are not co-expressed and label spatially separate neuron populations.

(M-N) Markers for Group-N (Prox1) and Group-E (Ebf1) are rarely co-expressed and are largely segregated into discrete domains.

(O) Quantification of molecular marker co-expression for Figure S4 and S5. Each dot represents one animal.

Figure S6

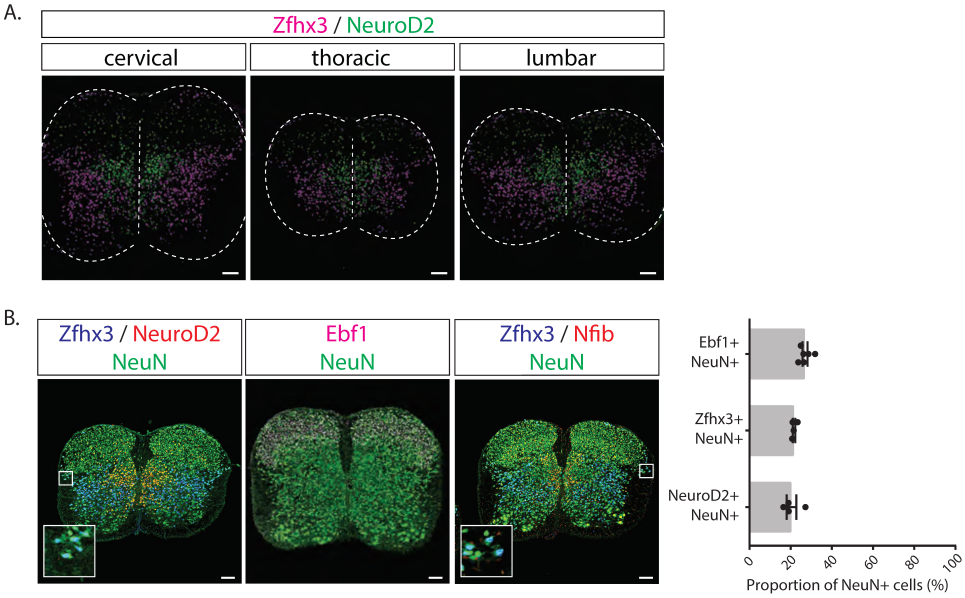

A.
Zfhx3 / NeuroD2
cervical
thoracic
lumbar
B.
Zfhx3 / NeuroD2
NeuN
Ebf1
NeuN
Zfhx3 / Nfib
NeuN
Ebf1+
NeuN+
Zfhx3+
NeuN+
NeuroD2+
NeuN+
0
20
40
60
80
100
Proportion of NeuN+ cells (%)

Fig. S6. Characterization of Group-N, -Z, -E marker expression along the rostrocaudal axis of spinal cord neurons

(A) Group-Z (Zfhx3) and Group-N (NeuroD2) marker expression detected with immunostaining in the P0 cervical, thoracic, and lumbar spinal cord. The relative location of Group-Z and Group-N neurons was similar at each level of the spinal cord. Note, lumbar image is from Figure 2E. 20um cryosections. Scale bar 100um.

(B) Group-Z (Zfhx3), Group-N (NeuroD2), and Group-E (Ebf1) $NeuN^+$ neurons detected with immunostaining in the P0 lumbar spinal cord. Neurons in the lateral spinal nucleus, located within the dorsolateral funiculus, expressed Group-Z markers. Quantification of double-labeling reveals Group-Z, -N, and -E each represent a substantial (non-overlapping, see S5) portion of spinal neurons. 20um cryosections. Scale bar 100um.

Figure S7

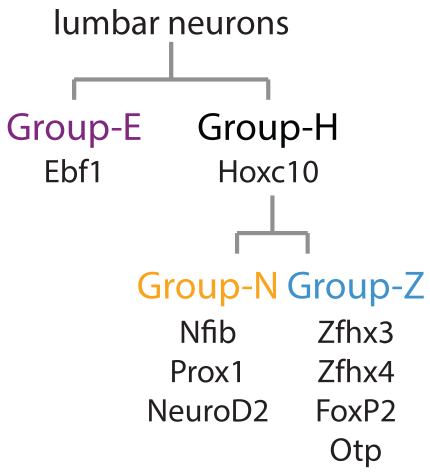

lumbar neurons
Group-E
Ebf1
Group-H
Hoxc10
Group-N
Nfib
Prox1
NeuroD2
Group-Z
Zfhx3
Zfhx4
FoxP2
Otp

Fig. S7. Summary dendrogram of marker genes for Group-H, -E, -Z, -N neurons

Data summarized from Figures 1-2, and S1-S5.

Figure S8

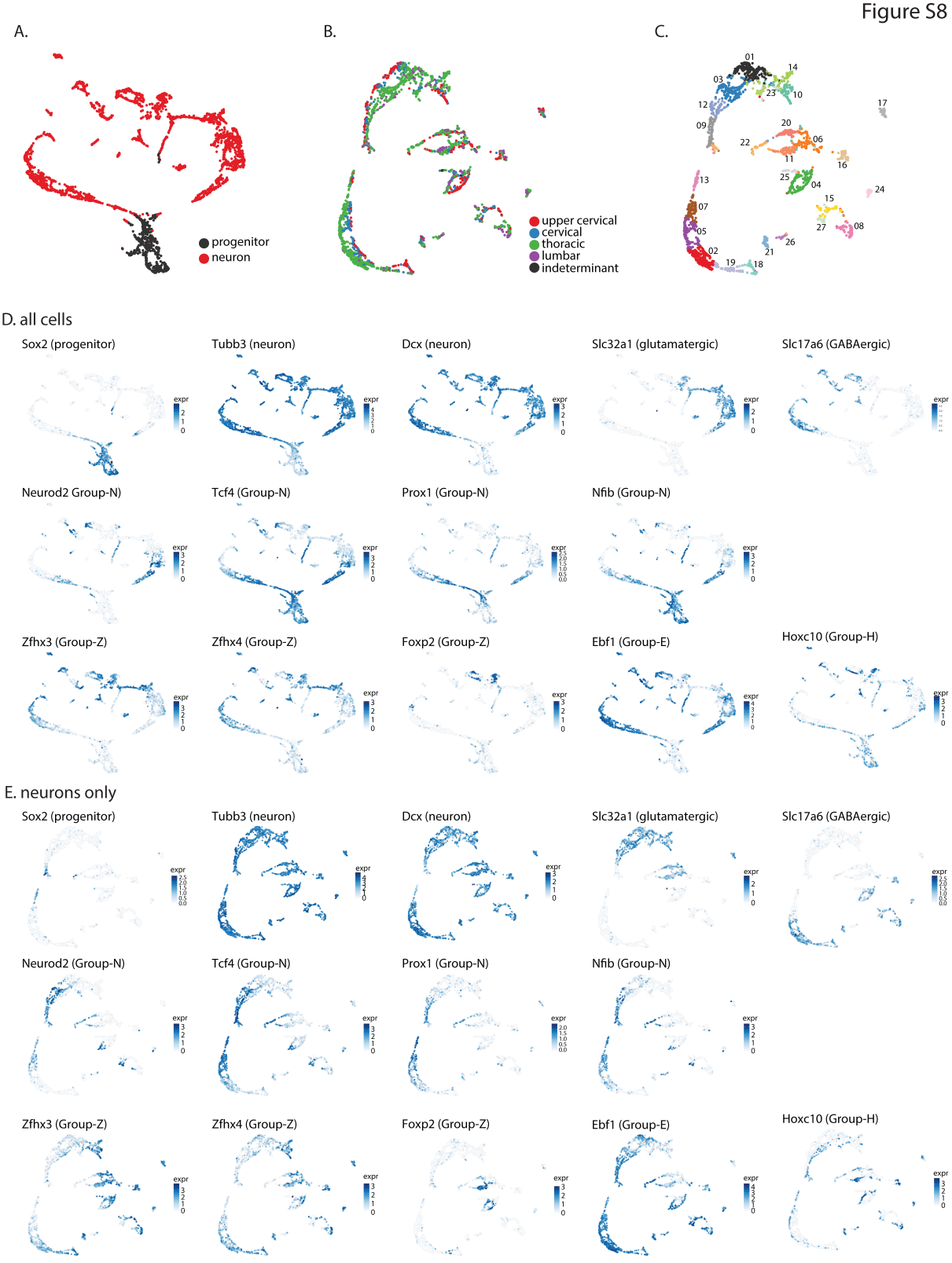

A.
progenitor
neuron
B.
upper cervical
cervical
thoracic
lumbar
indeterminant
C.
01
14
03
23
10
12
17
09
20
06
22
11
16
25
04
24
13
15
07
27
08
05
26
02
21
19
18
D. all cells
Sox2 (progenitor)
Tubb3 (neuron)
Dcx (neuron)
Slc32a1 (glutamatergic)
Slc17a6 (GABAergic)
Neurod2 Group-N)
Tcf4 (Group-N)
Prox1 (Group-N)
Nfib (Group-N)
Zfhx3 (Group-Z)
Zfhx4 (Group-Z)
Foxp2 (Group-Z)
Ebf1 (Group-E)
Hoxc10 (Group-H)
E. neurons only
Sox2 (progenitor)
Tubb3 (neuron)
Dcx (neuron)
Slc32a1 (glutamatergic)
Slc17a6 (GABAergic)
Neurod2 (Group-N)
Tcf4 (Group-N)
Prox1 (Group-N)
Nfib (Group-N)
Zfhx3 (Group-Z)
Zfhx4 (Group-Z)
Foxp2 (Group-Z)
Ebf1 (Group-E)
Hoxc10 (Group-H)

Fig. S8. E12.5 scRNA-seq analysis of neural tube cells

(A) Single cells from the E12.5 neural tube were isolated and scRNA-seq was performed. UMAP depicting progenitor cells and neurons based on marker expression. Neurons were selected for further analysis in B, C, E.

(B) The segmental identity of each E12.5 neuron was classified using Hox gene expression.

(C) 27 transcriptionally distinct clusters were identified in UMAP space. Clusters are not obviously divided based on their rostrocaudal segment identity (compare B and C).

(D) Individual gene expression level in each cell.

(E) Individual gene expression level in each neuron. The broad expression of Ebf1 and Hoxc10 in E12.5 cells suggests Group-E and Group-H identity is not yet fully established at this age.

Figure S9

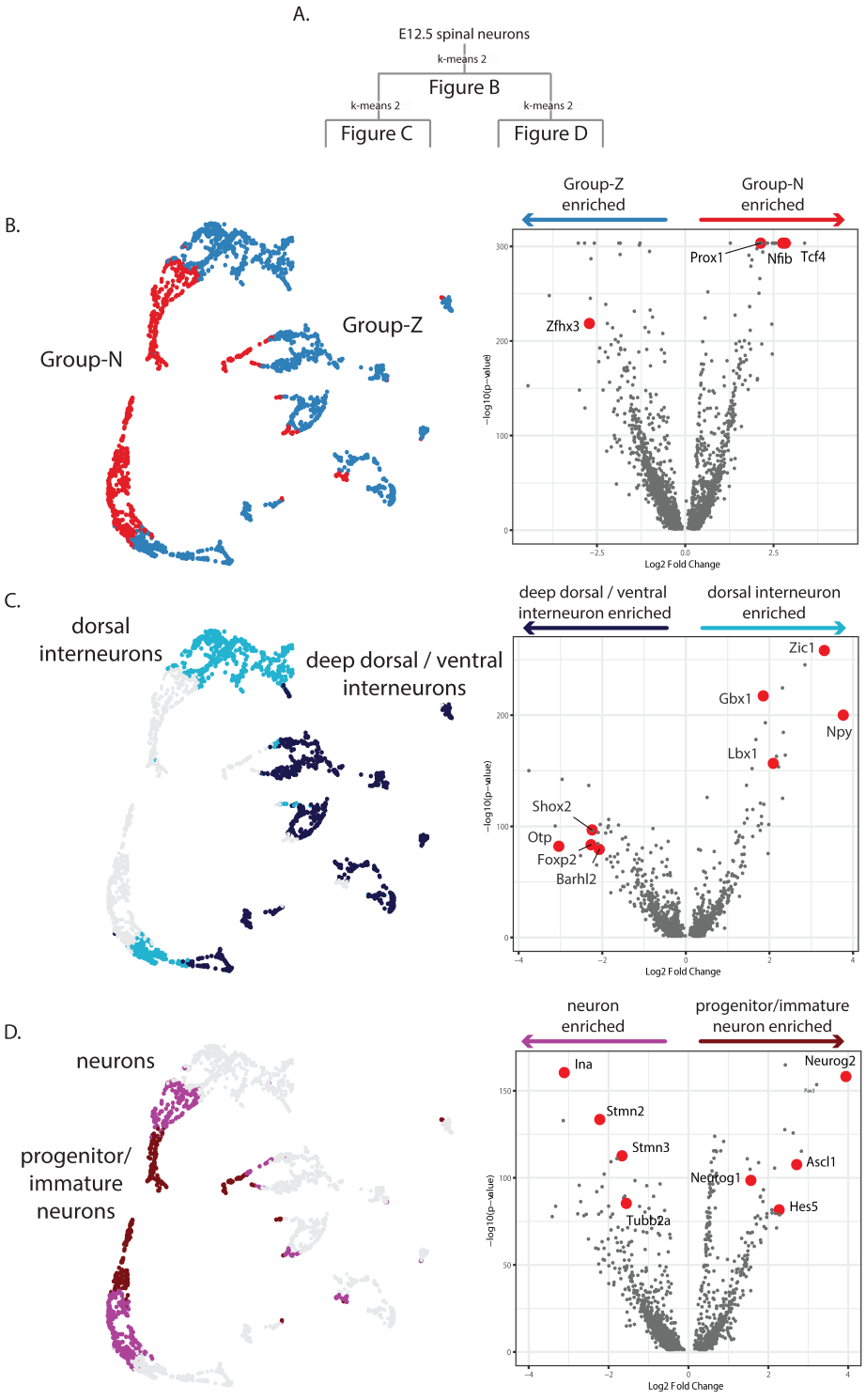

A.
E12.5 spinal neurons
k-means 2
Figure B
k-means 2
k-means 2
Figure C
Figure D
B.
Group-N
Group-Z
Group-Z enriched
Group-N enriched
Prox1
Nfib
Tcf4
Zfhx3
−log10(p−value)
Log2 Fold Change
C.
dorsal interneurons
deep dorsal / ventral interneurons
deep dorsal / ventral interneuron enriched
dorsal interneuron enriched
Zic1
Gbx1
Npy
Lbx1
Shox2
Otp
Foxp2
Barhl2
−log10(p−value)
Log2 Fold Change
D.
neurons
progenitor/ immature neurons
neuron enriched
progenitor/immature neuron enriched
Ina
Neurog2
Stmn2
Stmn3
Ascl1
Neurog1
Hes5
Tubb2a
−log10(p−value)
Log2 Fold Change

Fig. S9. k-means 2 divisions of E12.5 scRNA-seq reveal neuronal groups and states

(A) Hierarchical relationships across E12.5 embryonic neuron transcriptomes were identified via k-means 2 divisive clustering. Outline of sequential divisions is shown.

(B) Group-N and Group-Z markers were enriched in the cell populations identified by the first division.

(C) At E12.5 Group-Z interneurons can be further split into dorsal interneurons and deep dorsal/ventral interneurons. Dorsal interneuron population: 782 cells; Jaccard similarity 0.851, Deep dorsal/ventral interneuron population: 1189 cells; Jaccard similarity 0.933. Red dots indicate well established markers.

(D) At E12.5 Group-N neurons represent a mixture of progenitor/immature neurons and neurons, revealed by the differential gene expression in the volcano plot (red dots indicate well established markers). Neuron population: 570 cells; Jaccard similarity 0.902, progenitor/immature neuron population: 404 cells; Jaccard similarity 0.951.

Figure S10

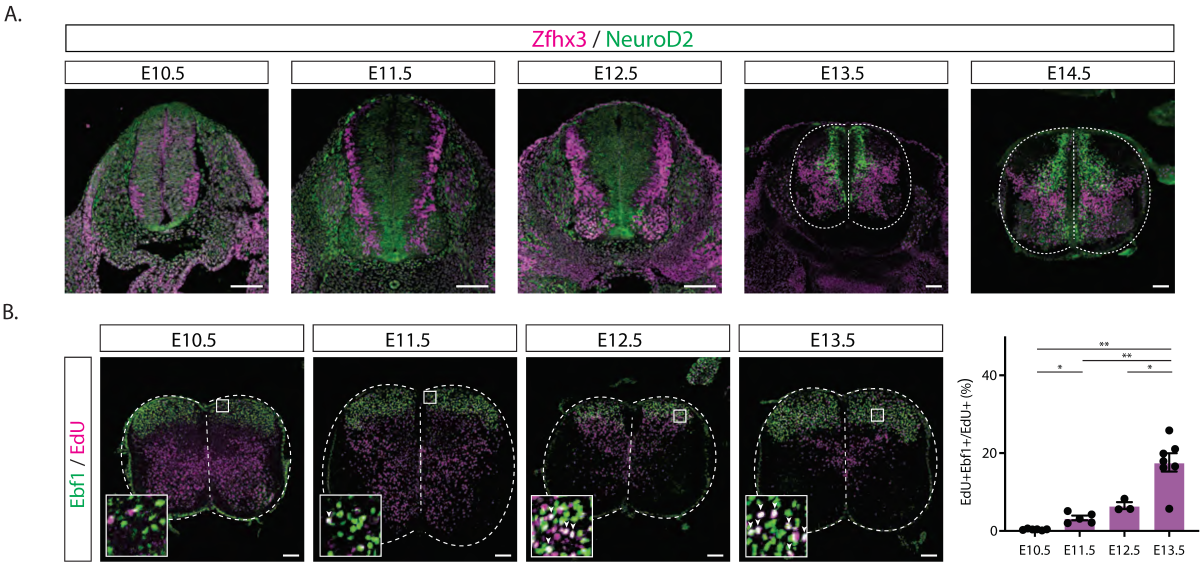

A.
Zfhx3 / NeuroD2
E10.5
E11.5
E12.5
E13.5
E14.5
B.
E10.5
E11.5
E12.5
E13.5
Ebf1 / EdU
EdU+Ebf1+/EdU+ (%)
40
20
0
**
**
*
*
E10.5
E11.5
E12.5
E13.5

Fig. S10. Embryonic development of Group-N, -Z, and -E neurons

(A) Immunostaining was conducted to detect Group-Z (Zfhx3) and Group-N (NeuroD2) cells in the developing spinal cord from E10.5-E14.5. Zfhx3 was detected in neurons beginning at E10.5, whereas NeuroD2 was not detected in mature neurons until E12.5. Lumbar spinal cord, 12um cryosections. Scale bar 100um.

(B) Birthdating analysis of Group-E neurons using EdU pulses at E10.5-E13.5, followed by immunostaining in the lumbar P0 spinal cord. Most Group-E neurons are born after E12.5 (detected as $Ebf1^{+}$ EdU^{+} colabeling). Co-expression of Ebf1 in EdU^{+} cells is quantified at each time point. Welch One-way ANOVA comparing every timepoint to every other timepoint, with Dunnett T3 correction for multiple comparisons. *$p \leq 0.05$, **$p \leq 0.01$, ***$p \leq 0.001$. 20um cryosections. Scale bar 100um.

Figure S11

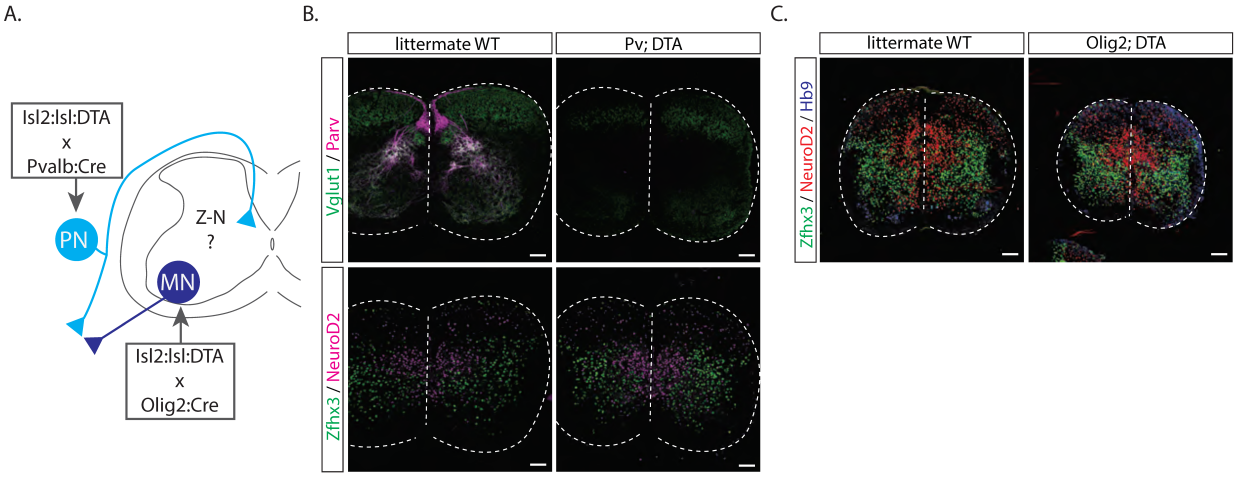

A.
Isl2:Isl:DTA
x
Pvalb:Cre
PN
Z-N
?
MN
Isl2:Isl:DTA
x
Olig2:Cre
B.
littermate WT
Pv; DTA
Vglut1 / Parv
Zfhx3 / NeuroD2
C.
littermate WT
Olig2; DTA
Zfhx3 / NeuroD2 / Hb9

Fig. S11. Group-N and -Z neurons develop properly in the absence of sensory or motor neurons

(A) Genetic strategy to selectively ablate either proprioceptors using Parvalbumin:Cre crossed to Isl2:lsl:DTA or motor neurons using Olig2:Cre crossed to Isl2:lsl:DTA mice.

(B) As expected, proprioceptor fibers and terminals ($Pvalb^{+}$ $Vglut1^{+}$) are absent in Parvalbumin:Cre x Isl2:lsl:DTA animals. Zfhx3 (Group-Z marker) and NeuroD2 (Group-N marker) were expressed normally in the P6 lumbar spinal cord of mice lacking proprioceptor inputs. 20um cryosections. Scale bar 100um.

(C) As expected, motor neurons ($Hb9^{+}$) are ablated in Olig2:Cre x Isl2:lsl:DTA mice. Zfhx3 (Group-Z marker) and NeuroD2 (Group-N marker) were expressed normally in the E17 lumbar spinal cord of mice lacking motor neurons. 12um cryosections. Scale bar 100um.

Figure S12

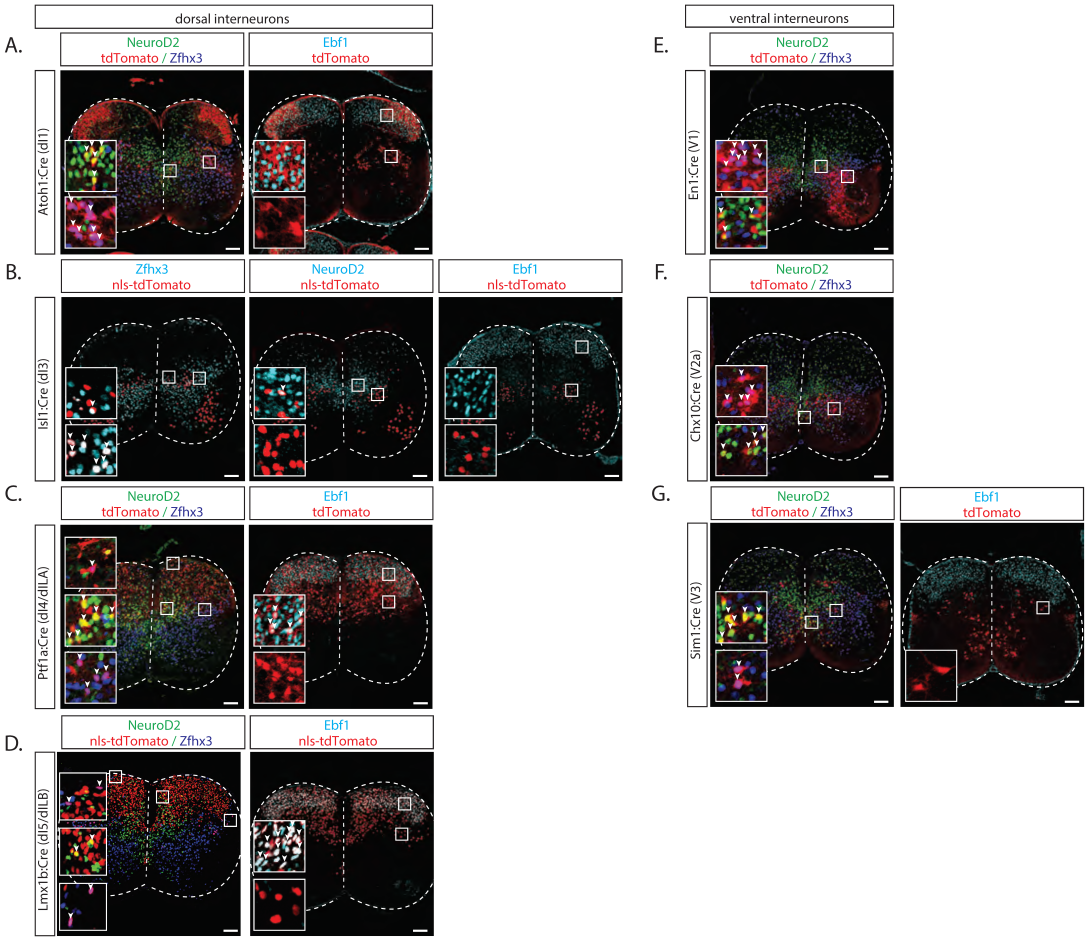

dorsal interneurons
A.
NeuroD2
tdTomato / Zfhx3
Ebf1
tdTomato
Atoh1:Cre (dI1)
B.
Zfhx3
nls-tdTomato
NeuroD2
nls-tdTomato
Ebf1
nls-tdTomato
Isl1:Cre (dI3)
C.
NeuroD2
tdTomato / Zfhx3
Ebf1
tdTomato
Ptf1a:Cre (dI4/dILA)
D.
NeuroD2
nls-tdTomato / Zfhx3
Ebf1
nls-tdTomato
Lmx1b:Cre (dI5/dILB)
ventral interneurons
E.
NeuroD2
tdTomato / Zfhx3
En1:Cre (V1)
F.
NeuroD2
tdTomato / Zfhx3
Chx10:Cre (V2a)
G.
NeuroD2
tdTomato / Zfhx3
Ebf1
tdTomato
Sim1:Cre (V3)

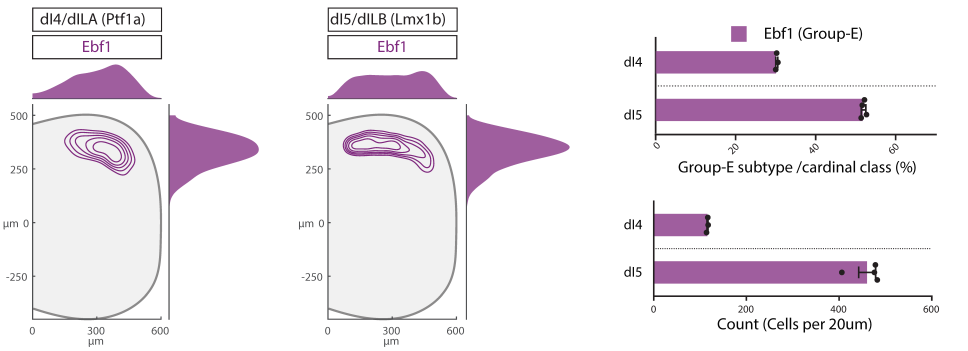
Fig. S12. Each cardinal neuron class is a mixture of both Group-N and Group-Z neurons

(A-G) Spinal neuron cardinal classes were genetically labeled using the indicated Cre lines with tdTomato reporters and immunostained with markers for Group-E (Ebf1), -N (NeuroD2), and -Z (Zfhx3) neurons at lumbar levels of P0 mice. All cardinal classes examined expressed Group-N and Group-Z markers (tdTomato$^+$ NeuroD2$^+$ and tdTomato$^+$ Zfhx3$^+$; white arrowheads in insets). Only neurons derived from the cardinal classes dI4 and dI5 expressed Group-E marker Ebf1.

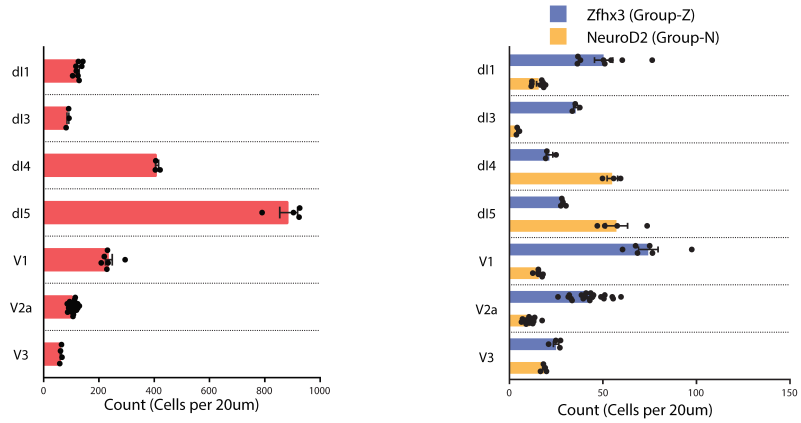
(C, D). Group-Z (Zfhx3) neurons found in the very superficial dorsal horn (i.e. lamina 1) arise from the dI4 and dI5 lineages. Some Group-Z neurons arising from the dI5 lineage were located in the lateral spinal nucleus (insets).

Figure S13

A.



B.



C.

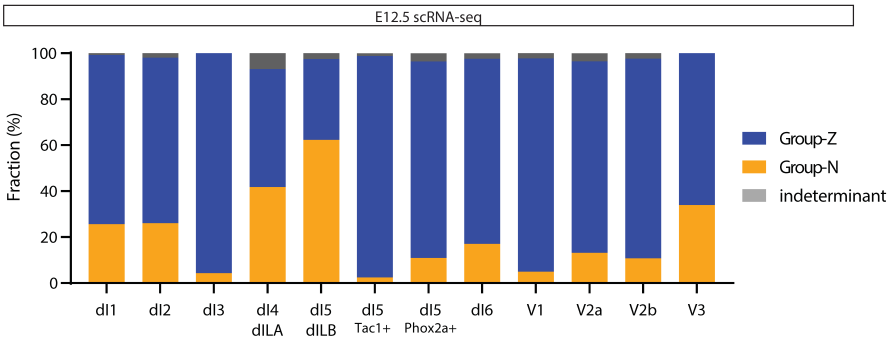


Fig. S13. Quantification of Group-E, -N, and -Z neurons that arise from each cardinal neuron class

(A) Spatial distribution plots (contour plots and cell quantification along the x-y axes) and neuron counts of Ebf1^{+} Group-E neurons derived from dI4/dILA and dI5/dILB neuron cardinal classes marked using Ptf1a:Cre (dI4/dILA) and Lmx1b:Cre (dI5/dILB) together with tdTomato reporters at P0.

(B) Quantification of Group-N (NeuroD2) and -Z (Zfhx3) neurons within each cardinal class marked by Cre and tdTomato (see Figure S12 for Cre lines) in the lumbar P0 spinal cord. Left histogram plots the number of cells from each cardinal class. Right histogram plots the number of Group-Z and Group-N cells comprising each cardinal class. Note, individual cardinal classes have different neuronal numbers and different fractions of Group-N and Group-Z neurons.

(C) scRNA-seq analysis reveals that the vast majority of identified cardinal class neurons express either Group-N or Group-Z markers at E12.5.

Figure S14

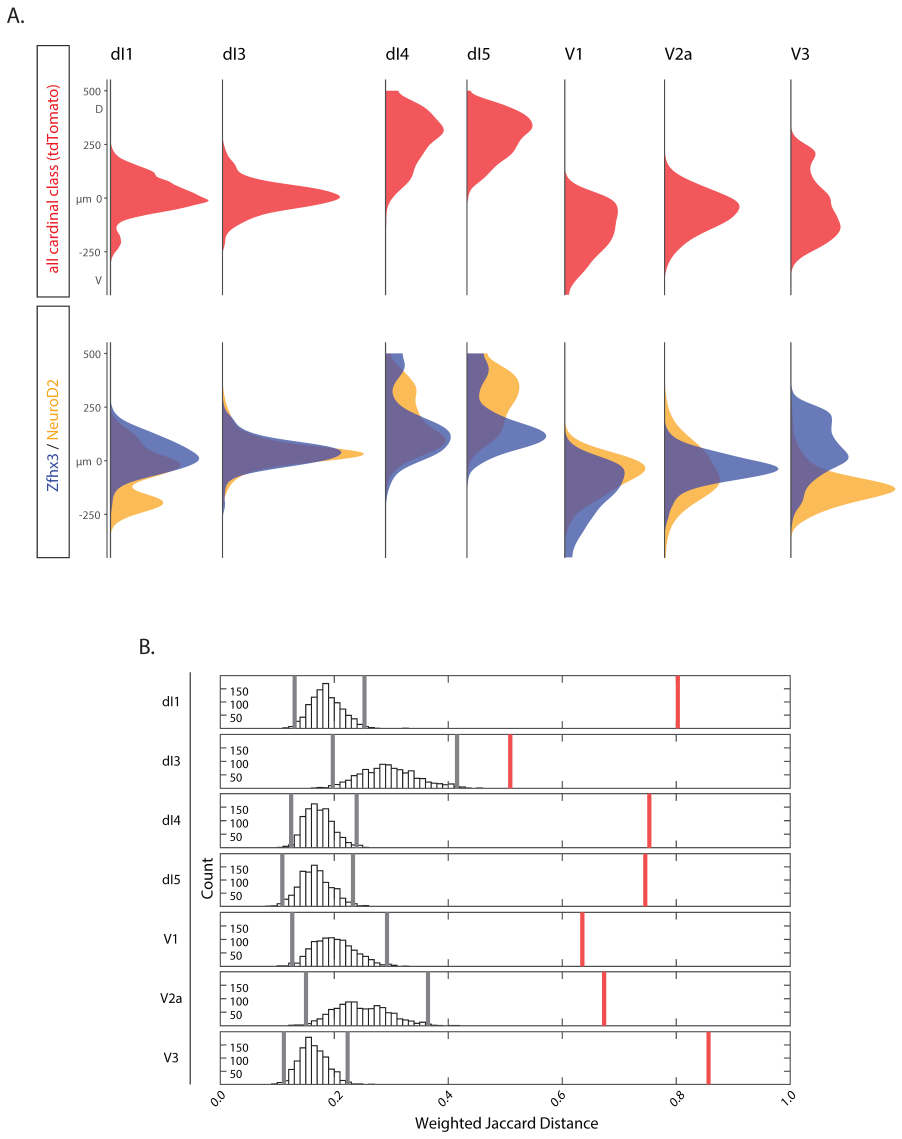

A.
dI1
dI3
dI4
dI5
V1
V2a
V3
all cardinal class (tdTomato)
Zfhx3 / NeuroD2
500
D
250
µm 0
-250
V
B.
Count
150
100
50
0.0
0.2
0.4
0.6
0.8
1.0
Weighted Jaccard Distance

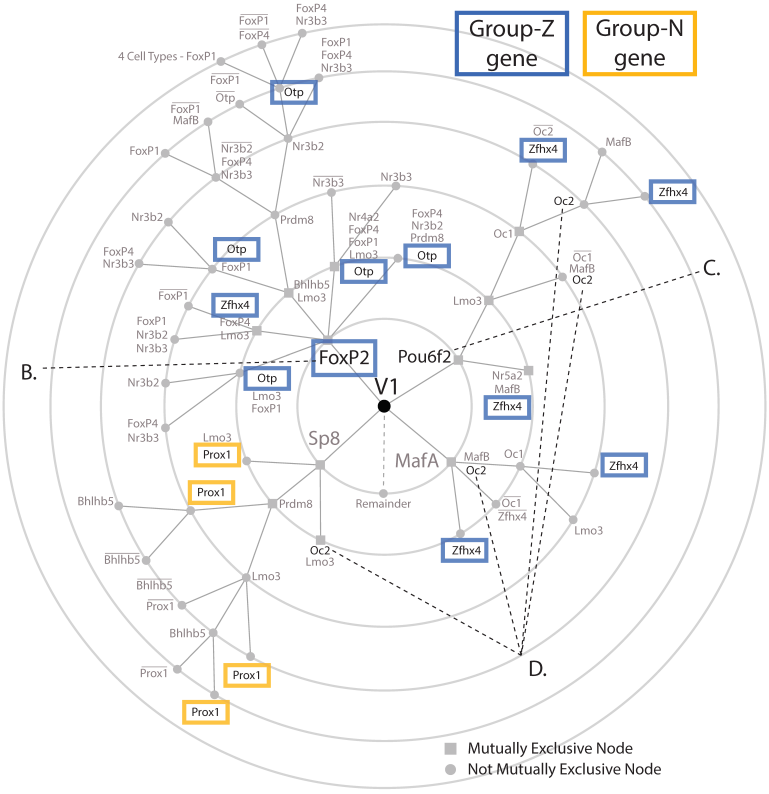
Fig. S14. Spatial characterization of Group-N and -Z neurons from each cardinal class

(A) Top row: cell densities for the cardinal neuron classes labeled using Cre and tdTomato (Cre lines indicated in Fig S12) plotted along the dorsoventral axis of the lumbar P0 spinal cord (red). Cardinal neuron classes have broad but stereotypical settling patterns along the dorsoventral axis of the spinal cord.

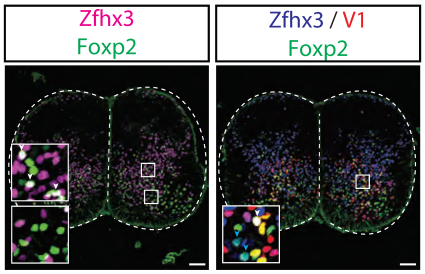
Bottom row: the Group-N (NeuroD2) and Group-Z (Zfhx3) composition and position of each cardinal class is plotted along the dorsoventral axis in yellow and blue, respectively. Although Group-N and Group-Z neurons segregate along the mediolateral axis of the neural tube (see Fig 4), there was not a consistent dorsoventral separation of the subtypes when examined in the context of each cardinal interneuron class.

(B) Weighted Jaccard distance for groups within each cardinal class. Red line represents the measured distance between Group-N and Group-Z for each cardinal class. The group identities were shuffled and bootstrapped to create a distribution of Weighted Jaccard distances, the gray lines designate 1st and 99th percentiles for bootstrapped distances (see methods). This analysis indicates that Group-N and Group-Z neurons form discrete cell populations that segregate greater than chance.

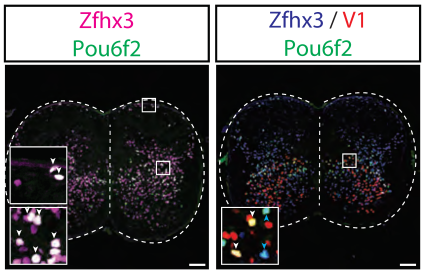
A. Adapted from Gabitto et al. 2016



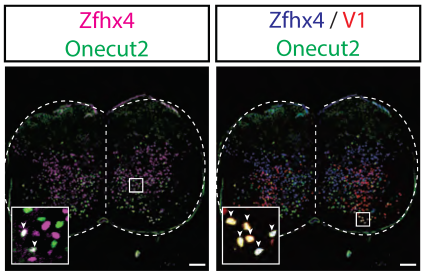
B.



C.



D.



E.

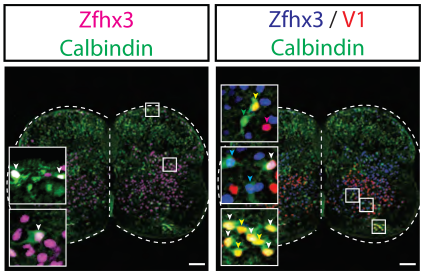


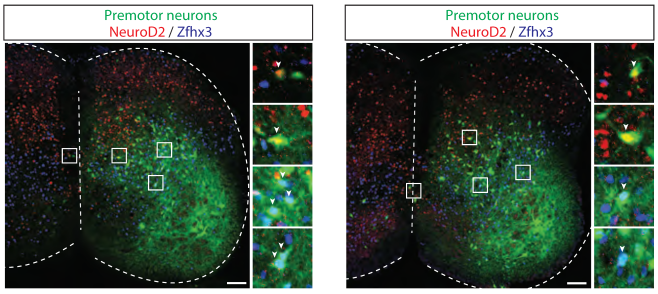
Fig. S15. Group-N and -Z divisions amongst the V1 cardinal class clades

(A) Diagram adapted from Gabitto et al., 2016 (*10, 20*), showing that the V1 interneuron cardinal class can be further divided into four molecularly distinct clades based on the expression profile of FoxP2, Pou6f2, MafA, and Sp8. Division of the four main clades into further subtypes is indicated by additional branches. Group-N and Group-Z markers are highlighted in this diagram in yellow and blue, respectively. Three clades, FoxP2, Pou6f2, and MafA express Group-Z genes (blue boxes), while subtypes in the Sp8 clade express Group-N genes (yellow boxes). As per original figure, a bar above a transcription factor name denotes lack of expression. Transcription factor names in black are Group-N, Group-Z, and/or are analyzed below in panels B-D.

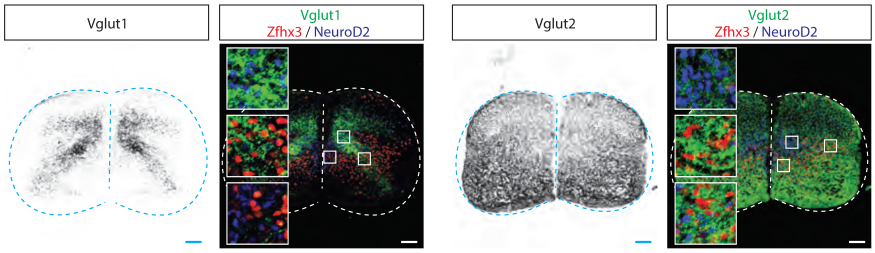
(B-E) En1:Cre was crossed to a tdTomato reporter to label the entire V1 neuron cardinal class. Immunostaining for clade and Group-Z markers demonstrates that Pou6f2 and Foxp2 clades express Zfhx3 consistent with the prediction in (A). Renshaw cells represent a well characterized subpopulation of V1 neurons marked by Calbindin. We found Zfhx3^{+} Calbindin^{+} V1 (En1:Cre) neurons, indicating some Group-Z neurons are Renshaw cells. Note panel (B) is from Fig S4C. P0 lumbar spinal cord. 20um cryosections. Scale bar 100um.

Figure S16

A.



B.



C.

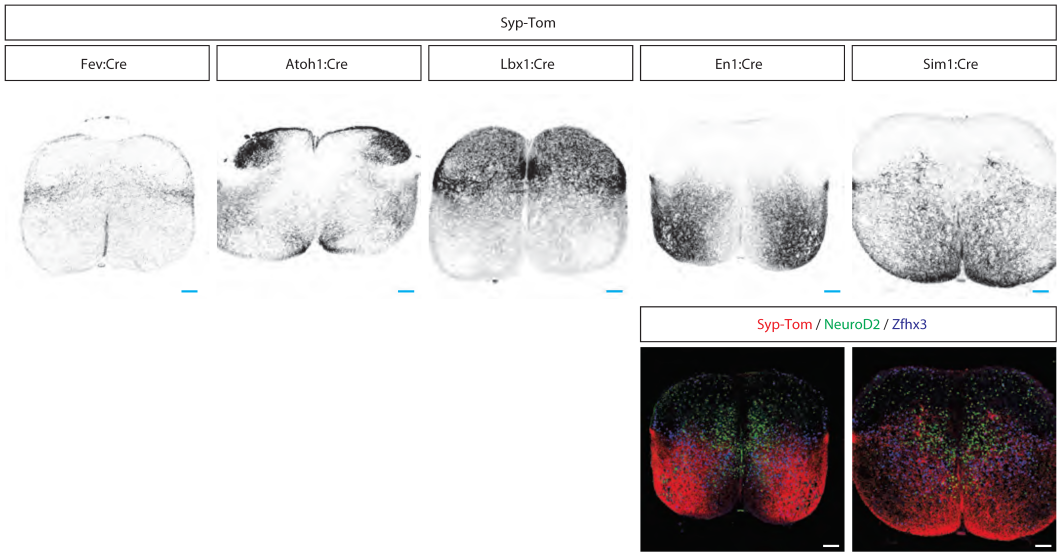


Fig. S16. Group-N and -Z neurons synapse with motor neurons and receive diverse inputs

(A) AAV6-CAG-Flex-oG-WPRE-SV40-pA was injected into TA muscles of P4 ChAT:Cre mice, followed by the injection of ΔG-GFP rabies at P7 to monosynaptically label premotor spinal neurons in lumbar segments at P14. $GFP^{+}Zfhx3^{+}$ cells represent premotor Group-Z neurons, and $GFP^{+}NeuroD2^{+}$ cells correspond to premotor Group-N neurons. 60um cryosections. Scale bar 100um.

(B) $Vglut1^{+}$ terminals are primarily from DRG sensory neurons, whereas $Vglut2^{+}$ terminals are primarily CNS-derived in the neonatal spinal cord (*24*). Triple labeling revealed that both Group-Z (Zfhx3) and Group-N (NeuroD2) neurons receive $Vglut1^{+}$ and $Vglut2^{+}$ inputs. 20um cryosections. Scale bar 100um.

(C) Indicated Cre lines were crossed to a tdTomato-Synaptophysin reporter to identify the synaptic terminals of genetically-defined spinal neurons within the P1 lumbar cord. V1 neurons marked by En1:Cre, and V3 neurons marked by Sim1:Cre have post-synaptic targets within the ventral spinal cord that include both Group-N (NeuroD2) and Group-Z (Zfhx3) cells. 20um cryosections. Scale bar 100um.

Figure S17

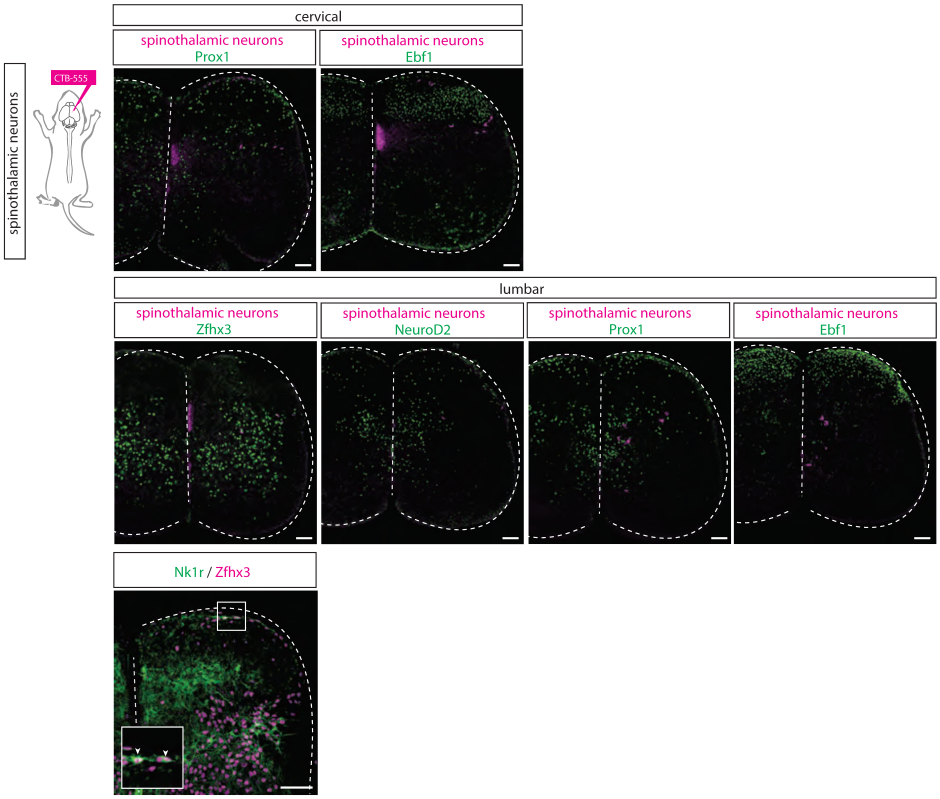

spinothalamic neurons
CTB-555
cervical
spinothalamic neurons
Prox1
spinothalamic neurons
Ebf1
lumbar
spinothalamic neurons
Zfhx3
spinothalamic neurons
NeuroD2
spinothalamic neurons
Prox1
spinothalamic neurons
Ebf1
Nk1r / Zfhx3

Fig. S17. Cervical and lumbar spinothalamic neurons express Group-Z markers

CTB was injected into the thalamus to label spinothalamic neurons located in the cervical and lumbar spinal cord. Staining was performed with markers for Group-Z (Zfhx3), Group-E (Ebf1), and Group-N (NeuroD2, Prox1) neurons. The majority of CTB^+ spinothalamic cells were marked by Zfhx3, but not Ebf1, NeuroD2 or Prox1. The $Zfhx3^+$ cells in the superficial region of lamina 1 expressed spinothalamic neuron marker Nk1r (*5*), providing independent confirmation that these neurons project to the thalamus. 20um cryosections. Scale bar 100um.

Figure S18

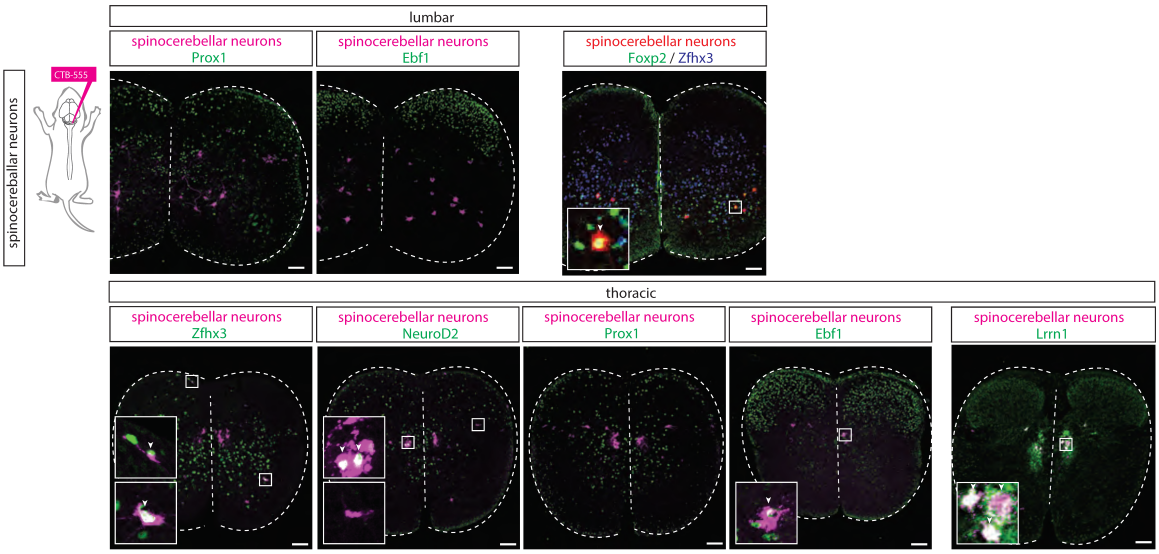

lumbar
spinocerebellar neurons
Prox1
spinocerebellar neurons
Ebf1
spinocerebellar neurons
Foxp2 / Zfhx3
spinocerebellar neurons
CTB-555
thoracic
spinocerebellar neurons
Zfhx3
spinocerebellar neurons
NeuroD2
spinocerebellar neurons
Prox1
spinocerebellar neurons
Ebf1
spinocerebellar neurons
Lrrn1

Fig. S18. Lumbar spinocerebellar neurons express Group-Z markers

CTB was injected into the cerebellum to label spinocerebellar neurons located in the lumbar and thoracic spinal cord. Staining was performed with markers for Group-Z (Zfhx3, Foxp2), Group-E (Ebf1), and Group-N (NeuroD2, Prox1) neurons. The majority of CTB^+ spinocerebellar neurons were marked by Zfhx3 and/or Foxp2, but not Ebf1, NeuroD2 or Prox1. In thoracic segments, spinocerebellar neurons form a discrete group called Clark's column, marked by Lrrn1 (*28*). Although Clark's column is comprised of projection neurons, a fraction of Clark's column neurons expressed NeuroD2, a Group-N marker. Thoracic spinocerebellar neurons that were not part of Clark's column lacked NeuroD2 and expressed Zfhx3 as expected for projection neurons. 20um cryosections. Scale bar 100um.

Figure S19

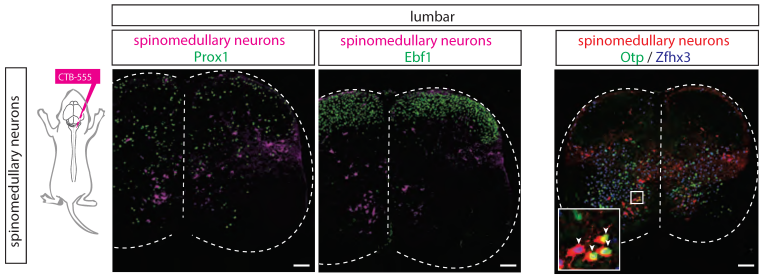

lumbar
spinomedullary neurons
Prox1
spinomedullary neurons
Ebf1
spinomedullary neurons
Otp / Zfhx3
spinomedullary neurons
CTB-555

Fig. S19. Spinomedullary neurons express Group-Z markers

CTB was injected into the medulla to label spinomedullary neurons located in the lumbar spinal cord. Staining was performed with markers for Group-Z (Zfhx3, Otp), Group-E (Ebf1), and Group-N (Prox1) neurons. The majority of CTB^{+} spinomedullary cells were marked by Zfhx3 and/or Otp, but not Ebf1 or Prox1. 20um cryosections. Scale bar 100um.

Figure S20

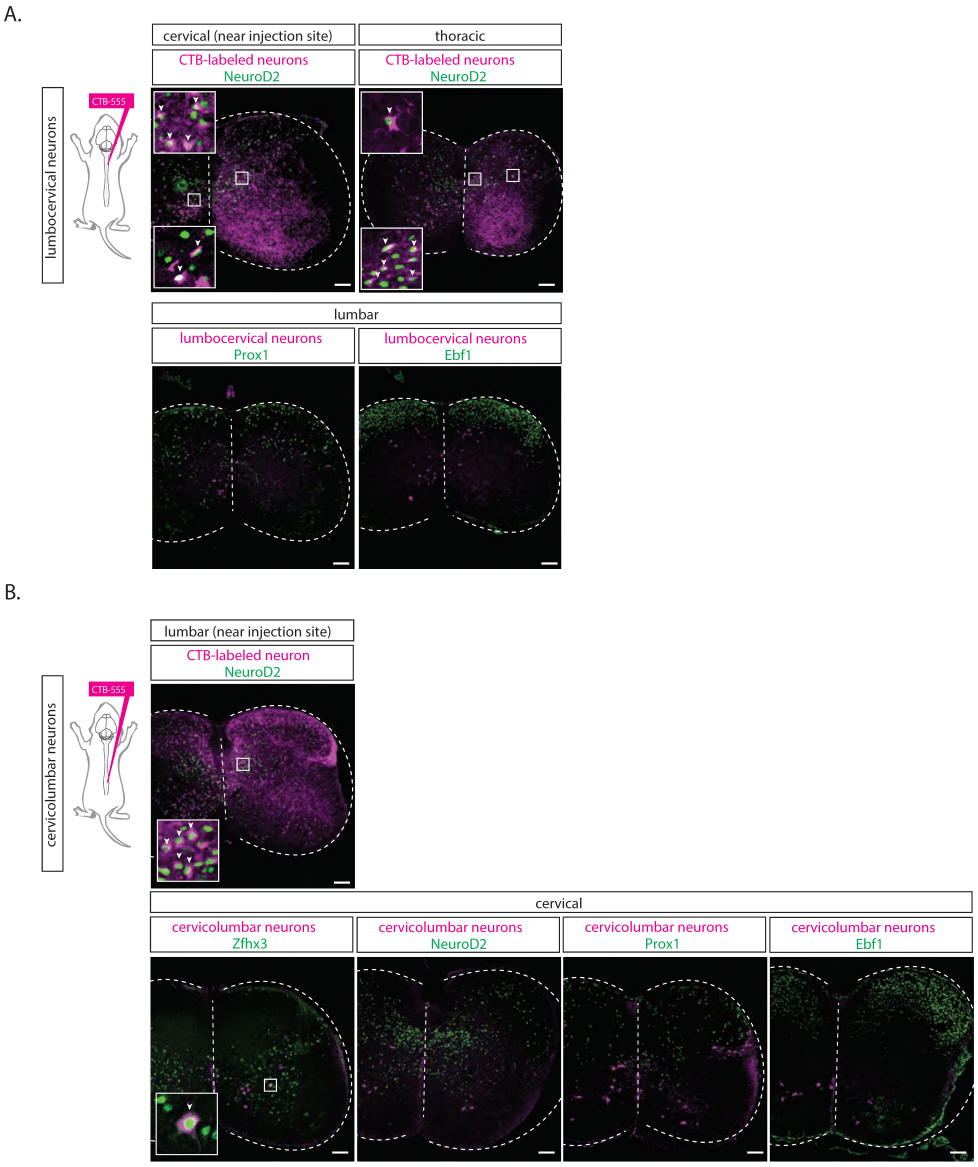

A.
cervical (near injection site)
thoracic
CTB-labeled neurons
NeuroD2
CTB-labeled neurons
NeuroD2
lumbocervical neurons
CTB-555
lumbar
lumbocervical neurons
Prox1
lumbocervical neurons
Ebf1
B.
lumbar (near injection site)
CTB-labeled neuron
NeuroD2
cervicolumbar neurons
CTB-555
cervical
cervicolumbar neurons
Zfhx3
cervicolumbar neurons
NeuroD2
cervicolumbar neurons
Prox1
cervicolumbar neurons
Ebf1

Fig. S20. Propriospinal cervicolumbar and lumbocervical neurons express Group-Z markers

(A) CTB was injected into the cervical spinal cord. Immunostaining for Group-N (NeuroD2) markers labeled local CTB^+ neurons in the cervical and thoracic spinal cord near the injection site. However, lumbocervical neurons (in lumbar cord) did not express Group-N (Prox1) or Group-E (Ebf1) makers. 20um cryosections. Scale bar 100um.

(B) CTB was injected into the lumbar spinal cord. Immunostaining for Group-E (Ebf1), Group-N (NeuroD2, Prox1), and Group-Z (Zfhx3) markers revealed that Group-N neurons were labeled near the lumbar injection site. However, propriospinal cervicolumbar neurons (in the cervical cord) expressed the Group-Z marker Zfhx3 and lacked Group-N/E markers. 20um cryosections. Scale bar 100um.

Figure S21

A.

Intersectional neuronal features

	Group-N (NeuroD2)	Group-Z (Zfhx3)
dI1 (Atoh1)	Glutamatergic; mixed; dorsal	
	medial; short-range; late-born	lateral; long-range; early-born
dI2 (Ngn1)	Glutamatergic; mixed; dorsal	
	medial; short-range; late-born	lateral; long-range; early-born
dI3 (Isl1)	Glutamatergic; ipsilateral; dorsal	
	medial; short-range; late-born	lateral; long-range; early-born
dI4 (Ptf1a)	GABAergic; mixed; dorsal	
	medial; short-range; late-born	lateral; long-range; early-born
d5 (Lmx1b)	Glutamatergic; mixed; dorsal	
	medial; short-range; late-born	lateral; long-range; early-born
dI6 (Wt1)	GABAergic; mixed; ventral;	
	medial; short-range; late-born	lateral; long-range; early-born
V0 (Evx1)	mix (Glut: V0v; GABA: V0d; ACh: V0c); mixed; ventral	
	medial; short-range; late-born	lateral; long-range; early-born
V1 (En1)	GABAergic; ipsilateral; ventral	
	medial; short-range; late-born	lateral; long-range; early-born
V2a (Chx10)	Glutamatergic; ipsilateral; ventral	
	medial; short-range; late-born	lateral; long-range; early-born
V2b (Gata3)	GABAergic; ipsilateral; ventral	
	medial; short-range; late-born	lateral; long-range; early-born
V3 (Sim1)	Glutamatergic; mixed; ventral	
	medial; short-range; late-born	lateral; long-range; early-born

B.

Anatomical studies of cardinal projection pathways

	Projection Neuron target (predicted Group-Z)
dI1 (Atoh1)	spinocerebellar projecting (Yuengert et al. 2015; Sakai et al. 2012)
dI2 (Ngn1)	spinocerebellar projecting (Sakai et al. 2012)
dI3 (Isl1)	LRN projecting (Pivetta et al. 2014)
dI4 (Ptf1a)	propriospinal projecting (Nishida and Ito 2017)
d5 (Lmx1b)	spinothalamic projecting (Nishida and Ito 2017; (Roome et al. 2020)
dI6 (Wt1)	
V0 (Evx1)	cervicolumbar projecting (Ruder et al. 2016)
V1 (En1)	LRN projecting (Pivetta et al. 2014)
V2a (Chx10)	LRN projecting (Pivetta et al. 2014; Azim et al. 2014; Hayashi et al. 2018) cervicolumbar projecting (Ruder et al. 2016)
V2b (Gata3)	cervicolumbar projecting (Flynn et al. 2017)
V3 (Sim1)	LRN projecting (Pivetta et al. 2014)

Fig. S21. Summary of neuronal features encapsulated by cardinal class and Group-Z/N identity

(A) Most cardinal classes have stereotyped dorsoventral settling position, neurotransmitter status, and ipsilateral or mixed projection patterns. Group-N neurons are late-born during development, medially located, and have short range projections. Group-Z neurons are early born, laterally located, and have long range projections. Given the cardinal class and Group-N/Z identity of a given neuron in the spinal cord, many neuronal properties can be predicted.

(B) Many studies have shown evidence for various cardinal classes containing long range projections to assorted targets. Long range neurons tend to express Group-Z markers, thus the long projecting cardinal neurons identified in each study are predicted to be Group-Z neurons. While long range neurons express Group-Z markers, the intersection of cardinal class and Group-Z status appears to yield additional information on each sub-set's long range target specificity.

Table S1. P0 neuron 45 cluster solution enriched genes and cardinal class identification

Table showing enriched genes from clustering solution depicted in 1C, 1D. Top row is predicted cardinal class based on marker genes. Second row is cluster number. Genes highlighted in yellow were used for cardinal class predictions based on literature.

Table S2. Top differentially expressed genes between Group-N and Group-Z neurons

Related to Figure 1I. Table showing top 25 genes enriched for each group when comparing Group-N neurons to Group-Z neurons. Columns indicate gene id, adjusted p-value, average expression in each group, and log fold change.

Table S3. E12.5 neuron 27 cluster solution enriched genes and cardinal class identification

Table showing enriched genes from clustering solution depicted in 3B. Top row is predicted cardinal class based on marker genes. Second row is cluster number. Genes highlighted in yellow were used for cardinal class predictions based on literature.

Table S4. GO terms analysis comparing Group-N/Z neurons

Columns indicate term id, db name, description, enrichment score, adjusted p-value, and drivers (genes underlying term).

Table S5. Animal and marker counts for experiments

Table showing the number of animals and markers analyzed for each experiment. Columns indicate the corresponding figure, the number of animals in the experiment, and the total markers counted across all animals for the experiment.

References and Notes

1. D. C. Lu, T. Niu, W. A. Alaynick, Molecular and cellular development of spinal cord locomotor circuitry. *Front. Mol. Neurosci.* **8**, 25 (2015). doi:10.3389/fnmol.2015.00025 Medline

2. H. C. Lai, R. P. Seal, J. E. Johnson, Making sense out of spinal cord somatosensory development. *Development* **143**, 3434–3448 (2016). doi:10.1242/dev.139592 Medline

3. O. Kiehn, Decoding the organization of spinal circuits that control locomotion. *Nat. Rev. Neurosci.* **17**, 224–238 (2016). doi:10.1038/nrn.2016.9 Medline

4. S. C. Koch, D. Acton, M. Goulding, Spinal circuits for touch, pain, and itch. *Annu. Rev. Physiol.* **80**, 189–217 (2018). doi:10.1146/annurev-physiol-022516-034303 Medline

5. A. J. Todd, Neuronal circuitry for pain processing in the dorsal horn. *Nat. Rev. Neurosci.* **11**, 823–836 (2010). doi:10.1038/nrn2947 Medline

6. J. Jiang, E. Azim, C. F. Ekerot, B. Alstermark, Direct and indirect spino-cerebellar pathways: Shared ideas but different functions in motor control. *Front. Comput. Neurosci.* **9**, 75 (2015). doi:10.3389/fncom.2015.00075 Medline

7. P. J. Osseward 2nd, S. L. Pfaff, Cell type and circuit modules in the spinal cord. *Curr. Opin. Neurobiol.* **56**, 175–184 (2019). doi:10.1016/j.conb.2019.03.003 Medline

8. J. Ericson, P. Rashbass, A. Schedl, S. Brenner-Morton, A. Kawakami, V. van Heyningen, T. M. Jessell, J. Briscoe, Pax6 controls progenitor cell identity and neuronal fate in response to graded Shh signaling. *Cell* **90**, 169–180 (1997). doi:10.1016/S0092-8674(00)80323-2 Medline

9. M. Hayashi, C. A. Hinckley, S. P. Driscoll, N. J. Moore, A. J. Levine, K. L. Hilde, K. Sharma, S. L. Pfaff, Graded Arrays of Spinal and Supraspinal V2a Interneuron Subtypes Underlie Forelimb and Hindlimb Motor Control. *Neuron* **97**, 869–884.e5 (2018). doi:10.1016/j.neuron.2018.01.023 Medline

10. J. B. Bikoff, M. I. Gabitto, A. F. Rivard, E. Drobac, T. A. Machado, A. Miri, S. Brenner-Morton, E. Famojure, C. Diaz, F. J. Alvarez, G. Z. Mentis, T. M. Jessell, Spinal inhibitory interneuron diversity delineates variant motor microcircuits. *Cell* **165**, 207–219 (2016). doi:10.1016/j.cell.2016.01.027 Medline

11. M. Häring, A. Zeisel, H. Hochgerner, P. Rinwa, J. E. T. Jakobsson, P. Lönnerberg, G. La Manno, N. Sharma, L. Borgius, O. Kiehn, M. C. Lagerström, S. Linnarsson, P. Ernfors, Neuronal atlas of the dorsal horn defines its architecture and links sensory input to transcriptional cell types. *Nat. Neurosci.* **21**, 869–880 (2018). doi:10.1038/s41593-018-0141-1 Medline

12. A. Sathyamurthy, K. R. Johnson, K. J. E. Matson, C. I. Dobrott, L. Li, A. R. Ryba, T. B. Bergman, M. C. Kelly, M. W. Kelley, A. J. Levine, Massively parallel single nucleus transcriptional profiling defines spinal cord neurons and their activity during behavior. *Cell Rep.* **22**, 2216–2225 (2018). doi:10.1016/j.celrep.2018.02.003 Medline

13. J. Delile, T. Rayon, M. Melchionda, A. Edwards, J. Briscoe, A. Sagner, Single cell transcriptomics reveals spatial and temporal dynamics of gene expression in the

developing mouse spinal cord. *Development* **146**, dev173807 (2019). doi:10.1242/dev.173807 Medline

14. D. Arendt, J. M. Musser, C. V. H. Baker, A. Bergman, C. Cepko, D. H. Erwin, M. Pavlicev, G. Schlosser, S. Widder, M. D. Laubichler, G. P. Wagner, The origin and evolution of cell types. *Nat. Rev. Genet.* **17**, 744–757 (2016). doi:10.1038/nrg.2016.127 Medline

15. O. Hobert, P. Kratsios, Neuronal identity control by terminal selectors in worms, flies, and chordates. *Curr. Opin. Neurobiol.* **56**, 97–105 (2019). doi:10.1016/j.conb.2018.12.006 Medline

16. D. Arendt, P. Y. Bertucci, K. Achim, J. M. Musser, Evolution of neuronal types and families. *Curr. Opin. Neurobiol.* **56**, 144–152 (2019). doi:10.1016/j.conb.2019.01.022 Medline

17. H. Zeng, J. R. Sanes, Neuronal cell-type classification: Challenges, opportunities and the path forward. *Nat. Rev. Neurosci.* **18**, 530–546 (2017). doi:10.1038/nrn.2017.85 Medline

18. D. R. Ladle, E. Pecho-Vrieseling, S. Arber, Assembly of motor circuits in the spinal cord: Driven to function by genetic and experience-dependent mechanisms. *Neuron* **56**, 270–283 (2007). doi:10.1016/j.neuron.2007.09.026 Medline

19. B. Tasic, Z. Yao, L. T. Graybuck, K. A. Smith, T. N. Nguyen, D. Bertagnolli, J. Goldy, E. Garren, M. N. Economo, S. Viswanathan, O. Penn, T. Bakken, V. Menon, J. Miller, O. Fong, K. E. Hirokawa, K. Lathia, C. Rimorin, M. Tieu, R. Larsen, T. Casper, E. Barkan, M. Kroll, S. Parry, N. V. Shapovalova, D. Hirschstein, J. Pendergraft, H. A. Sullivan, T. K. Kim, A. Szafer, N. Dee, P. Groblewski, I. Wickersham, A. Cetin, J. A. Harris, B. P. Levi, S. M. Sunkin, L. Madisen, T. L. Daigle, L. Looger, A. Bernard, J. Phillips, E. Lein, M. Hawrylycz, K. Svoboda, A. R. Jones, C. Koch, H. Zeng, Shared and distinct transcriptomic cell types across neocortical areas. *Nature* **563**, 72–78 (2018). doi:10.1038/s41586-018-0654-5 Medline

20. M. I. Gabitto, A. Pakman, J. B. Bikoff, L. F. Abbott, T. M. Jessell, L. Paninski, Bayesian sparse regression analysis documents the diversity of spinal inhibitory interneurons. *Cell* **165**, 220–233 (2016). doi:10.1016/j.cell.2016.01.026 Medline

21. A. E. Stepien, M. Tripodi, S. Arber, Monosynaptic rabies virus reveals premotor network organization and synaptic specificity of cholinergic partition cells. *Neuron* **68**, 456–472 (2010). doi:10.1016/j.neuron.2010.10.019 Medline

22. M. Tripodi, A. E. Stepien, S. Arber, Motor antagonism exposed by spatial segregation and timing of neurogenesis. *Nature* **479**, 61–66 (2011). doi:10.1038/nature10538 Medline

23. A. J. Levine, C. A. Hinckley, K. L. Hilde, S. P. Driscoll, T. H. Poon, J. M. Montgomery, S. L. Pfaff, Identification of a cellular node for motor control pathways. *Nat. Neurosci.* **17**, 586–593 (2014). doi:10.1038/nn.3675 Medline

24. F. J. Alvarez, R. M. Villalba, R. Zerda, S. P. Schneider, Vesicular glutamate transporters in the spinal cord, with special reference to sensory primary afferent synapses. *J. Comp. Neurol.* **472**, 257–280 (2004). doi:10.1002/cne.20012 Medline

25. A. Yuan, M. V. Rao, R. A. Veeranna, R. A. Nixon, Neurofilaments and neurofilament proteins in health and disease. *Cold Spring Harb. Perspect. Biol.* **9**, a018309 (2017). doi:10.1101/cshperspect.a018309 Medline

26. C. Pivetta, M. S. Esposito, M. Sigrist, S. Arber, Motor-circuit communication matrix from spinal cord to brainstem neurons revealed by developmental origin. *Cell* **156**, 537–548 (2014). doi:10.1016/j.cell.2013.12.014 Medline

27. E. Azim, J. Jiang, B. Alstermark, T. M. Jessell, Skilled reaching relies on a V2a propriospinal internal copy circuit. *Nature* **508**, 357–363 (2014). doi:10.1038/nature13021 Medline

28. M. Baek, V. Menon, T. M. Jessell, A. W. Hantman, J. S. Dasen, Molecular Logic of Spinocerebellar Tract Neuron Diversity and Connectivity. *Cell Rep.* **27**, 2620–2635.e4 (2019). doi:10.1016/j.celrep.2019.04.113 Medline

29. R. Yuengert, K. Hori, E. E. Kibodeaux, J. X. McClellan, J. E. Morales, T. P. Huang, J. L. Neul, H. C. Lai, Origin of a non-Clarke's column division of the dorsal spinocerebellar tract and the role of caudal proprioceptive neurons in motor function. *Cell Rep.* **13**, 1258–1271 (2015). doi:10.1016/j.celrep.2015.09.064 Medline

30. A. W. Hantman, T. M. Jessell, Clarke's column neurons as the focus of a corticospinal corollary circuit. *Nat. Neurosci.* **13**, 1233–1239 (2010). doi:10.1038/nn.2637 Medline

31. K. Nishida, S. Ito, Developmental origin of long-range neurons in the superficial dorsal spinal cord. *Eur. J. Neurosci.* **46**, 2608–2619 (2017). doi:10.1111/ejn.13736 Medline

32. Z. Zhang, S. Wei, H. Du, Z. Su, Y. Wen, Z. Shang, X. Song, Z. Xu, Y. You, Z. Yang, Zfhx3 is required for the differentiation of late born D1-type medium spiny neurons. *Exp. Neurol.* **322**, 113055 (2019). doi:10.1016/j.expneurol.2019.113055 Medline

33. M. Tambalo, R. Mitter, D. G. Wilkinson, A single cell transcriptome atlas of the developing zebrafish hindbrain. *Development* **147**, dev184143 (2020). doi:10.1242/dev.184143 Medline

34. S. A. Wilke, B. J. Hall, J. K. Antonios, L. A. Denardo, S. Otto, B. Yuan, F. Chen, E. M. Robbins, K. Tiglio, M. E. Williams, Z. Qiu, T. Biederer, A. Ghosh, NeuroD2 regulates the development of hippocampal mossy fiber synapses. *Neural Dev.* **7**, 9 (2012). doi:10.1186/1749-8104-7-9 Medline

35. L. C. Greig, M. B. Woodworth, M. J. Galazo, H. Padmanabhan, J. D. Macklis, Molecular logic of neocortical projection neuron specification, development and diversity. *Nat. Rev. Neurosci.* **14**, 755–769 (2013). doi:10.1038/nrn3586 Medline

36. C. Q. Doe, Temporal Patterning in the Drosophila CNS. *Annu. Rev. Cell Dev. Biol.* **33**, 219–240 (2017). doi:10.1146/annurev-cellbio-111315-125210 Medline

37. R. B. Roome, F. B. Bourojeni, B. Mona, S. Rastegar-Pouyani, R. Blain, A. Dumouchel, C. Salesse, W. S. Thompson, M. Brookbank, Y. Gitton, L. Tessarollo, M. Goulding, J. E. Johnson, M. Kmita, A. Chédotal, A. Kania, Phox2a defines a developmental origin of the anterolateral system in mice and humans. *Cell Rep.* **33**, 108425 (2020). doi:10.1016/j.celrep.2020.108425 Medline

38. L. Ruder, A. Takeoka, S. Arber, Long-distance descending spinal neurons ensure quadrupedal locomotor stability. *Neuron* **92**, 1063–1078 (2016). doi:10.1016/j.neuron.2016.10.032 Medline

39. M. J. Sternfeld, C. A. Hinckley, N. J. Moore, M. T. Pankratz, K. L. Hilde, S. P. Driscoll, M. Hayashi, N. D. Amin, D. Bonanomi, W. D. Gifford, K. Sharma, M. Goulding, S. L. Pfaff,

Speed and segmentation control mechanisms characterized in rhythmically-active circuits created from spinal neurons produced from genetically-tagged embryonic stem cells. *eLife* **6**, e21540 (2017). doi:10.7554/eLife.21540 Medline

40. T. V. Bui, T. Akay, O. Loubani, T. S. Hnasko, T. M. Jessell, R. M. Brownstone, Circuits for grasping: Spinal dI3 interneurons mediate cutaneous control of motor behavior. *Neuron* **78**, 191–204 (2013). doi:10.1016/j.neuron.2013.02.007 Medline

41. M. A. Sieber, R. Storm, M. Martinez-de-la-Torre, T. Müller, H. Wende, K. Reuter, E. Vasyutina, C. Birchmeier, Lbx1 acts as a selector gene in the fate determination of somatosensory and viscerosensory relay neurons in the hindbrain. *J. Neurosci.* **27**, 4902–4909 (2007). doi:10.1523/JNEUROSCI.0717-07.2007 Medline

42. K. L. Hilde, A. J. Levine, C. A. Hinckley, M. Hayashi, J. M. Montgomery, M. Gullo, S. P. Driscoll, R. Grosschedl, Y. Kohwi, T. Kohwi-Shigematsu, S. L. Pfaff, Satb2 is required for the development of a spinal exteroceptive microcircuit that modulates limb position. *Neuron* **91**, 763–776 (2016). doi:10.1016/j.neuron.2016.07.014 Medline

43. E. Dessaud, L. L. Yang, K. Hill, B. Cox, F. Ulloa, A. Ribeiro, A. Mynett, B. G. Novitch, J. Briscoe, Interpretation of the sonic hedgehog morphogen gradient by a temporal adaptation mechanism. *Nature* **450**, 717–720 (2007). doi:10.1038/nature06347 Medline

44. Y. Kawaguchi, B. Cooper, M. Gannon, M. Ray, R. J. MacDonald, C. V. E. Wright, The role of the transcriptional regulator Ptf1a in converting intestinal to pancreatic progenitors. *Nat. Genet.* **32**, 128–134 (2002). doi:10.1038/ng959 Medline

45. Y. Zhang, S. Narayan, E. Geiman, G. M. Lanuza, T. Velasquez, B. Shanks, T. Akay, J. Dyck, K. Pearson, S. Gosgnach, C.-M. Fan, M. Goulding, V3 spinal neurons establish a robust and balanced locomotor rhythm during walking. *Neuron* **60**, 84–96 (2008). doi:10.1016/j.neuron.2008.09.027 Medline

46. S. K. Lee, L. W. Jurata, J. Funahashi, E. C. Ruiz, S. L. Pfaff, Analysis of embryonic motoneuron gene regulation: Derepression of general activators function in concert with enhancer factors. *Development* **131**, 3295–3306 (2004). doi:10.1242/dev.01179 Medline

47. L. McFarlane, V. Truong, J. S. Palmer, D. Wilhelm, Novel PCR assay for determining the genetic sex of mice. *Sex Dev.* **7**, 207–211 (2013). doi:10.1159/000348677 Medline

48. A. Saxena, A. Wagatsuma, Y. Noro, T. Kuji, A. Asaka-Oba, A. Watahiki, C. Gurnot, M. Fagiolini, T. K. Hensch, P. Carninci, Trehalose-enhanced isolation of neuronal sub-types from adult mouse brain. *Biotechniques* **52**, 381–385 (2012). doi:10.2144/0000113878 Medline

49. P. Brennecke, S. Anders, J. K. Kim, A. A. Kołodziejczyk, X. Zhang, V. Proserpio, B. Baying, V. Benes, S. A. Teichmann, J. C. Marioni, M. G. Heisler, Accounting for technical noise in single-cell RNA-seq experiments. *Nat. Methods* **10**, 1093–1095 (2013). doi:10.1038/nmeth.2645 Medline

50. A. Subramanian, P. Tamayo, V. K. Mootha, S. Mukherjee, B. L. Ebert, M. A. Gillette, A. Paulovich, S. L. Pomeroy, T. R. Golub, E. S. Lander, J. P. Mesirov, Gene set enrichment analysis: A knowledge-based approach for interpreting genome-wide expression profiles. *Proc. Natl. Acad. Sci. U.S.A.* **102**, 15545–15550 (2005). doi:10.1073/pnas.0506580102 Medline

51. A. M. Henry, J. G. Hohmann, High-resolution gene expression atlases for adult and developing mouse brain and spinal cord. *Mamm. Genome* **23**, 539–549 (2012). doi:10.1007/s00335-012-9406-2 Medline

52. G. Paxinos, *Atlas of the Developing Mouse Brain at E17.5, P0 and P6*. (Elsevier, ed. 1, 2007).

Acknowledgements

Chapter 2, in full, is a reprint of the manuscript as it appears in: Osseward, Peter J., Neal D. Amin, Jeffrey D. Moore, Benjamin A. Temple, Bianca K. Barriga, Lukas C. Bachmann, Fernando Beltran, Miriam Gullo, Robert C. Clark, Shawn P. Driscoll, Samuel L. Pfaff, and Marito Hayashi. 2021. 'Conserved genetic signatures parcellate cardinal spinal neuron classes into local and projection subsets', *Science*, 372: 385. The manuscript was written in collaboration with Marito Hayashi and Samuel L. Pfaff.

We thank K. Lettieri, B. O'Leary, H. Forman, A. J. Levine, M. J. Sternfeld, K. L. Hilde, members of the Pfaff laboratory, the FCCF core (C. O'Connor and C. Fitzpatrick; NIH-NCI CCSG: P30 014195), the NGS core (N. Hah; NIH-NCI CCSG: P30 014195, the Chapman Foundation and the Helmsley Charitable Trust), the UCSD IGM Genomic Center (K. Jepsen and other members), the Biophotonics core (NIH-NCI CCSG: P30 014195 and the Waitt Foundation), the GT3 core (J. Naughton, J. Marlett, and R. Armendariz; NIH-NCI CCSG: P30 014195, NINDS R24 Core Grant, funding from NEI), and the Janelia Viral Vector Core for technical support and advice; M. Goulding, G. Gatto, members of the Goulding laboratory, E. J. Kim and E. M. Callaway for providing reagents and advice; and S. Ackerman, K. Asahina, K. Baldwin, T. Komiyama, and Y. Zou for discussions and advice. Funding: P.J.O. was supported by the Christopher and Dana Reeve Foundation. N.D.A. is supported by the NIMH T32 Training Grant T32MH019938 J.D.M. is supported by NIH-NICHD K99 HD096512. B.K.B. is supported by the UCSD Cell and Molecular Genetics Training Program (T32 GM007240) and the Timken-Sturgis Foundation. M.H. was supported by the Japanese Ministry of Education, Culture, Sports,

Science, and Technology Long-Term Student Support Program and the Timken-Sturgis Foundation. S.L.P. is a Benjamin H. Lewis chair in neuroscience. This research was supported by funding from the Howard Hughes Medical Institute, the Christopher and Dana Reeve Foundation, the Sol Goldman Charitable Trust, and National Institutes of Health (1 U19 NS112959-01). Author contributions: Conceptualization: M.H., P.J.O., and S.L.P. Methodology: M.H., P.J.O., J.D.M., and S.P.D. Software: S.P.D., J.D.M., and P.J.O. Validation: M.H., P.J.O., L.C.B., and R.C.C. Formal analysis: S.P.D., J.D.M., P.J.O., and M.H. Investigation: M.H., P.J.O., N.D.A., B.A.T., B.K.B., L.C.B., F.B., and R.C.C. Resources: M.G., S.P.D., J.D.M., P.J.O., and M.H. Data curation: S.P.D., J.D.M., and P.J.O. Writing, original draft: M.H., P.J.O., and S.L.P. Writing, review and editing: M.H., P.J.O., N.D.A., J.D.M., B.A.T., B.K.B., S.P.D., and S.L.P. Visualization: M.H., P.J.O., and S.P.D. Supervision: M.H., P.J.O., and S.L.P. Project administration: M.H., P.J.O., and S.L.P. Competing interests: The authors declare no competing interests. Data and materials availability: All data are available in the main text or the supplementary materials. The accession number for the scRNA-seq data reported in this paper is NIH GEO: GSE171607, GSE171605, and GSE171606.

Chapter 3: An intersectional genetic system to access interneuron subtypes arrayed across the spinal cord

Abstract

The spinal cord contains a variety of interneurons for processing sensory and motor information. During embryonic development, neural progenitors can be divided into cardinal classes which arise from discrete progenitor domains. Concurrently, the timing of neurogenesis correlates with neurons expressing Group-N or Group-Z markers, across all cardinal classes. These two developmental frameworks correspond to various aspects of cell type identity, including spatial position, neurotransmitter status, and axonal output. However, it is unclear the degree to which this intersection produces functionally distinct cell types. We generated transgenic mouse lines to selectively label Group-N and Group-Z neurons in the spinal cord. To label Group-N/Z subsets within each cardinal class, we developed an intersectional genetic approach. Each intersection of cardinal class and Group-N/Z lines labeled neurons with distinct locations within the spinal cord. Leveraging tools to trace and manipulate intersectional neural populations will allow for the systematic analysis of spinal interneuron function.

Introduction

Spinal neuron function has been examined through various perspectives, including spinal cord injury, projections, physiology, and development (Ahuja et al., 2017; Lai, Seal, & Johnson, 2016; Lu, Niu, & Alaynick, 2015). Tract tracing, physiological, and spinal cord injury studies demonstrate correlations between damage to specific spinal cord tracts or projection neurons and resulting patterns of sensorimotor loss (Ahuja et al., 2017; Ruder, Takeoka, & Arber, 2016). Developmentally, genetic mouse lines labeling spinal cardinal classes have been used to perturb or ablate specific neuron populations, which consequently produce distinct physiological and behavioral deficits (Kiehn, 2016; Lai et al., 2016). To illustrate, ablation of V0 interneurons

results in loss of left-right limb alternation, while V1 ablation results in limb hyperflexion (Britz et al., 2015; Talpalar et al., 2013). However, the correspondence between cardinal classes and spinal cord projection status is low. Cardinal classes are a mixture of local and long-range neurons, making it is difficult to interpret whether phenotypes derived from cardinal class manipulations can be attributed to their long-range neuronal subsets, their local neuronal subsets, or both (P. J. Osseward, 2nd & Pfaff, 2019; P. J. Osseward et al., 2021). Furthermore, individual spinal tracts and are composed of multiple cardinal classes – thus, tract lesions generally cannot be attributed to projection subpopulations of individual cardinal classes (Pivetta, Esposito, Sigrist, & Arber, 2014). As a result, there have been limited studies examining spinal neuron function through both the lens of cardinal class and projection status simultaneously (Azim, Jiang, Alstermark, & Jessell, 2014).

We recently showed that the Group-N/Z division of spinal neurons corresponds to local versus long range projections, as well as timing of neurogenesis, and is a major molecular division among all cardinal classes (Chapter 2, (P. J. Osseward et al., 2021)). We sought to generate genetic tools to better asses the properties and functions of each Group-N/Z subset of each cardinal class.

Results

Genetic labeling of Group-N and Group-Z neurons

To gain genetic access to Group-N and Group-Z neurons, we generated two transgenic knock-in mouse lines in which P2A-Flpo was introduced into the NeuroD2 and Zfhx3 loci (Figure 1, A and B). We crossed the knock-in animals to ROSA-CAG-FSF-Tdtomato animals to

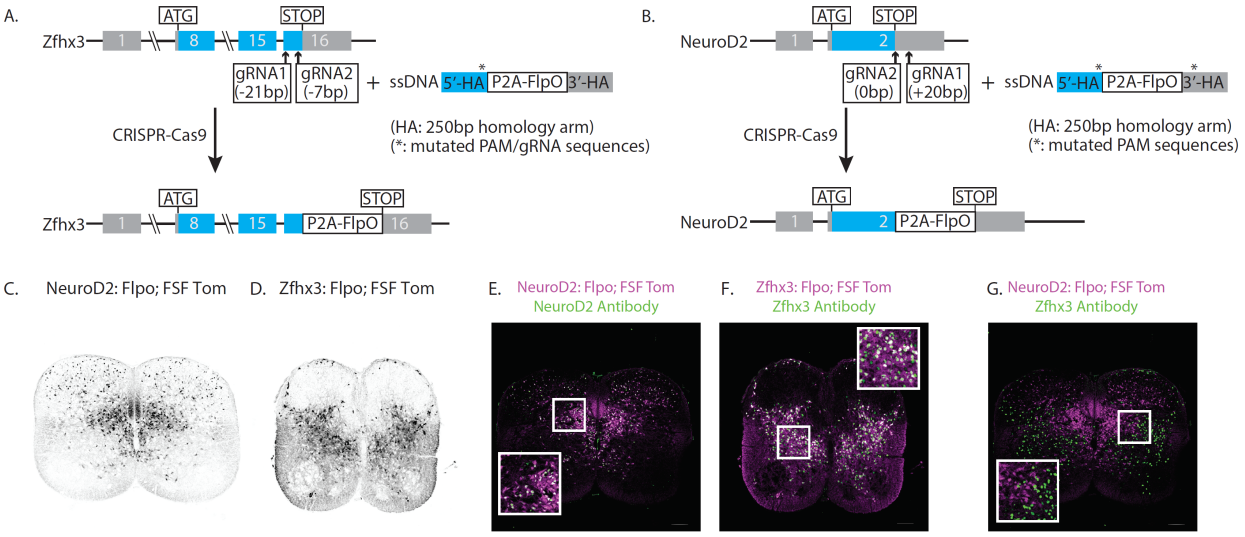
Figure 1 - Genetic labeling of Group-N and Group-Z neurons in the spinal cord

(A and B) Schematic for the generation of the NeuroD2:Flpo and Zfhx3:Flpo mouse lines. Targeted insertion of P2A-Flpo into the last exon before the stop codon.

(C-F) Crossing NeuroD2:Flpo or Zfhx3:Flpo with the reporter line Rosa-CAG-FSF-TdTomato recapitulates the pattern of expression seen with antibody staining.

(G) Immunostaining for the opposite N-Z marker reveals low incidences of colocalization.

All cryosections are lumbar, P0, 12μm. Scale bars, 100μm.


A.
ATG
STOP
Zfhx3
1
8
15
16
gRNA1 (-21bp)
gRNA2 (-7bp)
+ ssDNA 5′-HA P2A-FlpO 3′-HA
CRISPR-Cas9
(HA: 250bp homology arm)
(*: mutated PAM/gRNA sequences)
ATG
STOP
Zfhx3
1
8
15
P2A-FlpO
16
B.
ATG
STOP
NeuroD2
1
2
gRNA2 (0bp)
gRNA1 (+20bp)
+ ssDNA 5′-HA P2A-FlpO 3′-HA
CRISPR-Cas9
(HA: 250bp homology arm)
(*: mutated PAM sequences)
ATG
STOP
NeuroD2
1
2
P2A-FlpO

C. NeuroD2: Flpo; FSF Tom
D. Zfhx3: Flpo; FSF Tom
E. NeuroD2: Flpo; FSF Tom
NeuroD2 Antibody
F. Zfhx3: Flpo; FSF Tom
Zfhx3 Antibody
G. NeuroD2: Flpo; FSF Tom
Zfhx3 Antibody

indelibly label Zfhx3 and NeuroD2 expressing cells (Figure 1, C and D). To confirm that the Flpo lines recapitulated NeuroD2 and Zfhx3 expression, we compared NeuroD2 and Zfhx3 genetic labeling with antibody expression (Figure 1, E and F). Additionally, staining for the opposing Group-N/Z marker revealed low overlap, as predicted from earlier colocalization studies (Figure 1G) (Chapter 2, (P. J. Osseward et al., 2021)). Together, these studies indicate that the mouse lines effectively label Group-N and Group-Z neurons within the spinal cord.

Intersectional genetics to systematically label spinal neuron types

Each cardinal class is comprised of both Group-N and Group-Z subtypes (Chapter 2, (P. J. Osseward et al., 2021)). To label the Group-N/Z subset of cardinal classes, we crossed cardinal class Cre lines to Group-N or Group-Z Flpo lines, in combination with intersectional tdTomato reporter mice (ROSA-CAG:fsf:lsl:tdTomato). From our previous work (Chapter 2, (P. J. Osseward et al., 2021)), we displayed the positional densities of each cardinal class neuron type and their Group-N/Z subsets identified through antibody staining as heatmaps (Figure 3A-C, left panel). With each cardinal class tested intersectionally, the genetic labeling pattern matched the antibody labeling pattern (Figure 3, B and C, right panel). The intersection of cardinal class and Group-N/Z markers yielded higher spatial specificity when compared to the entire cardinal class or Group-N/Z lines alone (Figure 1 and 3). Thus, this intersectional genetic system can be used to systematically and reproducibly compare and contrast spinal interneuron types arrayed across the cord.

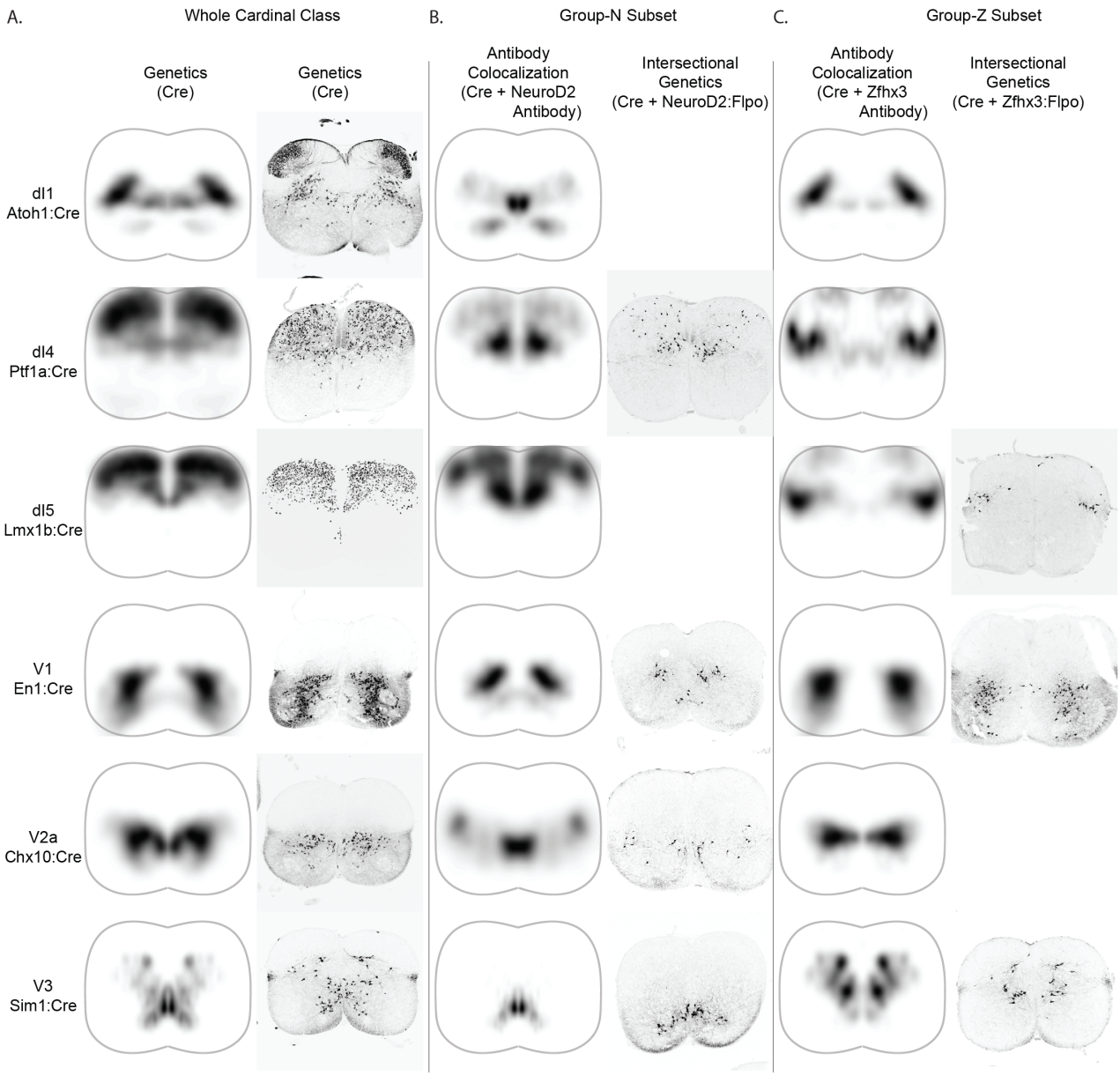
Figure 2 – Intersectional genetics recapitulates cardinal class immunostaining with Group-N and Z markers

(A) Left panel: Heatmaps depicting the spatial density of each cardinal class, labeled using Cre lines. Right panel: Representative image of each cardinal class.

(B) Left panel: Colocalization of genetically labeled cardinal class with Group-N marker NeuroD2 antibody staining. The Group-N subtypes within each cardinal class have refined, predominately medial, densities when compared to the entire cardinal class. Right panel: The Group-N subtype of each cardinal class labeled intersectionally with cardinal class Cre line, NeuroD2:Flpo, and tdTomato reporter.

(C) Left panel: Colocalization of genetically labeled cardinal class with Group-Z marker Zfhx3 antibody staining. The Group-Z subtypes within each cardinal class have lateral densities when compared to the entire cardinal class. Right panel: The Group-Z subtype of each cardinal class labeled intersectionally with cardinal class Cre line, Zfhx3:Flpo, and tdTomato reporter.

For all images, cryosections 20μm. Intersectional crosses not shown are ongoing.


A.
Whole Cardinal Class
Genetics (Cre)
Genetics (Cre)
B.
Group-N Subset
Antibody Colocalization (Cre + NeuroD2 Antibody)
Intersectional Genetics (Cre + NeuroD2:Flpo)
C.
Group-Z Subset
Antibody Colocalization (Cre + Zfhx3 Antibody)
Intersectional Genetics (Cre + Zfhx3:Flpo)
dI1 Atoh1:Cre
dI4 Ptf1a:Cre
dI5 Lmx1b:Cre
V1 En1:Cre
V2a Chx10:Cre
V3 Sim1:Cre

Discussion

In this chapter, we have developed and verified genetic tools for systematically studying spinal neuron cardinal class and projection diversity. In future work, we hope to examine the anatomy and function of each subset in greater detail. Cre and Flpo dependent AAVs - such as the INTERSECT system - can be used to restrict labeling to spinal segments, avoiding potentially labeling brain cells which may confound experiments (Fenno, Mattis, Ramakrishnan, & Deisseroth, 2017). Activation or ablation of cardinal class Group-N/Z subsets will allow for analysis of how each local and long-range subtype contribute to sensorimotor behaviors. Additionally, the synaptic inputs and outputs of each subtype may be analyzed. Many sensory synaptic inputs into the spinal cord have stereotyped spatial distributions of synaptic contacts (Lai et al., 2016). The refined spatial settling of each cardinal class Group-N/Z subset suggests that each may receive selective inputs. In support, Satb2 expressing interneurons are located medially in the deep dorsal horn, where they receive proprioceptive sensory inputs. Deletion of *Satb2* results in the interneurons to misposition laterally and consequently lose proprioceptive input (Hilde et al., 2016). For synaptic output, many long-range neurons in the spinal cord also possess short range collaterals (Azim et al., 2014; Pivetta et al., 2014). Thus, for a single cardinal class, we hope to compare the synaptic local output of the Group-N subset to short range collaterals of the Group-Z subset. In summary, the intersectional system developed here appears to be a simple but powerful system for assessing spinal interneuron function along developmental and axonal projection axes.

Methods

<u>Mouse lines</u>

The following strains of mice were used:

ROSA-CAG:lsl:tdTomato (Ai14, JAX, 007908),

ROSA-CAG:lsl:H2B-tdTomato (Ai75, JAX, 025106),

ROSA-CAG:fsf:lsl:tdTomato (Ai65, JAX, 021875),

Atoh1:Cre (JAX, 011104),

Chx10:Cre *(Sternfeld et al., 2017)*,

En1:Cre (JAX, 007916),

Lmx1b:Cre (provided by R. Johnson, University of Texas MD Anderson Cancer Center, *(Hilde et al., 2016)*),

Ptf1a:Cre *(Kawaguchi et al., 2002)*,

Sim1:Cre *(Zhang et al., 2008)*

Mouse lines obtained from the JAX laboratory were maintained in a C57BL/6J background, and all other lines were maintained in a CB6F1/J background. All mouse work was conducted in accordance with IACUC guidelines of the Salk Institute for Biological Studies. Both male and female mice were used in all studies.

Generation of NeuroD2:Flpo and Zfhx3:Flpo knock-in mouse lines:

The transgenic mice were generated based off the Easi-CRISPR protocol, a method for creating knock-in and conditional knockout mouse models using long ssDNA donors (Miura, Quadros, Gurumurthy, & Ohtsuka, 2018). For both NeuroD2 and Zfhx3, a P2A-Flpo with flanking 250bp homology arms was designed to be inserted into the last exon before the stop codon. Animals were genotyped using primer sequences for Flpo, as well as primers spanning

the region upstream and downstream from the Flpo sequence. Founder candidates were crossed to FSF Tomato mouse to compare genetic labeling with NeuroD2 and Zfhx3 immunostaining.

Tissue preparation, immunohistochemistry, and imaging:

Primary antibodies used were:

Rabbit anti-NeuroD2 (abcam, AB104430, lot# GR3263783-2/GR3185621-1, 1:1000),

Sheep anti-Zfhx3 (Novus, AF7384, lot# CGHE011709A/ CGHE0111121, 1:1000)

Secondary antibodies and counter stains used were:

Donkey anti-rabbit (Thermo Fisher, 1:1000), anti-sheep (Thermo Fisher, 1:1000)

Tissue preparation, fixation, immunostaining, and imaging was all performed in the same manner as chapter 2.

References

Ahuja, C. S., Wilson, J. R., Nori, S., Kotter, M. R. N., Druschel, C., Curt, A., & Fehlings, M. G. (2017). Traumatic spinal cord injury. *Nat Rev Dis Primers, 3*, 17018. doi:10.1038/nrdp.2017.18

Azim, E., Jiang, J., Alstermark, B., & Jessell, T. M. (2014). Skilled reaching relies on a V2a propriospinal internal copy circuit. *Nature, 508*(7496), 357-363. doi:10.1038/nature13021

Britz, O., Zhang, J., Grossmann, K. S., Dyck, J., Kim, J. C., Dymecki, S., . . . Goulding, M. (2015). A genetically defined asymmetry underlies the inhibitory control of flexor-extensor locomotor movements. *Elife, 4*. doi:10.7554/eLife.04718

Fenno, L. E., Mattis, J., Ramakrishnan, C., & Deisseroth, K. (2017). A Guide to Creating and Testing New INTRSECT Constructs. *Curr Protoc Neurosci, 80*, 4 39 31-34 39 24. doi:10.1002/cpns.30

Hilde, K. L., Levine, A. J., Hinckley, C. A., Hayashi, M., Montgomery, J. M., Gullo, M., . . . Pfaff, S. L. (2016). Satb2 Is Required for the Development of a Spinal Exteroceptive Microcircuit that Modulates Limb Position. *Neuron, 91*(4), 763-776. doi:10.1016/j.neuron.2016.07.014

Kawaguchi, Y., Cooper, B., Gannon, M., Ray, M., MacDonald, R. J., & Wright, C. V. (2002). The role of the transcriptional regulator Ptf1a in converting intestinal to pancreatic progenitors. *Nat Genet, 32*(1), 128-134. doi:10.1038/ng959

Kiehn, O. (2016). Decoding the organization of spinal circuits that control locomotion. *Nat Rev Neurosci, 17*(4), 224-238. doi:10.1038/nrn.2016.9

Lai, H. C., Seal, R. P., & Johnson, J. E. (2016). Making sense out of spinal cord somatosensory development. *Development, 143*(19), 3434-3448. doi:10.1242/dev.139592

Lu, D. C., Niu, T., & Alaynick, W. A. (2015). Molecular and cellular development of spinal cord locomotor circuitry. *Front Mol Neurosci, 8*, 25. doi:10.3389/fnmol.2015.00025

Miura, H., Quadros, R. M., Gurumurthy, C. B., & Ohtsuka, M. (2018). Easi-CRISPR for creating knock-in and conditional knockout mouse models using long ssDNA donors. *Nat Protoc, 13*(1), 195-215. doi:10.1038/nprot.2017.153

Osseward, P. J., 2nd, & Pfaff, S. L. (2019). Cell type and circuit modules in the spinal cord. *Curr Opin Neurobiol, 56*, 175-184. doi:10.1016/j.conb.2019.03.003

Osseward, P. J., Amin, N. D., Moore, J. D., Temple, B. A., Barriga, B. K., Bachmann, L. C., . . . Hayashi, M. (2021). Conserved genetic signatures parcellate cardinal spinal neuron classes into local and projection subsets. *Science, 372*(6540), 385. doi:10.1126/science.abe0690

Pivetta, C., Esposito, M. S., Sigrist, M., & Arber, S. (2014). Motor-circuit communication matrix from spinal cord to brainstem neurons revealed by developmental origin. *Cell, 156*(3), 537-548. doi:10.1016/j.cell.2013.12.014

Ruder, L., Takeoka, A., & Arber, S. (2016). Long-Distance Descending Spinal Neurons Ensure Quadrupedal Locomotor Stability. *Neuron, 92*(5), 1063-1078. doi:10.1016/j.neuron.2016.10.032

Sternfeld, M. J., Hinckley, C. A., Moore, N. J., Pankratz, M. T., Hilde, K. L., Driscoll, S. P., . . . Pfaff, S. L. (2017). Speed and segmentation control mechanisms characterized in rhythmically-active circuits created from spinal neurons produced from genetically-tagged embryonic stem cells. *Elife, 6*. doi:10.7554/eLife.21540

Talpalar, A. E., Bouvier, J., Borgius, L., Fortin, G., Pierani, A., & Kiehn, O. (2013). Dual-mode operation of neuronal networks involved in left-right alternation. *Nature, 500*(7460), 85-88. doi:10.1038/nature12286

Zhang, Y., Narayan, S., Geiman, E., Lanuza, G. M., Velasquez, T., Shanks, B., . . . Goulding, M. (2008). V3 spinal neurons establish a robust and balanced locomotor rhythm during walking. *Neuron, 60*(1), 84-96. doi:10.1016/j.neuron.2008.09.027

Acknowledgements

Chapter 3 is preliminary material being prepared for submission. Authors include Peter J. Osseward, Marito Hayashi, Lukas C. Bachmann, Hannah Forman, and Samuel L. Pfaff. The manuscript was written in collaboration with Samuel L. Pfaff.

We thank K. Lettieri, M. Gullo, members of the Pfaff laboratory, the GT3 core (J. Naughton, J. Marlett, and R. Armendariz; NIH-NCI CCSG: P30 014195, NINDS R24 Core Grant, funding from NEI), and the Transgenic Core Facility of the Salk Institute (Y. Dayn and Tsung-Chang Sung; NIH-NCI CCSG: P30 014195). Funding: P.J.O. was supported by the Christopher and Dana Reeve Foundation. M.H. was supported by the Japanese Ministry of Education, Culture, Sports, Science, and Technology Long-Term Student Support Program and the Timken-Sturgis Foundation. S.L.P. is a Benjamin H. Lewis chair in neuroscience. This research was supported by funding from the Howard Hughes Medical Institute, the Christopher and Dana Reeve Foundation, the Sol Goldman Charitable Trust, and National Institutes of Health (1 U19 NS112959-01).